AN INVESTIGATION OF LIQUEFACTION EFFECTS ON PIERS AND PILES OF SEGMENTAL PRECAST BALANCED CANTILEVER BRIDGES

A THESIS SUBMITTED TO
THE GRADUATE SCHOOL OF NATURAL AND APPLIED SCIENCES
OF
MIDDLE EAST TECHNICAL UNIVERSITY

BY

ÖZER GÜNDÜZ

IN PARTIAL FULFILLMENT OF THE REQUIREMENTS
FOR
THE DEGREE OF MASTER OF SCIENCE
IN
EARTHQUAKE STUDIES

DECEMBER 2019

Approval of the thesis:

AN INVESTIGATION OF LIQUEFACTION EFFECTS ON PIERS AND PILES OF SEGMENTAL PRECAST BALANCED CANTILEVER BRIDGES

submitted by **ÖZER GÜNDÜZ** in partial fulfillment of the requirements for the degree of **Master of Science in Earthquake Studies Department, Middle East Technical University** by,

Prof. Dr. Halil Kalıpçılar
Dean, Graduate School of **Natural and Applied Sciences** _____

Prof. Dr. Ayşegül Askan Gündoğan
Head of Department, **Earthquake Studies** _____

Prof. Dr. Alp Caner
Supervisor, **Earthquake Studies, METU** _____

Assoc. Prof. Dr. Mustafa Tolga Yılmaz
Co-Supervisor, **Engineering Sciences, METU** _____

Examining Committee Members:

Prof. Dr. Ayşegül Askan Gündoğan
Earthquake Studies, METU _____

Prof. Dr. Alp Caner
Earthquake Studies, METU _____

Assoc. Prof. Dr. Mustafa Tolga Yılmaz
Engineering Sciences, METU _____

Prof. Dr. Sadık Bakır
Civil Engineering, METU _____

Assoc. Prof. Dr. Mustafa Kerem Koçkar
Civil Engineering, Hacettepe University _____

Date: 06.12.2019

I hereby declare that all information in this document has been obtained and presented in accordance with academic rules and ethical conduct. I also declare that, as required by these rules and conduct, I have fully cited and referenced all material and results that are not original to this work.

Name, Surname: Özer Gündüz

Signature:

ABSTRACT

AN INVESTIGATION OF LIQUEFACTION EFFECTS ON PIERS AND PILES OF SEGMENTAL PRECAST BALANCED CANTILEVER BRIDGES

Gündüz, Özer
Master of Science, Earthquake Studies
Supervisor: Prof. Dr. Alp Caner
Co-Supervisor: Assoc. Prof. Dr. Mustafa Tolga Yılmaz

December 2019, 153 pages

In this thesis, the seismic behavior of a typical segmental precast balanced cantilever bridge over liquefiable soils is investigated. Liquefaction is a phenomenon that is triggered by large movements of the sand layer during earthquakes and cause damage to structures. The subject is still under investigation, approaches for liquefaction induced lateral spreading calculations can be found in the literature. Inertial and kinematic effects of the lateral spreading were studied with a total of four different approaches which are the non-liquefied scenario, liquefied scenario for inertial analysis, force-based method case and displacement-based method for kinematic analysis. The focus of this study is given to identify the changes in the structural response of case study bridge using different approaches. In inertial analysis, liquefaction effect on acceleration response spectrum was estimated via one-dimensional site response modeling. Some specifications have offered p-y curves for soil-pile interaction. Also, they suggest that the design response spectrum can be used in the case of liquefaction. Therefore, the liquefied and non-liquefied configuration was set up in this thesis for inertial analysis of this kind of bridge. In kinematic effects of soil, lateral spreading which is one of the major damaging mechanism of liquefaction also investigated. In this purpose, different soil profiles having different

peak ground accelerations, the shear strain of the soil were analyzed. P-y curves belonging to the soil profile had been modeled and their effects on superstructure and infrastructure were discussed. It was observed that the structure period is highly important in considering inertial analysis. Pier seismic design forces are critical in liquefied response-spectrum models than non-liquefied one which is design spectrum. Also, pile forces were more critical in displacement applied lateral spreading. Then other methods, liquefaction effects on the spectrum can significantly alter the structural response for long period structures.

Keywords: Liquefaction, Lateral Spreading, Precast Balanced Cantilever Bridge, Piles, Piers

ÖZ

DENGELİ KONSOL KÖPRÜLERİN AYAK VE KAZIKLARINDA SIVILAŞMA ETKİLERİNİN ARAŞTIRILMASI

Gündüz, Özer
Yüksek Lisans, Deprem Çalışmaları
Tez Danışmanı: Prof. Dr. Alp Caner
Ortak Tez Danışmanı: Doç. Dr. Mustafa Tolga Yılmaz

Aralık 2019, 153 sayfa

Bu tez çalışmasında, sıvılaşan bir zemin üzerinde bulunan önüretimli dengeli konsol köprülerin sismik davranışı incelenmiştir. Sıvılaşma, deprem anında zeminde bulunan kum tabakasının çok büyük hareketleri sonucu yapılara zarar veren bir olaydır. Hala araştırmalara konu olan bu konuda, depremden dolayı oluşan yanal kaymalar çeşitli yönetmeliklerde bulunabilir. Yanal yayılmanın atalet ve kinematic etkileri sıvılaşma durumu, sıvılaşmama durumu, kuvvete dayalı methodlar ve deplasmana dayalı methodlar olmak üzere dört farklı yöntemle incelenmiştir. Bu çalışmanın amacı, çeşitli yaklaşımlarla yapıda oluşan etkileri tanımlamaktır. Tek yönlü saha etki analizi ile, sıvılaşmanın spectral ivmelere etkisi hesaplanmıştır. Zemin-kazık etkileşimi için bazı yönetmelikler p-y eğrilerini önermiştir. Ayrıca, dizayn spektrumunun sıvılaşma durumunda kullanabileceği de eklenmiştir. Bu yüzden atalet analizlerinde hem sıvılaşma ve sıvılaşma olmayan Zemin için 2 ayrı hesap yöntemi kullanılmıştır. Zeminin kinematik etkilerinde, yanal yayılma incelenmiştir. Bu amaçla, farklı zemin profilleriyle beraber farklı pik ivmelerle şekil değiştirmeler bulunmuştur. Bu zeminlere ait p-y eğrileri modellenerek üstyapıya olan etkileri tartışılmıştır.Yapı periyodunun atalet analizinde çok önemli olduğu görüşmüştür. Ayakların tasarımında ise sıvılaşmanın gözlemlendiği ivme spektrumları daha kritik olarak gözlemlenmiştir.

Deplasman uygulanan kazıklarda, kuvvetlerin daha fazla olduğu görülmüştür. Sıvılaşmanın uzun periyotlu yapılara çok büyük ölçüde etkide bulunduğu görülmüştür.

Anahtar Kelimeler: Sıvılaşma, Yanal Akma, Önüretimli Dengeli Konsol Köprü, Kazıklar, Ayaklar

To my family…

ACKNOWLEDGEMENTS

I would like to declare my many thanks to my supervisor Prof. Dr. Alp Caner for providing me his guidance and experience. Also, I would like to declare my many thanks to my co-supervisor Assoc. Prof. Dr. Mustafa Tolga Yılmaz for his precious help on this study and widen my horizon in geotechnical earthquake engineering subjects.

I also would like to express the deepest gratitudes to dear committee members, Prof. Dr. Ayşegül Askan Gündoğan, Prof. Dr. Sadık Bakır, and Assoc. Prof. Dr. Mustafa Kerem Koçkar for their precious contributions, suggestions and comments for this study.

I am grateful to Mescioğlu Engineering since they provide me the support and opportunity to study.

I am thankful to my companions in thesis study road, who are Uğur Aşcı and Ayhan Akray for their motivation and support during this study. I owe many thanks to close friends, who are Berkay Doğan and Melis Deniz for being supportive in anything.

My deepest thanks belong to my family members, who are Öztürk Gündüz, Selfiraz Gündüz and Özgür Gündüz for their endless support and love. I am very grateful to Merve Gözütok for her moral support and trust on me during this study.

TABLE OF CONTENTS

LIST OF TABLES

TABLES

LIST OF FIGURES

FIGURES

LIST OF ABBREVIATIONS

AASHTO = American Association of State Highway and Transportation Officials

API = American Petroleum Institute

ASBI = American Segmental Bridge Institute

BNWF = Beam on Nonlinear Winkler Foundation

Caltrans = California Department of Transportation

CR = Cracked Model Results

CRR = Cyclic Resistance Ratio

CSR = Cyclic Stress Ratio

DBM = Displacement Based Method

ESA = Effective stress analysis

FBM = Force-Based Method

FC = Fine Content

FDM = Finite Difference Method

FEM = Finite Element Method

FS = Factor of Safety

GWT = Groundwater Table

LQ = Liquefaction Case Results

M_w = Moment Magnitude

NOLQ = No-Liquefaction Case Results

PEER = Pacific Earthquake Engineering Research

PGA = Peak Ground Acceleration

PSA = Pseudo Static Analysis

SP1 = Soil Profile – 1

SP2 = Soil Profile – 2

SP3 = Soil Profile – 3

SRSS = Square Root of The Sum Of The Squares

SS = Strike Slip Fault

SPT = Standard Penetration Test

PEER = Pacific Earthquake Engineering Research

TSA = Total Stress Analysis

UNCR = Uncracked Model Results

LIST OF SYMBOLS

D = permanent ground displacement and H is the in meters. in percent.

D_r = Relative density (%)

H = thickness of the liquefied layer

E_c = Modulus of Elasticity of Concrete

g = Acceleration of gravity (9.81 m/s2)

N_a = Fines Content Corrected SPT value

r_d = Depth reduction factor, also known as stress reduction coefficient (dimensionless)

s_u = Undrained shear strength in kPa

T = Period of the structure (s)

V_s = Shear wave velocity (m/s)

U_G = Ground displacement

U_P = Pile displacement due to inertial loads

γ = Unit weight kN/m^3

γ_{max} = Strain Potential Index

θ = Gradient of the bottom layer

a_{max} = Maximum horizontal acceleration at ground surface (m/s2)

σ_{v0} = Total vertical stress at the specified depth where the liquefaction analysis is required (kPa)

σ'_{v0} = Effective vertical stress at the specified depth where the liquefaction analysis is

required (kPa)

σ'_0 = initial effective confining stress

CHAPTER 1

INTRODUCTION

1.1. Introduction and Background

Liquefaction of soils during a seismic event is one of the reasons for damage on the bridge piles. The term “liquefaction” was first used by Mogami and Kubo (1953), according to Kramer (1996). If liquefiable soil is triggered by an earthquake, the ground changes its state from solid to almost liquid, which reduces the bearing capacity of foundations.

Liquefaction of soil is caused by the increase in pore-water pressure due to cyclic loading that is typically driven by the earthquake. In liquefied soils, increasing pore water pressure will decrease soil stiffness and shear strength. This yields to vertical and horizontal displacements. After some time, movements based on liquefaction may cause dilative behavior, and soil can regain its shear strength while pore pressure decreases (Day, 2012).

The factors that cause liquefaction are still under investigation. The most important factors to cause liquefaction are the site conditions and the susceptibility of soil type to liquefaction. Site conditions should include groundwater table level, soil density, and earthquake parameters such as distance to a fault, etc. Loose cohesionless soils and poorly compacted or non-compacted cohesionless fills tend to liquefaction, according to FHWA-NHI (2014).

The effects of the earthquake-induced liquefaction can be divided into two parts by considering soil-structure interaction. These are inertial and kinematic effects. Inertial effects are due to earthquake excitation. Kinematic effects are related to soil movement due to liquefaction. In liquefying soils, these two effects are considered for proper design. In inertial effects, it should be emphasized that liquefying soils has

effects on response spectra. These effects can be analyzed with site response analysis. Kinematic effects develop large forces on piles of structures due to moving soil. In the past, it had especially devastating impacts on bridges. (Youd and Carter, 2003)

Lateral spreading, which is one of the consequences of liquefaction, causes the most severe damage on bridges with pile foundations. The lateral spread is a very complicated process. Its consequences can be investigated by the equivalent stress method. Also, nonlinear dynamic models of the bridge and soil could be used for this purpose. Although nonlinear dynamic analysis of soils is more accurate than the equivalent stress analysis, it is time-consuming and not practical. Pseudo-static analysis (PSA) of the piled foundation involves the equivalent stress method. It is more practical but less accurate with respect to dynamic response analyses, according to Bowen and Cubrinovski (2008). However, the range of complexity continues by selecting the analysis parameters of PSA. The lateral spreading effects of liquefaction can be analyzed by applying forces or displacements on piles, according to Murashev (2014).

Precast balanced cantilever bridges are segmental structures for transportation. The manufacturing and construction processes of these types of bridges are easy and fast. However, the formwork is expensive. It is expected that if there are standardized cross-sections of the superstructure of the precast balanced cantilever, this type of bridge is very easy and fast for construction, according to Theryo (2005). The fundamental period of bridge given in a design example prepared by Theryo (2005), was categorized as in long period bridge type (T>1s). This situation may lead to a problem in liquefiable soils and should be investigated. (AASHTO, 2009).

Selection of the earthquakes, soil parameters, methods for the displacement, and forces driven by liquefaction are the essential components of PSA (Murashev, 2014). Moreover, liquefiable soils have effects on spectra that long period structures can be more dangerous than the design spectrum. Therefore, site response analysis should be carried according to Youd and Carter (2003).

The analysis method should contain soil and pile behavior. These can be achieved by bi-linear, tri-linear, or nonlinear soils springs. For nonlinear soil springs, p-y curves were used. P-y curves show the force-displacement relation for reaction of soil to pile displacements. The soil behavior was applied to piles by using these relations. (Murashev, 2014).

To sum up, liquefaction induced lateral spreading effects to piles and piers of precast balanced cantilever bridges were investigated. For this purpose, inertial and kinematic effects of lateral spreading was given in detail. Liquefaction effects on site response analysis with different types of soil profiles were investigated and compared to the design spectrum constructed according to AASHTO (2017) in order to understand the consequences of inertial effects. In kinematic analyses, applied load types classified as force and displacement-based. These two methods were applied, according to Caltrans (2013) and Cubrinovski (2008). In displacement-based analysis, shear strain of soil proposed by Shamoto et al. (1998) was used.

1.2. Liquefaction Failures

Possible failures of piles in liquefying soils can be summarized as according to Bhattacharya et al. (2009);

- Decreasing bearing capacity of the pile,
- Additional internal lateral loads due to lateral soil movement,
- Bending failure of piles due to the moving crust,
- Buckling failure due to additional second-order axial forces,
- Dynamic failures which are results of changing soil parameters and directly earthquake responses

Liquefaction mechanism in time domain vs. spatial domain was given in Figure 1.1. According to Wang R. (2016) liquefaction has lateral and vertical effects in three different time domain of earthquake, which are pre-liquefaction, post-liquefaction, and post-earthquake. In this study, only lateral effects of liquefaction were

investigated. Inertial and kinematic analyses which includes all times scenario was investigated in the lateral effects.

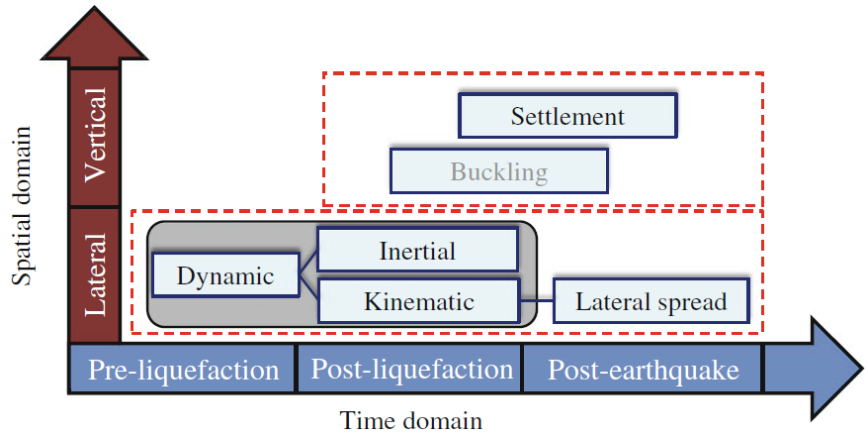

Figure 1.1. Liquefaction mechanism (Wang R., 2016)

Vertical effects were not included in analyses. Inertial effects are due to earthquake excitation. Kinematic effects are due to moving of soil subjected to liquefy. The failure mechanism of liquefaction was explained by Bhattacharya et al. (2009) in Figure 1.2.

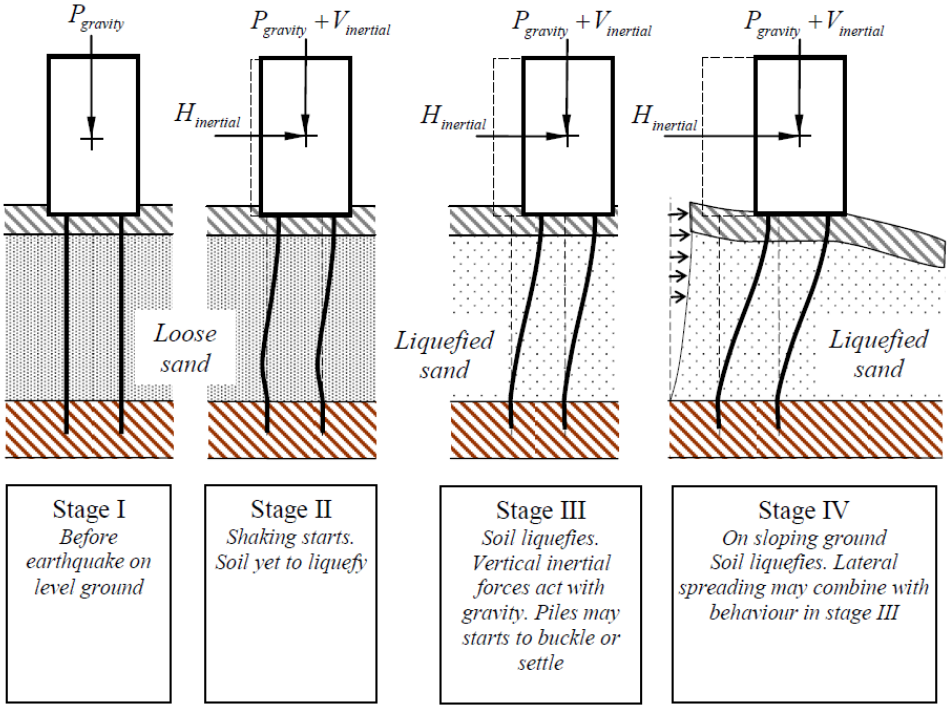

Figure 1.2. The stages of failure of piles after liquefaction (Bhattacharya et al., 2009)

The stages shown in Figure 1.2 show the mechanism of failure of piles due to liquefaction. In the first stage, structure resists against service loads. In the second stage, the earthquake excitation begins, and inertial earthquake loads are acting on the structure. In the third stage, soil begins to liquefy, and then to move vertically. As stated previously, bending, buckling failure of piles can be seen in that stage. Soil crust can cause some lateral displacement by moving. Serious settlements can also be observed. In the fourth stage, on sloping ground, the soil begins to move laterally. Therefore piles are subjected to serious damage due to moving soil. It should be noted that the pile is fixed bounded to the deep ground in every stage.

The collapse of bridges has many reasons; lateral spread is one of them. Niigata Earthquake (1964), which has a moment magnitude (M_w) of 7.6, created catastrophic failure on Showa Bridge as well as other infrastructure elements. Showa Bridge consists of 12 spans which side spans are 15m, and interior spans are 28m. Deck width was 24m.

Yoshida et al. (2007) stated that the Showa Bridge failed three minutes after the Niigata Earthquake based on local people's observations. They classified the external loads by earthquake that causes damage into three.

- Inertial forces at the time of the earthquake,
- Liquefaction induced by earthquake decreased subgrade elasticity modulus of soils, and that caused an increase in pile displacements,
- Liquefaction induced flow had given additional lateral load pile and caused large displacements.

These damages affected the structural stability of the Showa Bridge. The results can be seen in Figure 1.3. Bhattacharya et al. (2005) stated that the bending moment acting piles doubled the capacity during lateral spreading.

Figure 1.3. Collapse of the Showa Bridge after 1964 Niigata Earthquake (NISEE)

Another similarly collapsed bridge named “Million Dollar Bridge” was the victim of the Alaska Earthquake (1964). Liquefaction induced flow devastated the piles of interior piers, and affected the overall stability of the bridge. As a result, one of the spans falls from the caps into the Copper River as it can be seen in Figure 1.4.

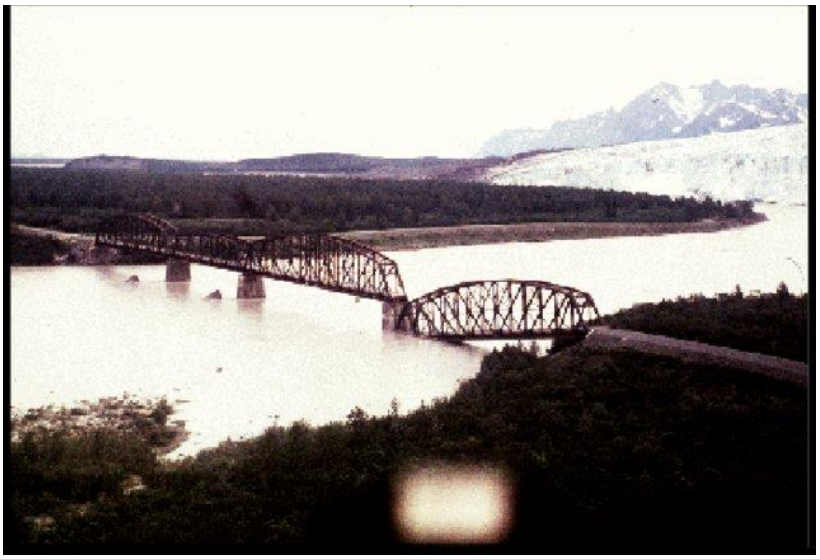

Figure 1.4. Collapse of Million Dollar Bridge (U.S. Geological survey data series 1995)

The Chi-Chi Earthquake (1999) destroyed many infrastructures, and one of them is the Wushi Bridge. Settlement due to liquefaction was the reason for the collapse of the Wushi Bridge. In Taiwan, Due to settlements caused by liquefaction, the foundation had lost its bearing capacity and started to settle. This behavior caused diagonal cracks in piers and differences in the elevation of the caps. As a result, the superstructure of the Wushi Bridge was collapsed. The collapsed superstructure can be seen in Figure 1.5.

Figure 1.5. Wushi Bridge after Taiwan 1999 Earthquake (Chang et al., 2000)

Llacolen Bridge had suffered damage from the Chile Earthquake in 2010. It was located in the Bio-Bio River in the city of Concepcion city and had a 2160m total span length and serves four lanes of vehicular traffic. Lateral spread was seen in the Bio-Bio River, and the damage resulted in unseating the decks of Llacolen Bridge, as shown in Figure 1.6. In the same river, three bridges located and liquefaction induced lateral spread had severely damaged these bridges.

Figure 1.6. Unseated decks of Llacolen Bridge (on left) and Bio-Bio Bridge (on right) after Chile Earthquake 2010 (Escribano and Bhattacharya, 2011)

In conclusion, failure mechanisms caused by the liquefaction can be typically classified into two types as the inertial and the kinematic effects. Inertial effects give damages due to seismic loads and kinematic effects are due to the movement of the soil. In the past, bridges mostly suffered damages from lateral spread in case of liquefaction. Both types of these effects will be discussed in this thesis.

1.3. Aim and Scope

The aim of this study is to investigate and to analyze the effect of liquefaction induced lateral spreading on a precast balanced cantilever bridge with a pile foundation.

To achieve this objective, post liquefaction scenarios, which are the inertial and kinematic effects of liquefaction on structural response were analyzed for a box girder bridge with five spans and a total length of 270 meters. As a result of these analyses, forces and displacements of piers and piles of the bridge were compared by considering cracked and uncracked moment of inertia of column sections. The effect of liquefiable soils on the response spectrum was investigated for three different soil profiles. For inertial analysis, both liquefied and non-liquefied scenarios were studied. Liquefiable soils and their thicknesses relations to the response spectrum were investigated in the liquefied scenario. A design spectrum for specified site conditions

proposed by AASHTO (2017) was used in the non-liquefied scenario. For kinematic analyses, two different methods for liquefaction-induced lateral spreading, which are the displacement-based and force-based methods, were examined.

1.4. Thesis Overview

This thesis contains six chapters.

Chapter 1 is about what is liquefaction, and the damages it gave to structures in the past. Aim and scope of this thesis are concluded in this part of the thesis.

Chapter 2 is the literature review of liquefaction and liquefaction-induced lateral spreading. Theoretical approaches for liquefaction, site response, soil structure interaction analyses were discussed in this section.

Chapter 3 is about the case study for bridge on pile foundations. Assumptions and simplifications for analysis are given in that chapter. The bridge information was given in this chapter. Each analysis type and scenarios, and methods were described in detail, without calculations.

Chapter 4 presents the parameters defining material behavior in the model. The soil profiles with their parameters, earthquake records selection, design spectrum and site response analysis calculations are presented in that chapter. The findings in this chapter are used in the analysis of the structure against liquefaction-induced lateral spreading.

Chapter 5 describes the results taken from the SAP2000 software. Analysis results were presented in this chapter. The results were discussed.

Chapter 6 presents the conclusions.

CHAPTER 2

LITERATURE REVIEW

2.1. Liquefaction and Lateral Spread Analysis

A lot of tests were conducted for researching the possible sources of liquefaction. There are widely known two studies in the past, which are presented by Seed and Lee (1965) and by Ishihara (1985), which related liquefaction to a number at soil parameters.

Cyclic triaxial tests on the sands of the Sacramento River were conducted by Seed and Lee (1965). Different sand specimens with different initial void ratios were used in these tests. Test results for acquiring 20% axial strain in the different sand specimens given in Figure 2.1. Seed and Lee (1965) concluded that the sands with lower void ratio (denser sands) are required more stress cycles to liquefy at the same cyclic deviator stress. In other words, test results show the relation between the number of cycles and the void ratio of soil for liquefaction.

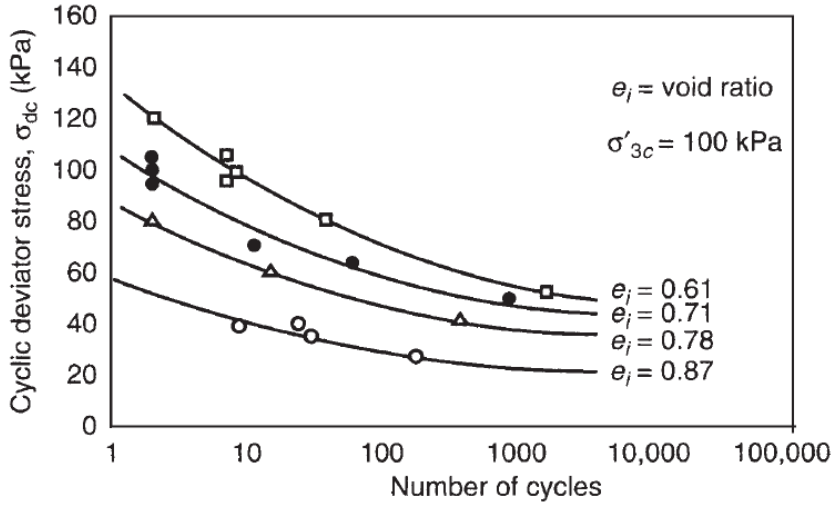

Figure 2.1. Cyclic tri-axial test results of Sacramento River sands (Seed and Lee, 1965)

After Seed and Lee (1965), Ishihara (1985) conducted tests for medium and dense sands from the Fuji River. He showed that the dense sand was not produced large strain even if pore pressure increases when comparing to medium sand. Test results for two specimens are shown in Figure 2.2.

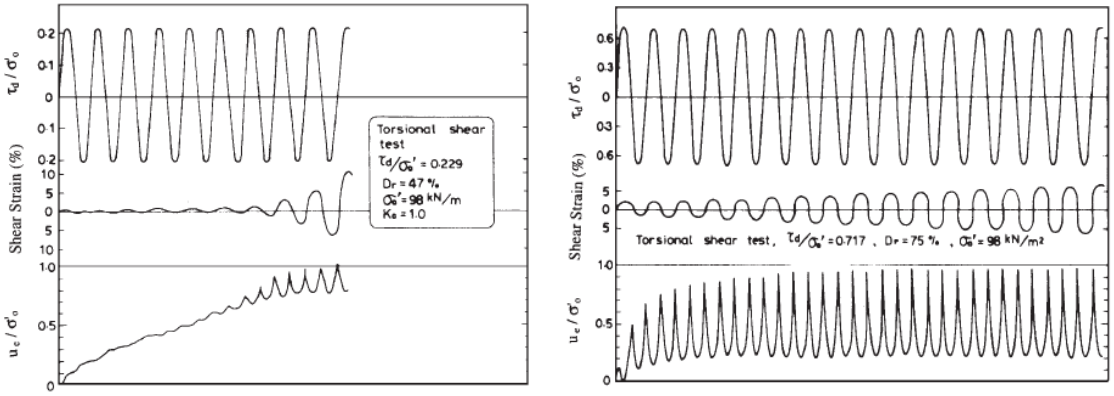

Figure 2.2. τd/σ'0 (Normalized Cyclic Shear Stress), Shear Strain and ue/σ'0, normalized excess pore water pressure results a) Dr=47% b) Dr=75% (Ishihara, 1985)

The graph of τ_d/σ_0' shows the normalized cyclic shear stress. The cyclic shear stress (τ_d) has constant amplitude and it is divided into initial effective confining stress, σ_0'. Shear strain in sand with low relative density (D_r = 47%) tend to increase suddenly after a number of stress cycles.

Normalized excess pore water pressure was reached to ratio of one for the medium density sand specimen. This means that the liquefaction had occurred in this condition. However, dense sand does produce large strain even if normalized excess pore water pressure reaches to one. This test results showed that the soil strains were highly dependent on soil density.

The factor of safety against liquefaction given in eq. 2-1 is calculated by using Cyclic Stress Ratio (CSR) over the Cyclic Resistance Ratio (CRR). CSR is also known as Shear Stress Ratio. (Day. R. W., 2012)

$$FS_{liq} = \frac{CRR}{CSR} \quad (2\text{-}1)$$

CRS in field is estimated by Youd et al. (1998);

$$CSR = \frac{\tau_{max}}{\sigma'_{v0}} = r_d \left(\frac{\sigma_{v0}}{\sigma'_{v0}}\right)\left(\frac{a_{max}}{g}\right) \quad (2\text{-}2)$$

Where, a_{max} is the maximum horizontal acceleration at ground surface in unit of m/s^2, g is the acceleration of gravity, which equals to 9.81 m/s^2, σ_{v0} is the total vertical stress at the specified depth where the liquefaction analysis is required in terms of kPa.

σ'_{v0} is the effective vertical stress at the specified depth where the liquefaction analysis is required in units of kPa, and r_d is the dimensionless depth reduction factor. According to Kayen et al. (1992);

$$r_d = 1 - 0.012z \quad (2\text{-}3)$$

The studies after the first CSR theory came up, are about depth reduction factor (r_d). Many researchers had tried to establish a reliable depth reduction factor for a reliable liquefaction evaluation. The depth reduction factor accounted for the behavior of the rigid column in the soil since the soil does not behave rigidly in the soil during an earthquake. While the soil depth increases, the depth reduction factor will decrease, and the depth reduction factor is to include deformable actions of soils under the loads, according to Day R. W. (2012).

CRR represents the resistance of the soil against liquefaction and can be determined by the in-situ soil tests such as Standard Penetration Test (SPT), Cone Penetration Test (CPT), and shear wave velocities. (Kramer, 1995)

CRR can be found from fine content corrected SPT-N value, $(N_1)_{60}$ by Seed et al. (1985). This plot was given in Figure 2.3 and used to determine the CRR for clean or silty sand for M = 7.5 earthquakes. The graph that was made by Seed et al. (1985) in Figure 2.4, based on the data from on liquefied sites.

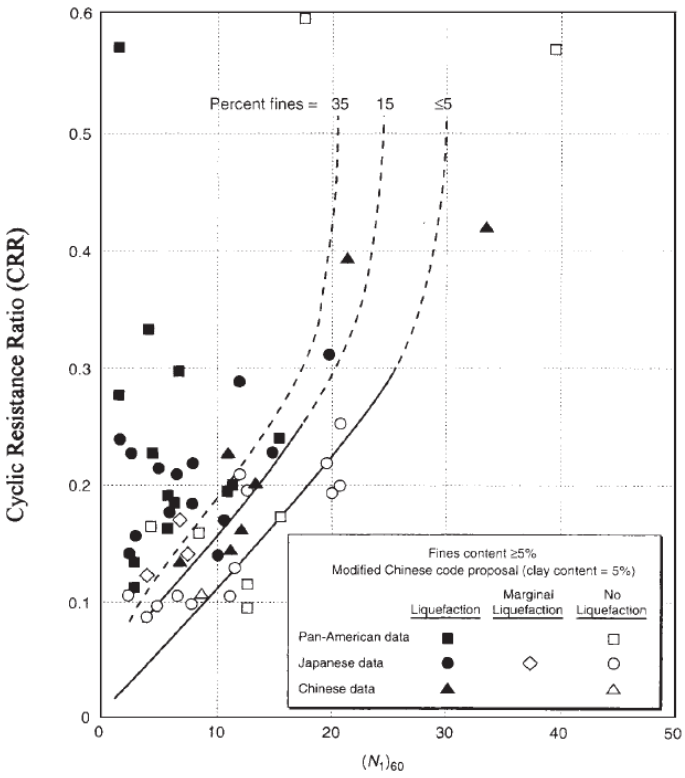

Figure 2.3. Determination of CRR in M =7.5 Earthquake (Seed et al. 1985)

Piles are the structural elements laterally and vertically supported by contacting soils. They usually transfer the superstructure loads acting on the foundation to the ground by skin friction and its tip. Pile friction and tip resistance determine the pile bearing capacity. In a multi-layered soil condition, liquefying soil weakens the skin friction, and the stiffer soil layer can be subjected to higher level loads. (Wang R., 2016)

Many kinds of research methods were tried to estimate the consequences of liquefaction. There are two methods for analyzing liquefaction effects on bridge's piles and piers. These are;

- Pseudo-static analysis (PSA)
- Dynamic Analysis

PSA is a simplified design-oriented analysis. The dynamic analysis contains direct time history analysis with constitutive models for soil behavior. The dynamic analysis

should be calibrated or tested. On the other hand, PSA has some uncertainties and should be performed carefully. (Murashev, 2014)

2.1.1. Pseudo Static Analysis

Nonlinear equivalent static analysis was used in the pseudo-static analysis approach. Linear or Nonlinear simple beam on a Winkler spring is the method for modeling soil-pile-bridge interaction. There are accepted analysis methods presented in the following sections.

The Method of Peer (Pacific Earthquake Engineering Research Center)

Ashford et al. (2011) prepared a report for the analysis of pile foundations against liquefaction-induced lateral spreading. The reaction of soil in contact with piles can be modeled using beam on the Winkler foundation method, as shown in Figure 2.4 Non-linear soil spring and moment-curvature relationships for reinforced concrete piles can be utilized. This method proposed to use non-linear p-y (force-displacement) curves for soil-pile interaction.

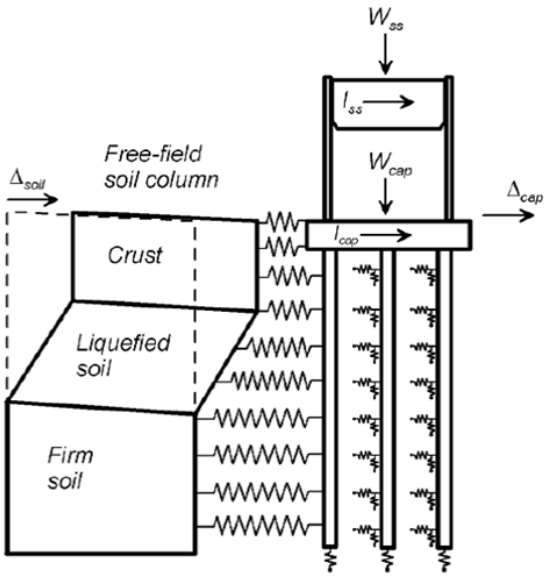

Figure 2.4. Schematic view of BNWF analysis with PSA (Ashford S.A. et al. 2011)

Ashford et al. (2011) stated that the effects of lateral spreading and dynamic shaking should be considered together. Three reasons that complicate the lateral spread are summarized as;

1. Liquefaction effects on seismic waves
2. Changing the displacement response spectrum by soil movement
3. The possibility of happening of inertial and kinematic demands at the same time

Several different approaches should be employed in the displacement-based design according to Ashford et al. Displacements belonging to selected approaches should be compared, and the critical displacements should be applied on non-linear soil springs that represent the soil-pile interaction as in Figure 2.5. In addition to these, nonlinear dynamic analysis is suggested for validation.

The Method of JRA (Japan Road Association)

Japan Road Association (JRA) developed the analysis of liquefaction for highway bridges. They divided the analysis into three cases; (JRA, 2002)

1. No-Liquefaction Case
2. Liquefied Soil Case
3. Lateral Spreading Case.

The JRA method offers bi-linear soil springs and tri-linear curvature-moment relation for soil-pile-structure interaction, as shown in Figure 2.5. Analytical model shows forces (M_0, V_0, H_0) acting to foundation in Figure 2.5.

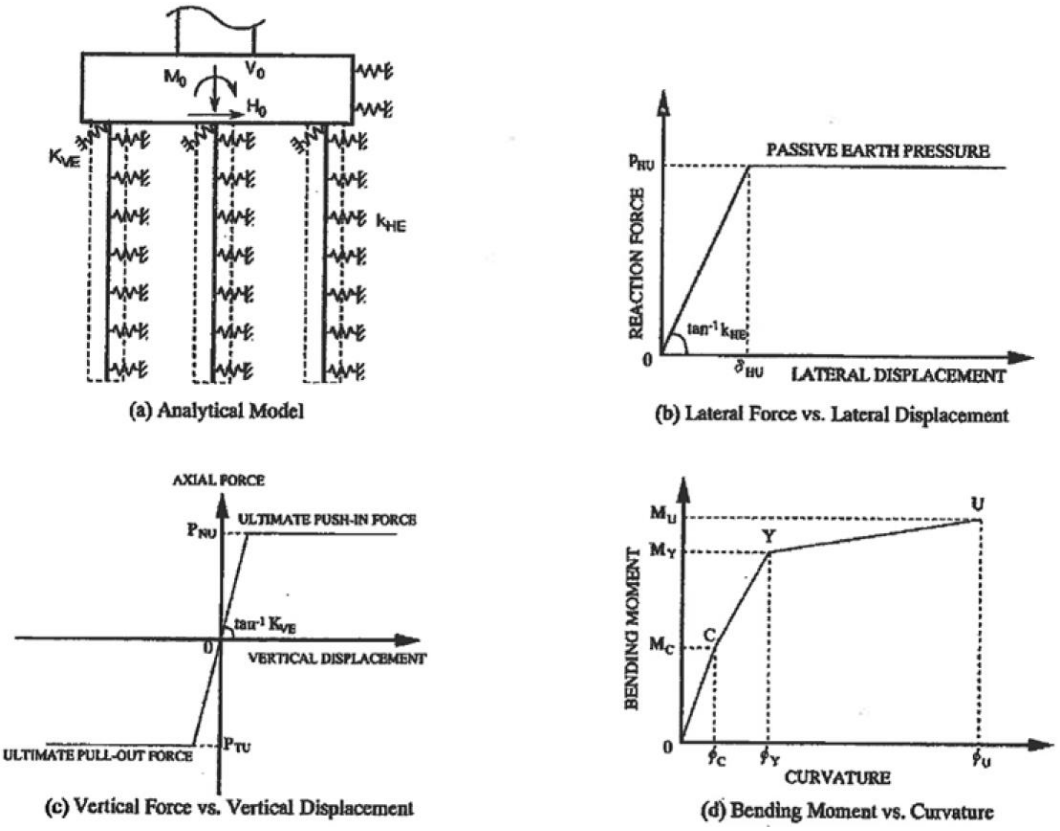

Figure 2.5. Liquefaction analysis scheme (Murashev et al., 2014)

Liquefaction effects on piles result in decreasing subgrade reaction coefficient, soil reaction, and skin friction capacity of piles in the liquefied layer. The force-based approach was considered when calculating the lateral movement of soil in the JRA method, as shown in Figure 2.6. Rankine passive soil pressures were calculated for non-liquefiable layer, and 30% of the overburden effective stress is applied on the liquefied layer. Murashev (2014) stated that the force-based approach was leading to incompatible soil loads and pile displacements.

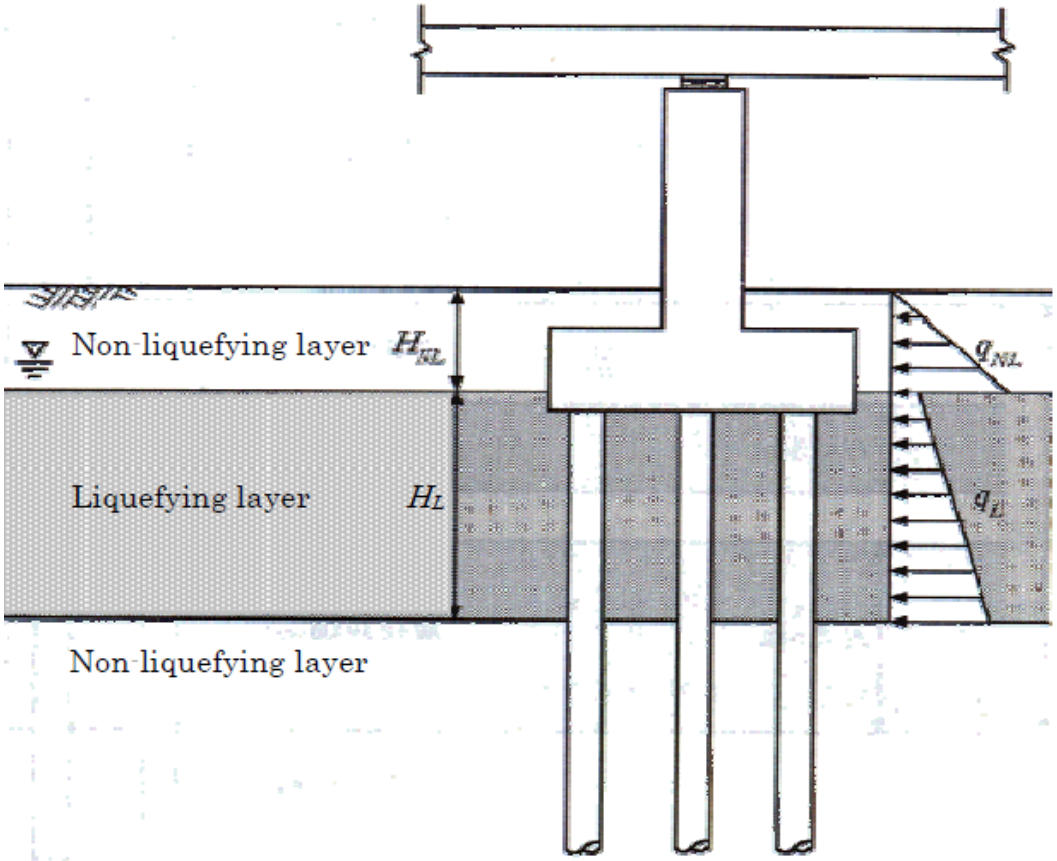

Figure 2.6. Calculation of lateral movement, Force-Based Approach (JRA, 2002)

The formulation of force-based method is given below.

q_{NL}: Lateral spreading force in crust per unit area (kN/m^2)

q_L : Lateral spreading force in liquefying layer per unit area (kN/m^2)

H_{NL}: Thickness of non-liquefying layer (m)

H_L: Thickness of non-liquefying layer (m)

The non-liquefying layer beneath the liquefying layer should not be considered. In the case of lateral spread, forces made by lateral movement of soil should be applied on the piles of the structure with consideration of depth.

The Method of Cubrinovski

Cubrinovski et al. (2009) studied the pseudo-static analysis of piles in lateral spreading. This method is very similar to the PEER method. Proposed PSA method was applied on a single-pile model, and it can be used with a pile group. The important part of this study was the estimation of soil strain caused by the cyclic phase of the earthquake excitation.

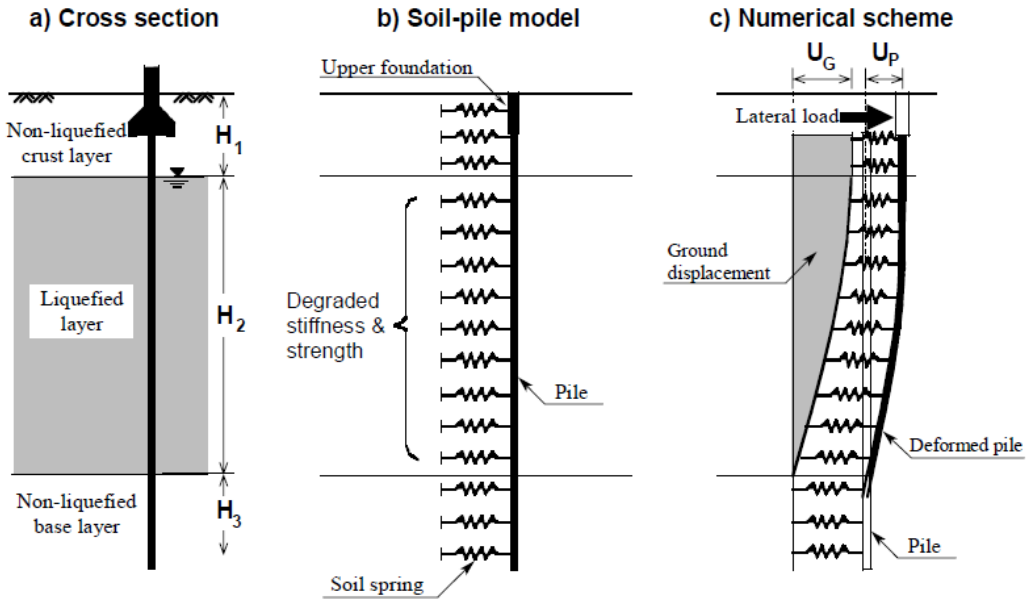

Figure 2.7. Scheme of the Pseudo Static Analysis model (Cubrinovski et al., 2009)

The proposed model in Figure 2.7 is simple but includes the non-linear relationship between pile and soil in order to include effects of liquefaction. The ground displacement due to moving soil, U_G, was applied to inertial pile displacement due to the earthquake, U_P. In that way, both inertial and kinematic effects of liquefaction on piles were taken into consideration.

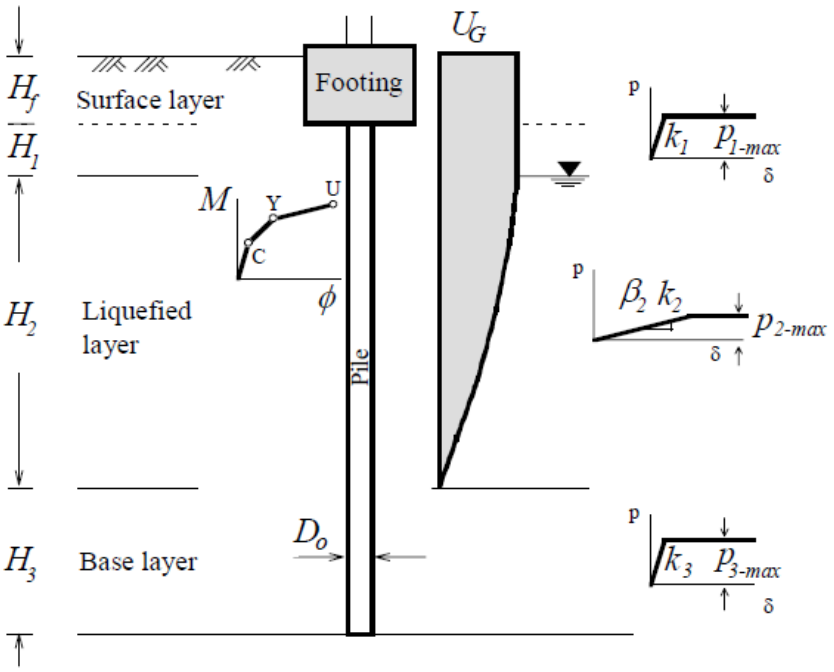

Figure 2.8. Non-linear soil-pile interaction and applied ground (Cubrinovski et al., 2009)

In Figure 2.8, bi-linear soil springs for every layer and tri-linear curvature-moment relation for the pile are shown. Cubrinovski et al. stated that the key requirement for the PSA is the estimated deformation of soil and behavior of nonlinear soil-pile interaction. They superimposed the inertial effects on piles due to the superstructure and kinematic effects, which are results of (cyclic or spreading loadings) due to soil movement.

Murashev et al. (2013) showed that the displacements and bending moment of piles can be analyzed with PSA suggested by Cubrinovski et al. (2009). Also, this method was used in design specifications of New Zealand according to Murashev et al. (2013).

The Method of AIJ (Architectural Institute of Japan)

AIJ method was gathered from Tokimatsu and Asaka (1998). The method was widely used in the design of pile foundations in Japan. As in the other stated methods, bi-linear springs and tri-linear curvature-moment relation was used in the models. The analysis is conducted according to the scheme in Figure 2.9.

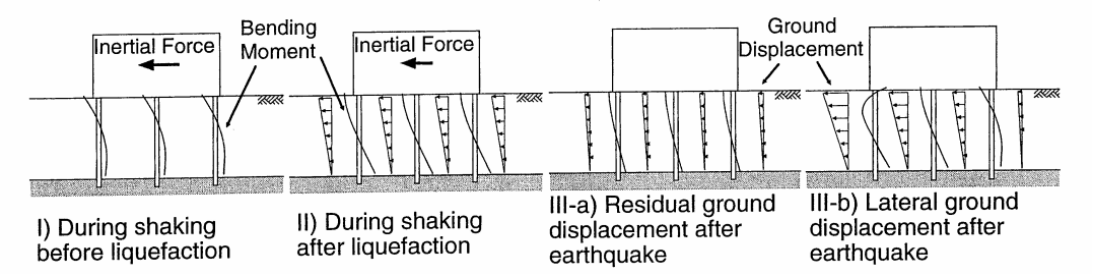

Figure 2.9. Earthquake load scenario for the soil-pile-structure interaction (Tokimatsu and Asaka, 1998)

There are three analysis cases. Case I implies that only the structure dominates the design before pore pressure increases. When pore pressure starts to increase, the cyclic shear strain will increase relatively, and massive ground displacement will occur in Case II. After that, permanent horizontal movements could be seen in Case III. In this case, earthquake stopped and the permanent ground displacements can be seen.

The only difference between the JRA method and the AIJ method is the solution method. AIJ has a displacement-based approach, and JRA has a force-based approach to modelling the effects of lateral spreading.

2.1.2. Dynamic Analysis

Dynamic Analysis of the liquefaction problems gives more reliable results than PSA if the dynamic model has realistic constitutive models calibrated by the tests. Because it includes every transient stage in it. However, it requires more knowledge and time. Finite element method (FEM) or finite difference methods (FDM) are employed mostly in the dynamic analysis of soils.

Dynamic analysis of soils can be achieved by two methods; effective-stress based and total-stress based analyses. Effective Stress Analysis (ESA) enables users to evaluate soil-pile interaction and liquefaction effects on piles. Total Stress Analysis (TSA) is similar to ESA but less accurate in liquefaction evaluation. Because TSA minimize the pore water pressure effects according to Murashev et al. (2014).

Liyanapathirana and Poulos (2002) developed a stress-based dynamic model to analyze liquefaction in the Port Island area. They had selected ESA to include the effects of liquefaction because of strength degradation due to changing pore pressure. They analyzed the Kobe earthquake within the Port Island soil profile, and their model showed degradation in stiffness and strength. Also, lateral displacement results are very close to the observations. They also concluded that most essential things in effective stress method in the dynamic analysis are plasticity, stress path gathered from laboratory tests, plastic volume change tendency due to pore pressure and undrained pore pressure response.

Elgamal A. (2010) states that the 3D simulation of soil-bridge foundation showed valuable results. The model was shown in Figure 2.10. Elgamal A. (2010) demonstrated that the structural response of a large bridge influenced by seismic ground deformation. Also, soil columns for remediation of liquefaction were modeled, and the mitigation of lateral soil deformation caused by liquefaction was evaluated.

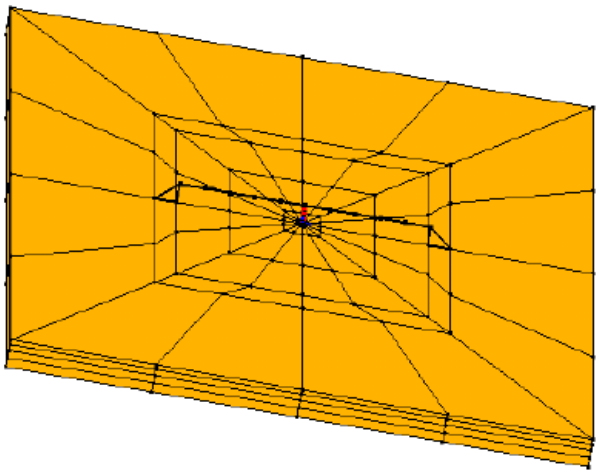

Figure 2.10. Bridge Foundation Meshes (Elgamal, 2010)

Yan (2006) used 3D dynamic analysis for The Humboldt Bay Middle Channel Bridge. Yan (2006) stated that lateral spreading in the longitudinal direction of bridges causes permanent ground deformation that can create additional moment and shear to bridge piers. The deformation of the model can be seen in Figure 2.11.

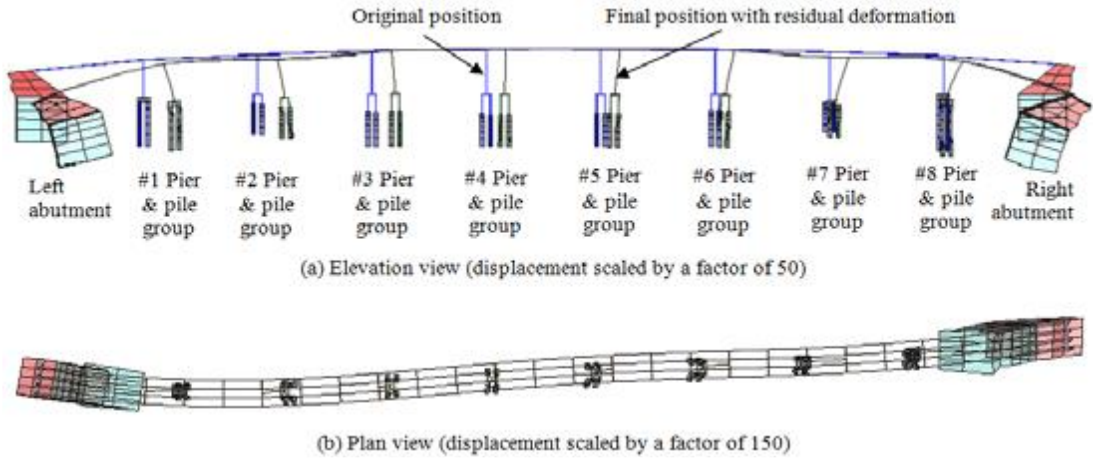

Figure 2.11. Effective Stress Based Analysis model results (Yan, 2006)

Bowen and Cubrinovski (2008) studied the case of Fitzgerald Bridge, to see the differences between the PSA and ESA methods. The results of the study was given in the Figure 2.12. It can be easily seen that ESA can capture non-linearity of the soil parameters when compared to PSA. In the shear strain diagram, they are likely to closer each other however, PSA is a stepwise linear.

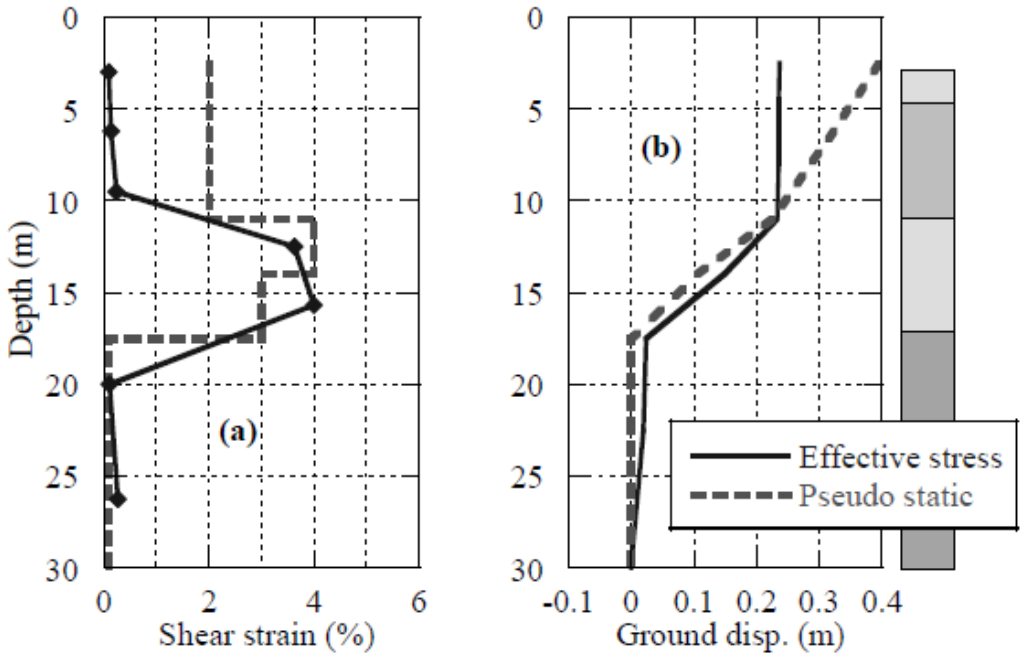

Figure 2.12. Shear strain and ground displacement comparisons between ESA and PSA (Bowen and Cubrinovski, 2008)

2.2. Site Response Analysis for Liquefiable Soils

From the results, it can Ziotopoulou et al. (2012) studied that three constitutive sand models with two-time history records, including liquefaction using one-dimensional dynamic analysis. In this study, user-defined models in the finite difference program FLAC (Itasca 2009) was used, and parametric analysis with reasonable variations was not sufficient to gather observed Port Island site responses within two earthquakes. Besides, reproducing post-triggering cyclic mobility behavior has an impact on spectral accelerations.

Youd and Carter (2003) prepared a report about the influence of liquefaction on response spectra. They simply combined the liquefaction records with the soil strata. They concluded that soil softening causes a reduction in a short period due to increased pore water pressure. In the range of 1-4 seconds of the response spectrum, a considerable increase in spectral acceleration was observed due to soil softening lengthening of the site period.

It is stated that if the soil is susceptible to liquefaction, Seismic Design Criteria should be evaluated as “D” by Imbsen (2007). AASHTO (2009) simply implied that the bridges which have longer periods (T>1s) should be investigated carefully in the liquefaction assessment.

Kramer et al. (2011) implied that an increase in the pore pressure reduces the amplitude of high-frequency ground motions and increases the amplitude of longer period components. Also, they stated that the constitutive models represent the liquefaction effect on the ground motion more accurately. In Figure 2.13, it is stated that in longer periods, the response spectral ratio was increased. This increase may lead to a problem for structures with a longer period.

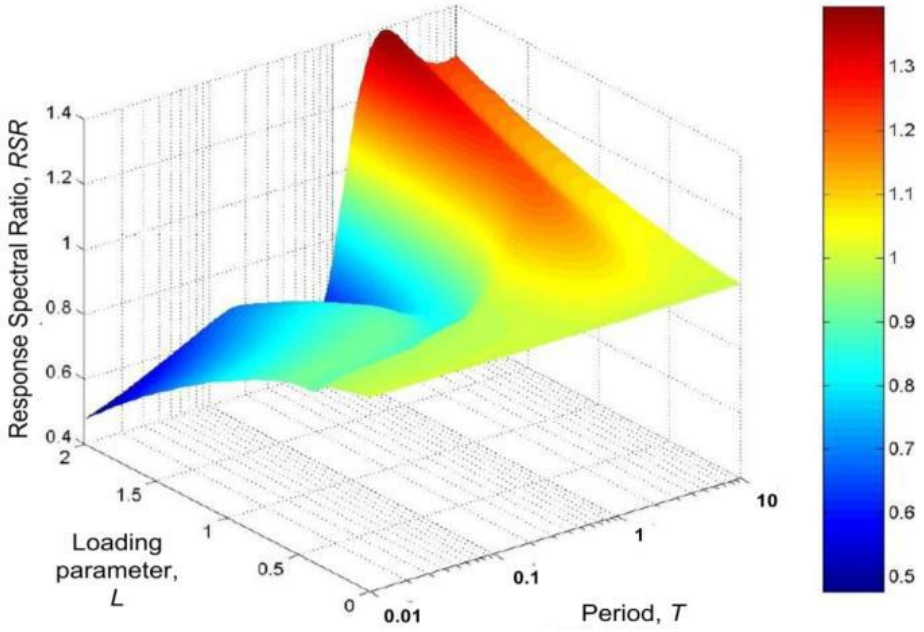

Figure 2.13. Graph of liquefaction effect (Kramer et al. 2011)

2.3. P-y Curves for Sands and Clays

P-y curves were used to illustrate the non-linear reaction of the soil to pile response. P is the soil resistance, y is the deflection regarding soil resistance. These curves were gathered by full-scale lateral loading experiments and creating theoretical methods that are fitting the experimental data. These relations are shown in Figure 2.14, are taken from the LPILE manual (2017). Some p-y methods were listed in this section. LPILE (2017) software contains the following p-y curves for the liquefying soils. Also, there are many more methods.

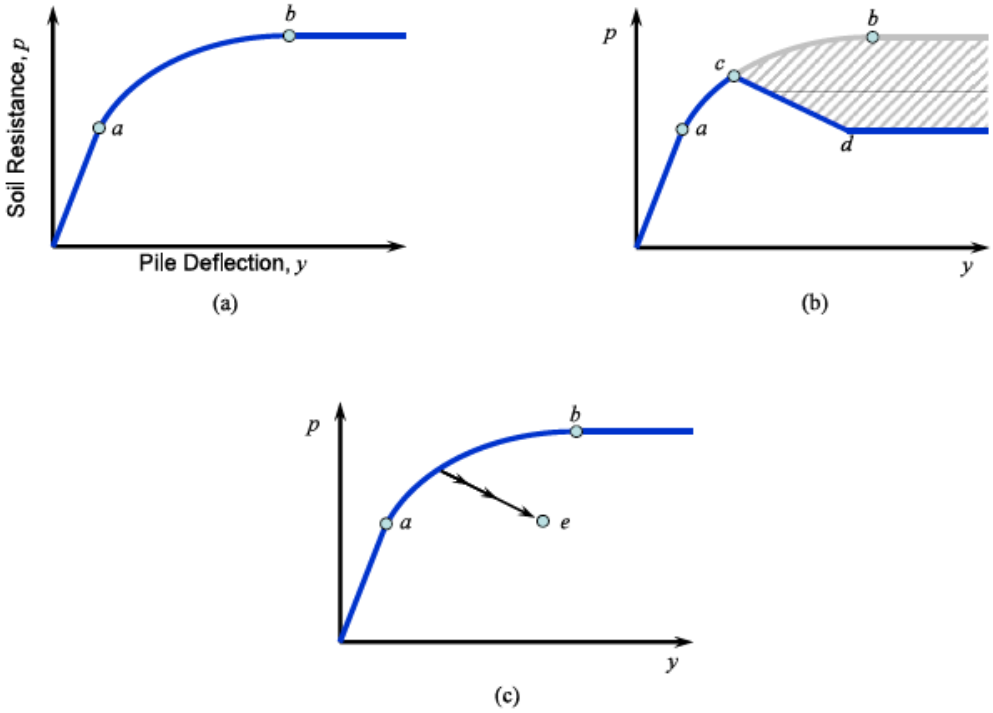

Figure 2.14. Conceptual charts for the p-y curves (Isenhower W. M. et al, 2017)

Researchers were using p-y curves for liquefying soils with the p-multiplier of any theoretical approach for cohesionless soils. Wang and Reese (1998) had studied the piles in liquefying soils. What they were doing was the modeling the soft clay as liquefying soil by equating the parameters clay and sand to each other. These parameters were cohesive strength of the clay and residual strength of liquefied sand.

Rollins (2005) developed a p-y curve for liquefied sands with a full-scale test on piles in the liquefying soil. The study shows that the liquefied soil layer got stiffer, increasing depth. Rollins found that concave up shape in the curve and the dilative effects of liquefied sand. This transition also related to pore pressure. As pore water pressure decreases, the shape would turn convex down. This type of behavior of sand is illustrated in Figure 2.15. The only limitation for the p-y curve that is made by Rollins was the pile diameter. It should be used between 0.3m and 2.6m. Also, the only correction is for pile diameter, and its trend is exponential.

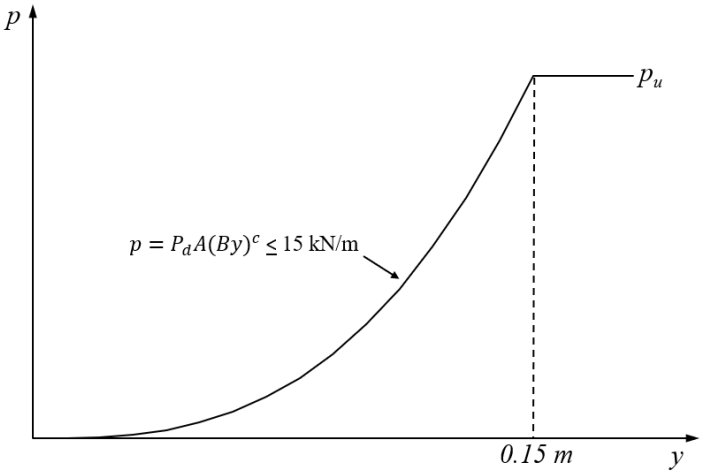

Figure 2.15. P-y relation of liquefied sands (Rollins, 2005)

Franke and Rollins (2013) proposed a hybrid model that combined the models of (Rollins et al. (2005) with that of Wang and Reese (1998). Sand lose its strength after it is liquefied. Therefore, y values remain stable after a while. This behavior was shown in Figure 2.16.

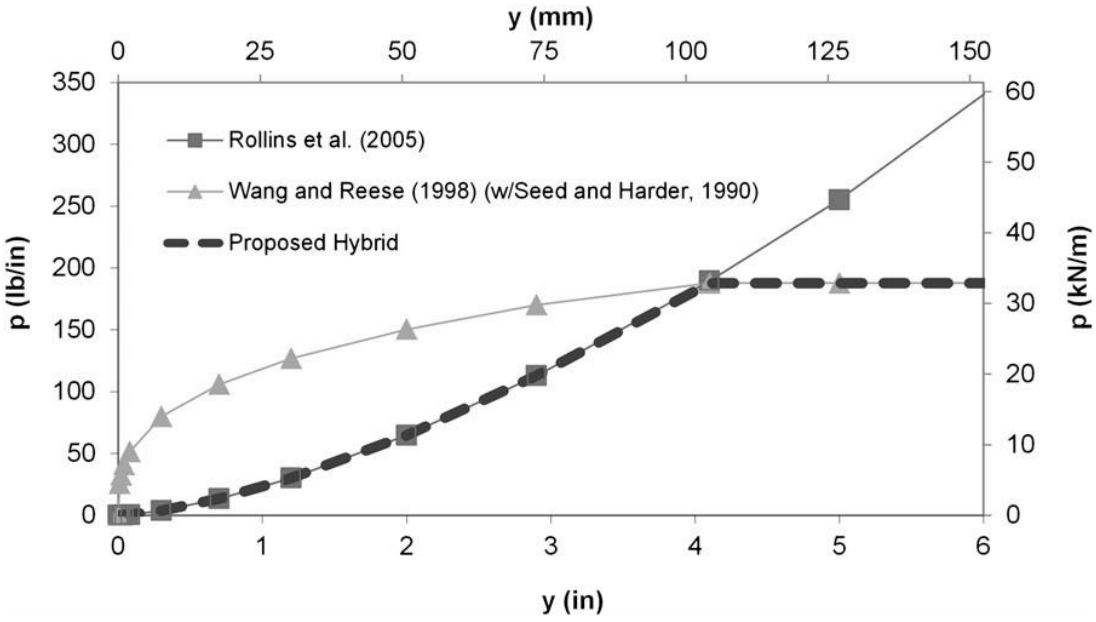

Figure 2.16. Hybrid P-y Curve (Franke and Rollins, 2013)

Franke and Rollins developed this hybrid curve combining two studies. As sand tries to densify during loading, excess pore water pressure increases. The decrease in the residual strength was considered with the hybrid p-y curve.

API (2014) developed a p-y curve for sand that considering cyclic and static loadings. API 2A sand model is a simple and widely used p-y curve. The database raised the theoretical background of API sand models; the internal friction angle was ranging between 34° and 42°. They did not suggested that any use out of that range cause trouble. P-y curve for API Sand was shown in Figure 2.17.

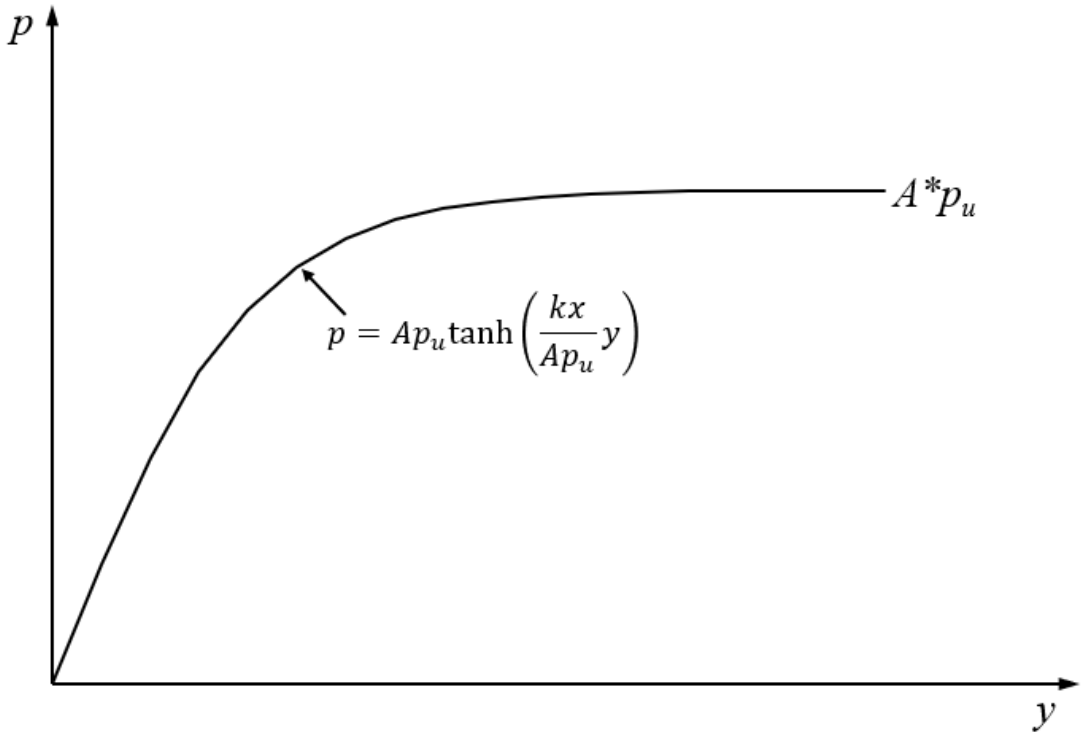

Figure 2.17. P-y curve for API Sand (Rocscience, 2018)

2.4. Deformations of Liquefiable Soils

Liquefying soil displacements are critical for the analysis and design of the pile foundation. Therefore, many researchers have been studied empirically to estimate the maximum shear strain of the liquefying soils. For the displacement-based analysis of kinematic effects of the bridges, a reliable evaluation of shear strain on soil profiles is necessary (Cubrinovski, 2009).

Hamada et al. (1987) stated a formula to predict the permanent displacement of soil induced by liquefaction with the data from Noshiro City, which was hit by an earthquake in 1983. Measured and evaluated displacements on sites of liquefaction are shown in Figure 2.18.

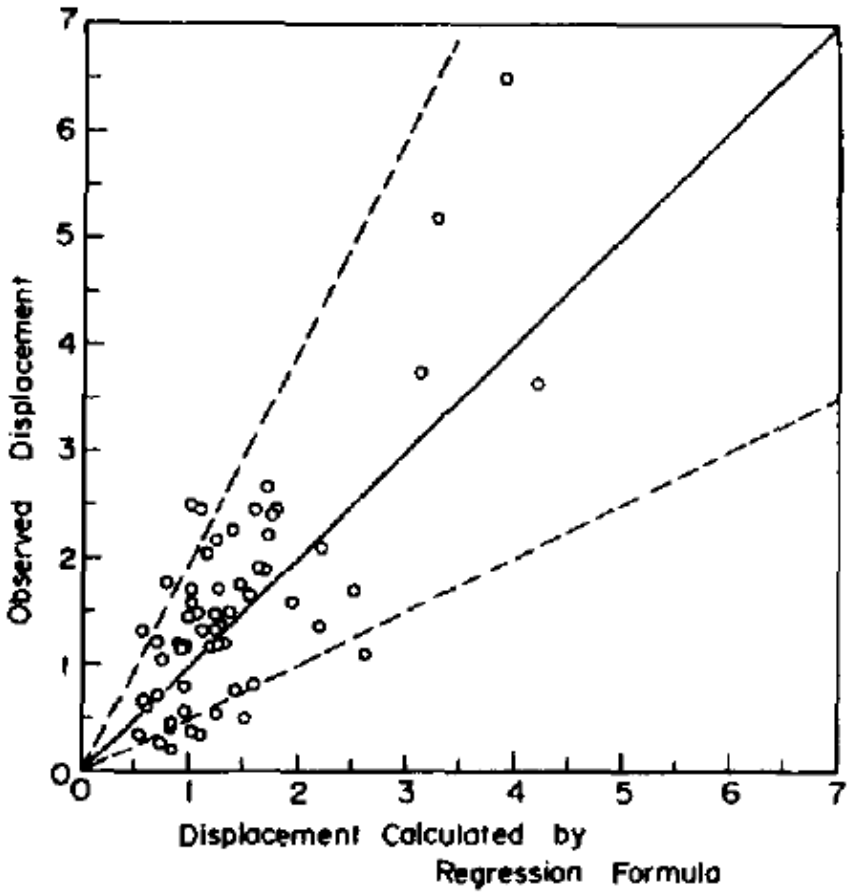

Figure 2.18. Measured and calculated displacement in meters (Hamada et al., 1987)

From these data, empirical relation gave the formula below.

$$D = 0.75\sqrt[2]{H}\sqrt[3]{\theta}$$

D is the permanent ground displacement, H is the thickness of the liquefied layer in meters, and θ is the gradient of the bottom layer in percent.

Youd et al. (2002) revised previous work on estimating liquefaction-induced deformation. His work in 1992 comprised of the earthquake data in Japan and the USA. The following formula was stated as Bartlett and Youd (1992, 1995) equation;

$$\text{Log } D_H = b_0 + b_{off} + b_1 M + b_2 \text{ Log } R + b_3 R + b_4 \text{ Log} W + b_5 \text{ Log } S + b_6 \text{ Log } T_{15} + b7 \text{ Log } (100\text{-}F_{15}) + b_8 D50_{15}$$

D_H is lateral ground displacement in meters, M is the moment magnitude of the earthquake, R is the distance to the seismic energy source, (km), T_{15} is the cumulative thickness of saturated granular layers with corrected blow counts, $(N_1)_{60}$, less than 15, in meters, F_{15} is the average fines content ~fraction of sediment sample passing a No. 200 sieve! for granular materials included within T_{15} , in percent, $D50_{15}$ is the average mean grain size for granular materials within T15 , in millimeters, S is the ground slope, in percent, and W is the free-face ratio defined as the height of the free face divided by the distance from the base of the free face to the point in question. The coefficients for this formula was given in Table 2.1.

Table 2.1. *Youd's regression formula coefficients (*Bartlett and Youd, 1992)

Parameters	Constants		M	Log R	R	Log W	Log S	Log T_{15}	Log $(100\text{-}F_{15})$	$D50_{15}$	Regression coefficient
Coefficients	b_o	b_{off}	b_1	b_2	b_3	b_4	b_5	b_6	b_7	b_8	R_c^2
Values	−15.787	−0.579	1.178	−0.927	−0.013	0.657	0.429	0.348	4.527	−0.922	82.6

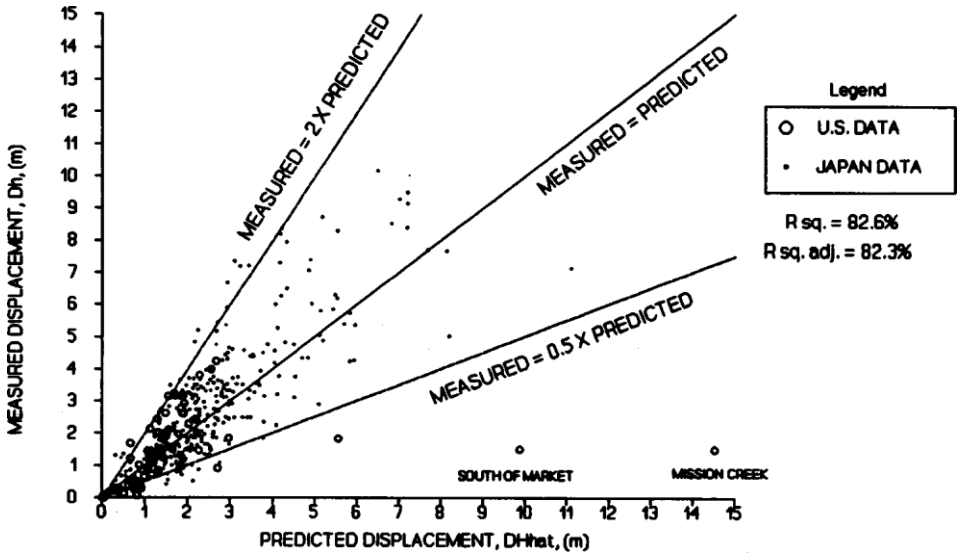

Figure 2.19. Predicted and measured displacement (Bartlett and Youd 1992)

Youd et al. (2002) compiled newer data and revised the formula of Bartlett and Youd (1992). The slope effects were also considered. The data was shown in Figure 2.19. Coefficients stated in Table 2.1 are changed to, as stated in the formulas below.

For the free face condition:

$$\text{Log } D_H = -16.713 + 1.532M - 1.406 \log R^* - 0.012R + 0.592 \log W + 0.540 \log T_{15} + 3.413 \log (100-F_{15}) - 0.795 \log (D50_{15} + 0.1 \text{ mm})$$

For the gently sloping ground:

$$\text{Log } D_H = -16.213 + 1.532M - 1.406 \log R^* - 0.012R + 0.338 \log S + 0.540 \log T_{15} + 3.413 \log (100-F_{15}) - 0.795 \log (D50_{15} + 0.1 \text{ mm})$$

They expressed that the displacement below 6m from the ground can be conservative. Also, for magnitudes greater than 8, this method gives unreliable results. (Youd et al., 2002)

Caltrans (2013) says that Idriss and Boulanger (2008) method for the estimation of the maximum shear strain of liquefying sands can be used. They incorporate with the potential strain index of Wu (2003) which is given in Figure 2.20.

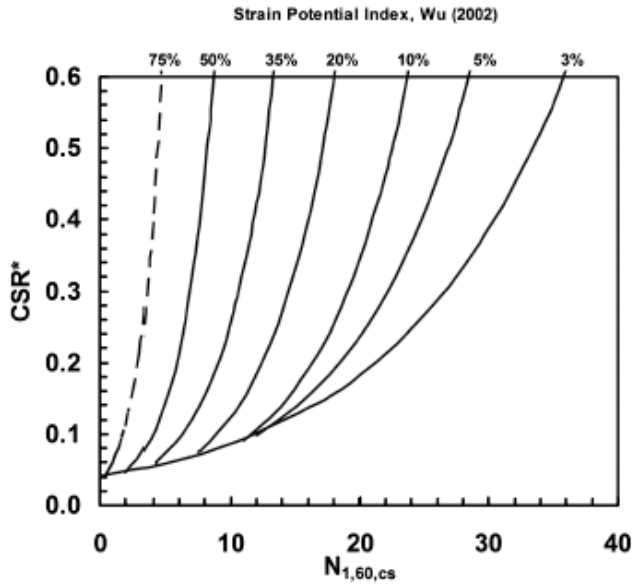

Figure 2.20. Chart of strain potential index (Caltrans, 2013)

Idriss and Boulanger (2008) evaluated and configured Wu's studies in many cases. The estimation of the γ_{max} (Strain Potential Index) was given in Figure 2.21. The formula contains fine content corrected SPT-N value, $N_{1,60,cs}$ and magnitude of earthquake corrected CSR.

$$\gamma_{max} = \begin{cases} 0 & CSR \leq 0.04 \\ \left(\frac{CSR-0.04}{l_1-0.04}\right)0.01 & N_{1,60,cs} \leq 15 \; AND \; 0.04 \leq CSR \leq l_1 \\ 0.01 + \left(\frac{CSR-l_1}{l_2-l_1}\right)0.02 & N_{1,60,cs} \leq 17.5 \; AND \; l_1 \leq CSR \leq l_2 \\ 1.859\left(1.1-\sqrt{\frac{N_{1,60,cs}+\Delta n}{46}}\right)^3 \geq 0 & N_{1,60,cs} > 17.5 \; OR \; CSR > l_2 \end{cases}$$

Figure 2.21. Estimation of γ_{max} by (Idriss and Boulanger, 2008)

l_1 and l_2 in the formula above were introduced for the accuracy of the γ_{max} in the low CSR values. According to the Caltrans (2013), these steps for estimation of the γ_{max} is reasonably accurate and simple.

Cetin et al. (2002) compared the shear strain formulations composed Hamada et al. (1987), Youd et al (2002) and Shamoto et al. (1998) for different 4 sites in Kocaeli earthquake. In Table 2.2, observed and computed results were shown. It was useful to see comparisons of the shear strains with real data.

Table 2.2. *Observed vs. calculated lateral spread displacements according three methods (Cetin et al. 2002)*

		Lateral ground spread (cm)			
Site	Borehole number	Observed	Shamoto et al. (1998)	Hamada et al. (1986)	Youd et al. (2002)
Police station	PS2	240	72	310	300
	PS3	10	10	120	180
	PS4	90	4	98	60
Soccer field	SF5	30	12	0	74
	SF6	120	49	0	240
Degirmendere nose	DN1	90	97	440	120
	DN2	0	3	440	0
Yalova harbor	YH1	20	20	0	79
	YH2	15	18	0	57
	YH3	5	20	0	61

They have concluded that strains offered by Shamoto and Hamada underpredict the lateral spreading displacement and strains offered by Youd overpredicts in some cases. The observed and calculated values can be seen in Table 2.2.

CHAPTER 3

ANALYSIS MODELS AND METHODS

The structure that was analyzed for the consequences of liquefaction is a precast balanced cantilever bridge with a piled foundation. Liquefaction induced lateral spreading causes a lot of damages to bridge structures in the past, as told in Chapter 1. There are many different approaches for analyzing lateral spreading effects on bridges. However, the results of these approaches are different from each other. Therefore, this study was performed to show the differences between these approaches.

The effects of lateral spreading are divided into two groups, which are inertial effects and kinematic effects. Inertial effects are due to earthquake excitation. Soil parameters change because of liquefaction. Kinematic effects are due to the movement of the soil due to liquefaction. For analyzing these two effects, some approaches should be granted, according to AASHTO (2017). For inertial analysis of a bridge, two configurations should be used as in AASHTO (2017). These are "Non-liquefied Configuration" and "Liquefied Configuration". As AASHTO (2017) says, if there are permanent liquefaction induced lateral ground displacements, it should be separated from the inertial evaluation. For the kinematic analysis of this bridge, two different methods can be employed, and the proper approach should be selected for design purposes. The evaluation of the bridge against liquefaction should include the potential of simultaneous occurrence of inertial and kinematic response of the bridge.

The analysis schema of liquefaction induced lateral spreading conducted in this study is shown in Figure 3.1. In this configuration, it is simply stated that the liquefaction induced lateral spreading analysis should include two analyses separately, which are inertial and kinematic analysis. These analysis types have different approaches. In

inertial analysis, the bridge should be analyzed for liquefaction and no-liquefaction scenario separately. In kinematic analysis, there are two methods that can be employed. In those analyses, bridge column parameters were changed in whether they cracked or not. For this purpose, the values of cracked modulus of elasticity of bridge columns were changed to half of the uncracked modulus of elasticity, according to AASHTO (2017).

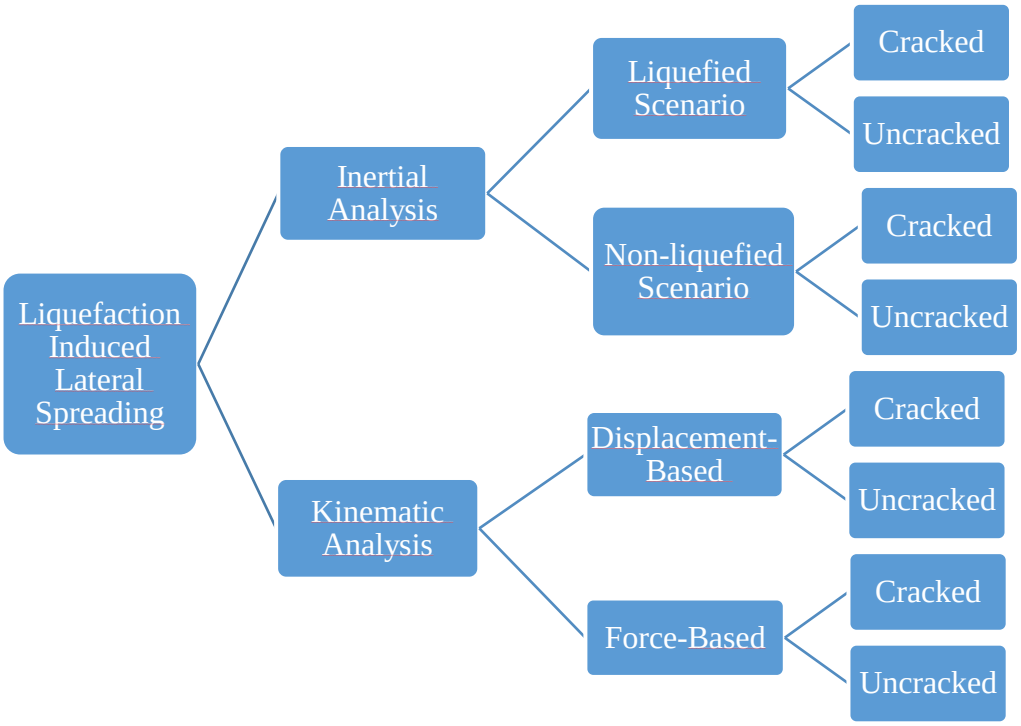

Figure 3.1. Configuration of the analysis of liquefaction induced lateral spreading

The more generalized flowchart for the liquefaction induced lateral spread analysis were shown in the Figure 3.1. The steps in those analysis were concluded in that flowchart. It is a general flowchart that was used in this study.

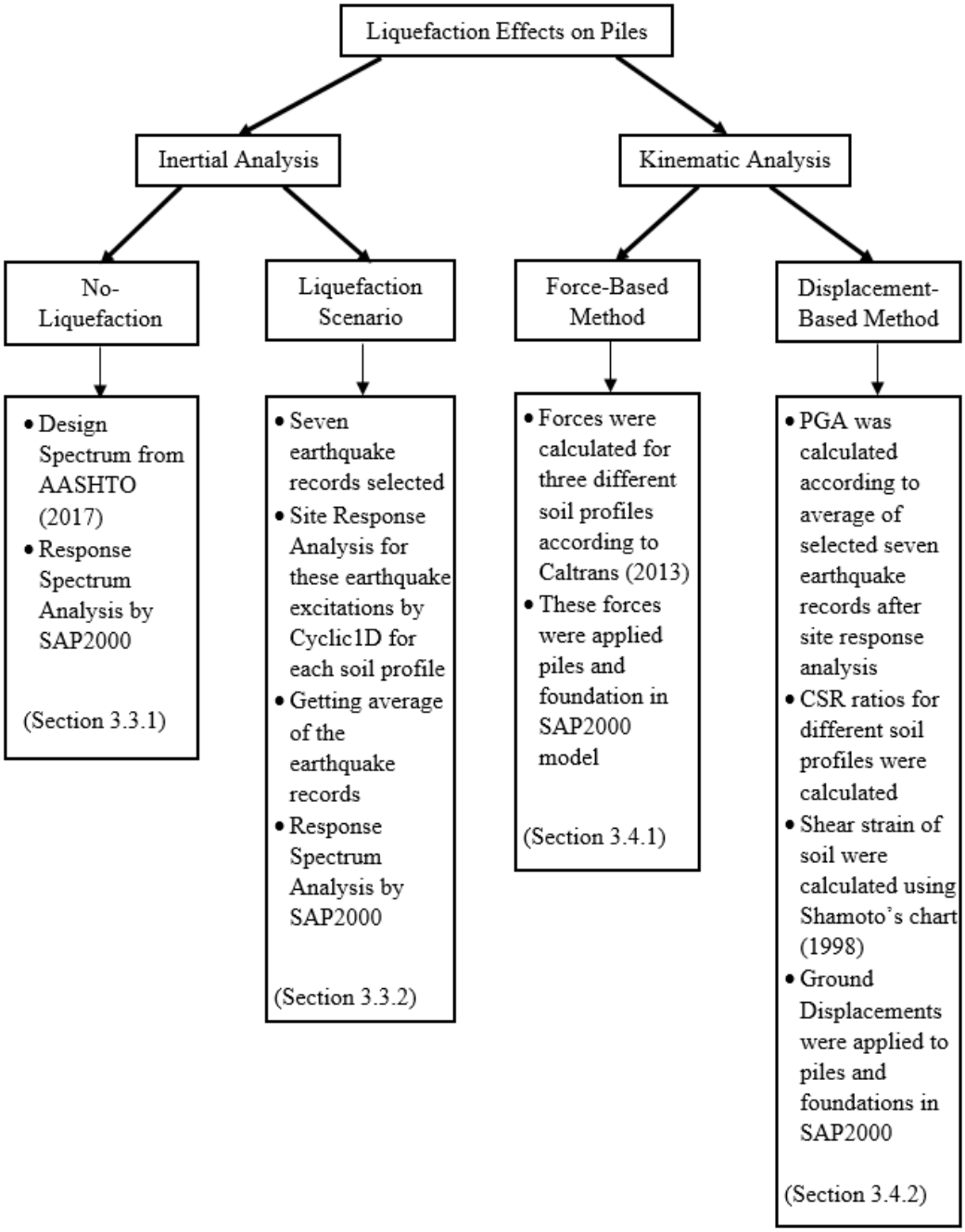

Figure 3.2. Flowchart for the analyses that were conducted in this study

3.1. Assumptions and Simplifications in Methods

In this study, some parameters are estimated for the sake of simplicity.

- All piles have the same length. The calculation of the lengths of the pile was based on the bearing capacity against the dead load of the bridge. The thicknesses of the first two layers were changed, since the damage created by lateral spreading is dependent on those layers thicknesses.
- The soil was considered as it only moves translationally in x and y directions. Piles were restrained in translation-Z direction.
- Generic soil profiles were used.
- Abutment effects were not considered and boundary conditions that are given by Theryo (2005) was used.
- Design of bearings and its effects to the period of the structure are not included.
- Fault's directivity and directionality effects and near-field fault effects were neglected.

These assumptions were given before the analysis model and methods to ease the understanding the context of this study. The necessary parts are mentioned in the relevant sections.

3.2. Precast Balanced Cantilever Bridge Parameters

The precast balanced cantilever bridge was taken from the design example prepared for American Segmental Bridge Institute (ASBI) by Theryo (2005). The dimensions are gathered from this example for simple design concerns. The bridge consists up of five spans total length of 270 meters involving two 45 meters long exterior span and three 60 meters long interior span. The deck width is 12.9 meters. The superstructure of bridge is Type 2700-2 AASHTO-PCI-ASBI Standard section with a height of 2700mm. Span to depth ratio is 22. The bridge is fixed at Pier 3 and the other piers and abutment have an expansion bearing in x-direction. Piers are restrained to superstructure in y and z directions. The boundary conditions and the span

arrangements are shown in Figure 3.3. Those bearings are free to move in longitudinal (x-direction) of the bridge which can be seen in Figure 3.2. In this study Pier 2, 3, 4, and 5 shown in Figure 3.3 was renamed as Pier 1 (P1), Pier 2 (P2), Pier 3 (P3), and Pier 4 (P4) respectively. The lengths of spans can be seen in Figure 3.5.

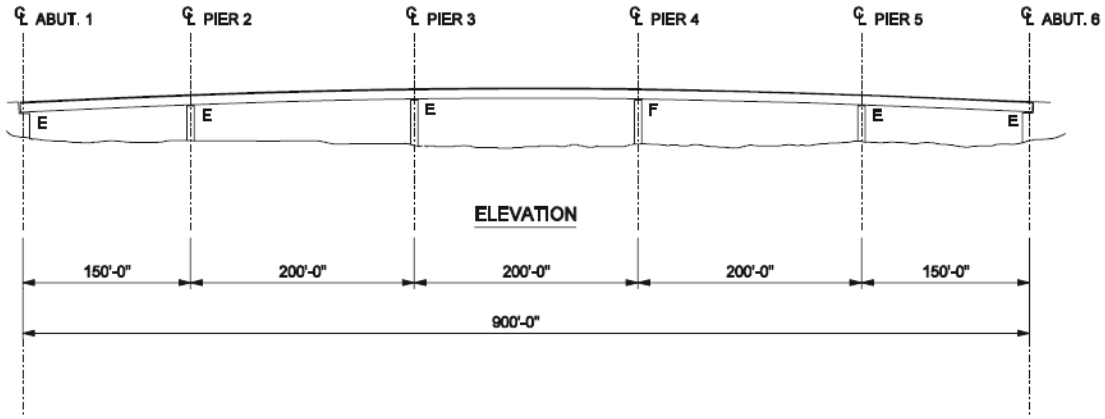

Figure 3.3. Elevation view and boundary conditions of precast balanced cantilever bridge (Theryo, 2005)

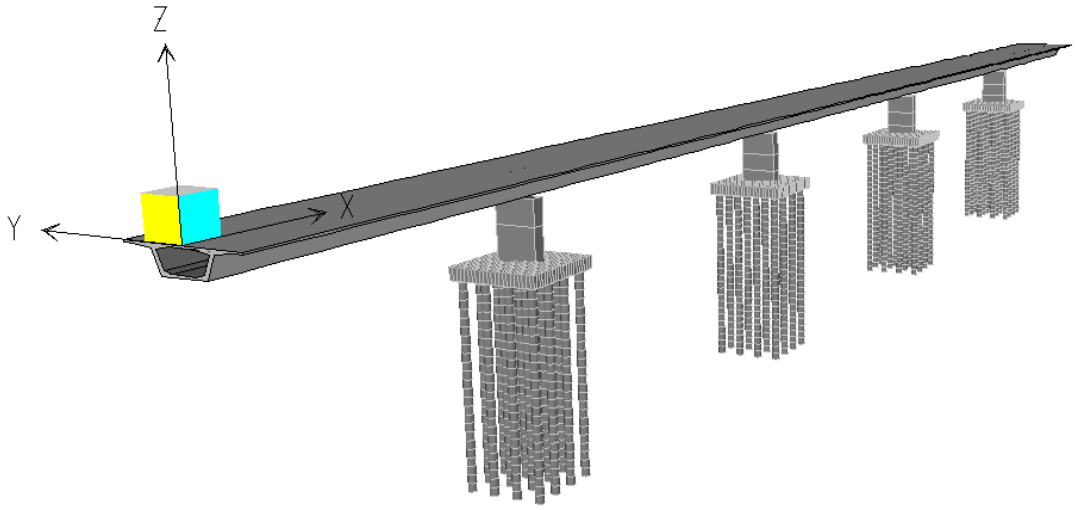

Figure 3.4. Analysis model and direction of global axes

It should be noted that the "X" direction of global axes is the longitudinal direction of the bridge. "Y" direction of the global axes is the transverse direction of the bridge as shown in the Figure 3.4.

This bridge has composed of concrete and structural steel reinforcement. Precast Box section girder consists of C50/60 class concrete. 50 and 60 are the cylindrical and cubic strength of the concrete in MPa, respectively. Piers, foundations, and piles are made of C30/37 class concrete.

The unit weight of concrete, γ_c, was taken as 23.5 kN/m^3 as stated in Theryo (2005). Unit weight of the superstructure, post-tensioned concrete was taken as 24.3 kN/m^3 and wearing surface load, 0.72 kN/m^2 was uniformly distributed along the bridge. The modulus of concrete is calculated by;

$$E_c=4800\sqrt{f'c} \qquad (3\text{-}1)$$

Hence, the modulus of elasticity of C30/37 and C50/60 concrete is 26.29 GPa and 33.94 GPa, respectively, from eq. 3-1. Dimensions of columns of the bridge are typical and length of 1.65m and width of 4.98m. All column heights are 8 meters. Foundations thicknesses are equal to 1.5 meters. The length and width of the foundation are equal to 11 meters. The pile diameter is 1 meter. They were spaced as three diameters of pile, 3 meters. Sixteen piles support each foundation, which is 25 meters in height. All of the profiles, plan drawings of structural elements of precast balanced cantilever bridges are drawn in Figure 3.5.

Considering the possibility of cracking of the column, AASTO (2017) states that cracked section properties should be used in the analysis. For this purpose, the rigidity of the columns was lowered to its one half the uncracked moment of inertia. All the methods clarified in Section 3, are solved under two different moments of inertia in both axes, x, and y. One is the uncracked column section properties, and the other is cracked column section properties.

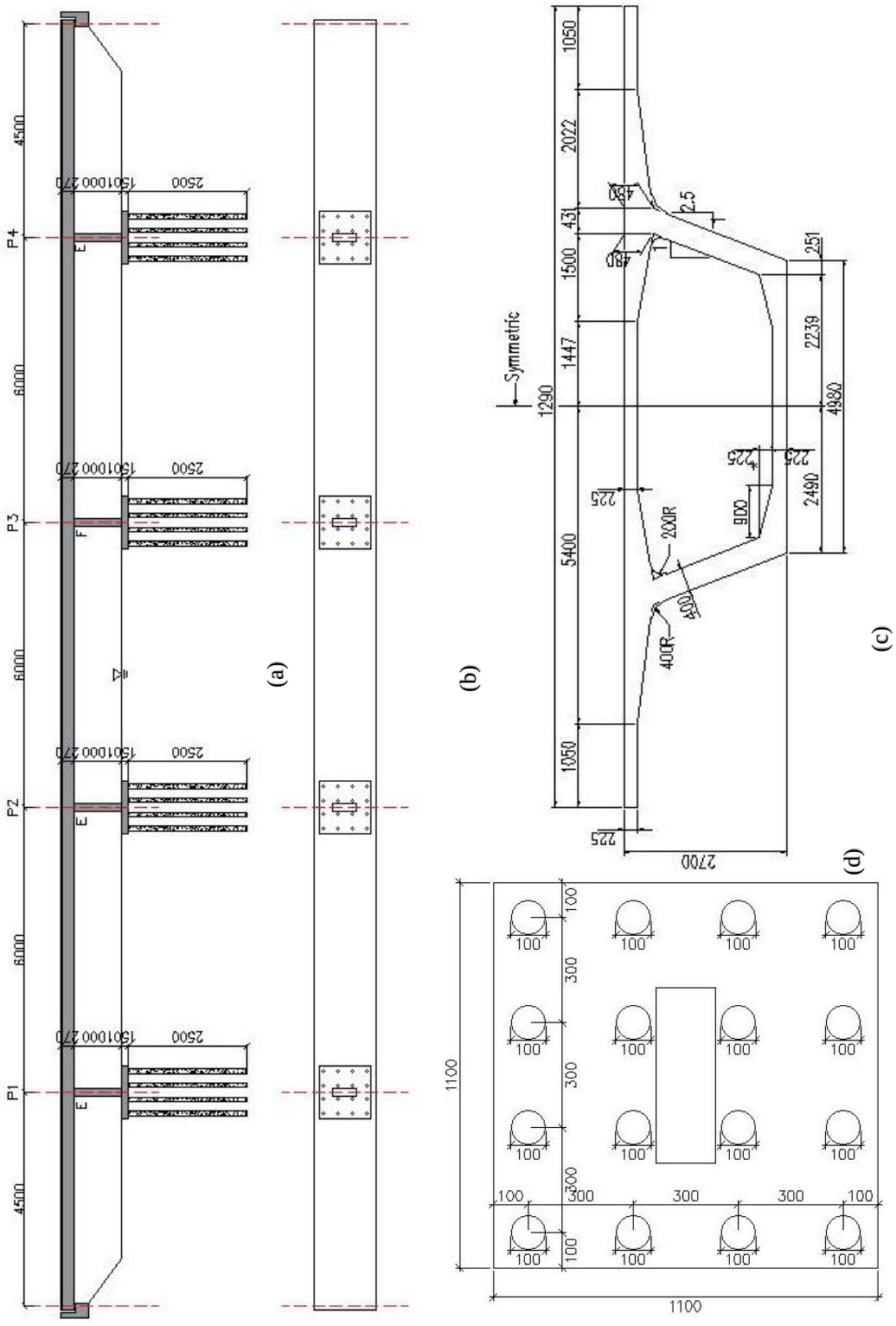

Figure 3.5. Profile (a), Plan view (b), Box section (c) and Plan view of foundation (d), in cm

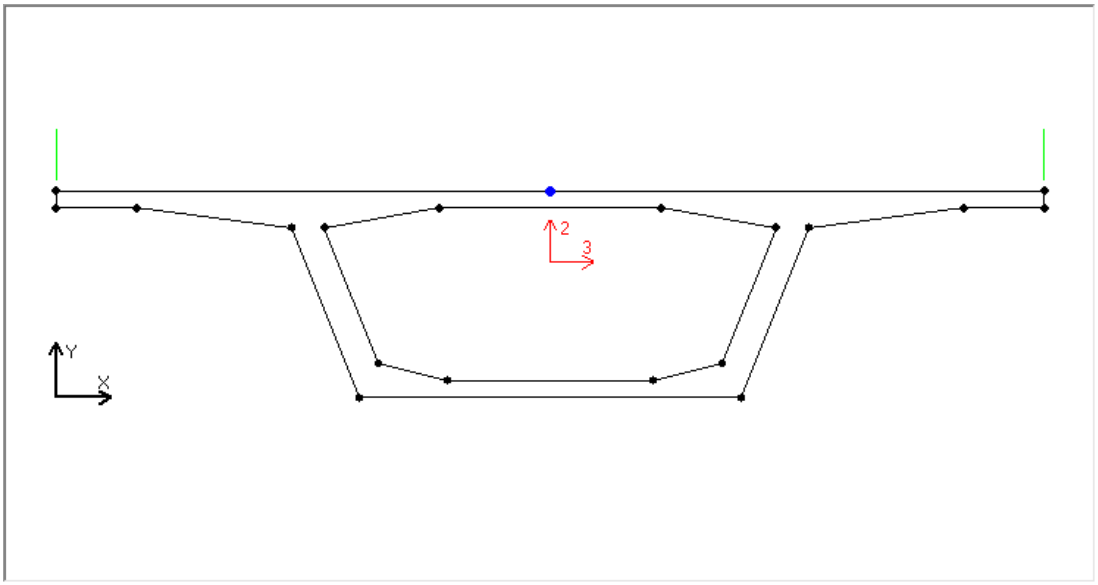

Figure 3.6. Cross section of superstructure of bridge

Section properties of the super structure were given below;

Area, A, is 7.06 m^2, St. Venant torsional inertia Mass Moment Inertia, J, equals 14.49 m^4, Moment of inertia, in weak direction (3) in Figure 3.6, I_{weak}, equals to 6.99 m^4, Moment of inertia, in strong direction (2) in Figure 3.3, I_{strong} , equals to 69.74 m^4, and the weight of the superstructure for 1 meter, w = 163.781 kN/m

3.3. Inertial Analyses

As stated previously, inertial analysis is the response of the structure against earthquake excitation. It does not include anything about the movement of the soil. It accounts only for the response of the structure against earthquakes. In inertial analysis, there are two scenarios given in the AASHTO (2017). The first scenario is based on the case of no liquefaction. And the second scenario is based on the case of liquefaction in load bearing soils.

3.3.1. No-liquefaction Scenario

The bridge was analyzed, assuming no liquefaction in soils. In this scenario, the ground response spectrum appropriate for site conditions should be calculated. The

design spectrum was considered as in AASHTO (2017). The construction of the design spectrum is shown in Figure 3.7.

Response spectrum analysis was used for analyzing the inertial effects of liquefaction in this study. Modes and periods of the structure are very important for this analysis type since the earthquake load is dependent on the spectral acceleration, Sa.

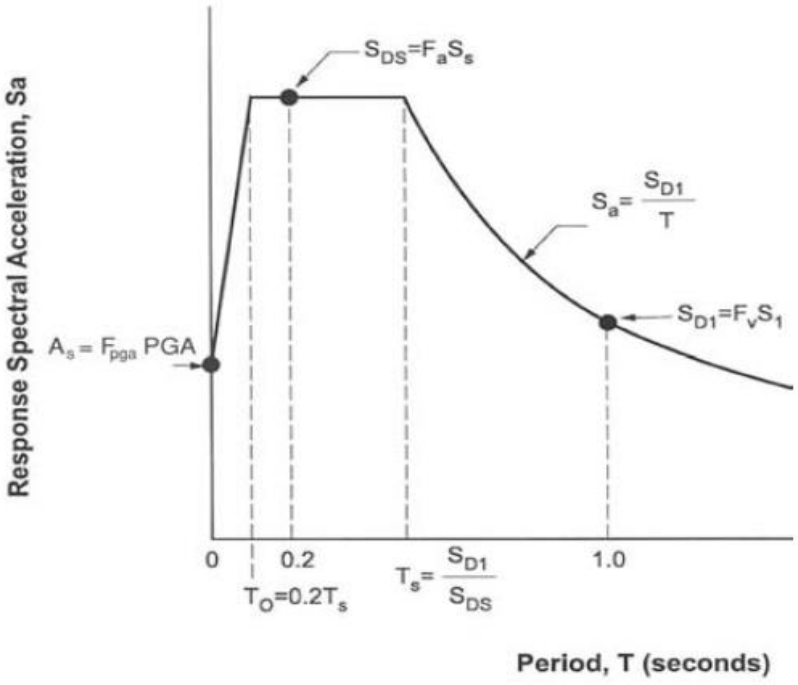

Figure 3.7. Design response spectrum (AASHTO, 2017)

The acceleration coefficient, A_s, the 0.2sec short period acceleration coefficient, S_{DS}, and the 1-sec period acceleration coefficient, S_{D1}, can be determined from Eqs. 3-2 through 3-4, respectively:

$$A_s = F_{pga}PGA \quad (3\text{-}2)$$

$$S_{DS} = F_aS_s \quad (3\text{-}3)$$

$$S_{D1} = F_vS_1 \quad (3\text{-}4)$$

F_{pga} is the site coefficient for peak ground acceleration (PGA) that is given in a table in AASHTO (2017). F_a and F_v is a site coefficient for 0.2-sec and 1.0 sec period spectral accelerations, respectively. S_s and S_1 are 0.2-sec and 1.0 sec period spectral acceleration coefficients on Class B rock, respectively.

The site class was selected from the Table 3.1. Selected values for constructing design spectrum is given in Table 3.1. Selected values can be seen in the Chapter 4, Calculations for Models section.

Table 3.1. *Soil class definitions (AASHTO, 2017)*

Site Class	Soil Type and Profile
A	Hard rock with measured shear wave velocity, $\bar{v}_s > 5000$ ft/sec
B	Rock with 2500 ft/sec $< \bar{v}_s < 5000$ ft/sec
C	Very dense soil and soil rock with 1200 ft/sec $< \bar{v}_s < 2500$ ft/sec, or with either $\bar{N} > 50$ blows/ft or $\bar{s}_u > 2.0$ ksf
D	Stiff soil with 600 ft/sec $< \bar{v}_s < 1200$ ft/sec, or with either 15 blows/ft $< \bar{N} < 50$ blows/ft or 1.0 ksf $< \bar{s}_u < 2.0$ ksf
E	Soil profile with $\bar{v}_s < 600$ ft/sec, or with either $\bar{N} < 15$ blows/ft or $\bar{s}_u < 1.0$ ksf, or any profile with more than 10 ft of soft clay defined as soil with $PI > 20$, $w > 40\%$, and $\bar{s}_u < 0.5$ ksf
F	Soils requiring site-specific ground motion response evaluations, such as: • Peats or highly organic clays ($H > 10$ ft of peat or highly organic clay, where H = thickness of soil) • Very high plasticity clays ($H > 25$ ft with $PI > 75$) • Very thick soft/medium stiff clays ($H > 120$ ft)

Table 3.2. *Coefficients tables of PGA, S_s, and S_1 (AASHTO, 2017)*

Site Class	Peak Ground Acceleration Coefficient (PGA)[1]				
	$PGA <$ 0.10	$PGA =$ 0.20	$PGA =$ 0.30	$PGA =$ 0.40	$PGA >$ 0.50
A	0.8	0.8	0.8	0.8	0.8
B	1.0	1.0	1.0	1.0	1.0
C	1.2	1.2	1.1	1.0	1.0
D	1.6	1.4	1.2	1.1	1.0
E	2.5	1.7	1.2	0.9	0.9
F[2]	*	*	*	*	*

Site Class	Spectral Acceleration Coefficient at Period 0.2 sec (S_S)[1]				
	$S_S <$ 0.25	$S_S =$ 0.50	$S_S =$ 0.75	$S_S =$ 1.00	$S_S >$ 1.25
A	0.8	0.8	0.8	0.8	0.8
B	1.0	1.0	1.0	1.0	1.0
C	1.2	1.2	1.1	1.0	1.0
D	1.6	1.4	1.2	1.1	1.0
E	2.5	1.7	1.2	0.9	0.9
F[2]	*	*	*	*	*

Site Class	Spectral Acceleration Coefficient at Period 1.0 sec (S_1)[1]				
	$S_1 <$ 0.1	$S_1 =$ 0.2	$S_1 =$ 0.3	$S_1 =$ 0.4	$S_1 >$ 0.5
A	0.8	0.8	0.8	0.8	0.8
B	1.0	1.0	1.0	1.0	1.0
C	1.7	1.6	1.5	1.4	1.3
D	2.4	2.0	1.8	1.6	1.5
E	3.5	3.2	2.8	2.4	2.4
F[2]	*	*	*	*	*

3.3.2. Liquefaction Scenario

The potential effects of liquefaction in soils and foundations shall be evaluated in the liquefaction scenario. In order to calculate the effects of liquefaction, one should investigate the effects of a site that is susceptible to liquefy to ground motions. Therefore, site response analysis for the bridge should be performed. Besides, for this site, ground motion record selection and scaling is an important issue.

Imbsen (2007) advised that the magnitude and the source to site distances of the selected earthquakes should be closer to each other, since, these are the characters having a strong influence on response spectral content. Also, he indicates that the time histories of the selected earthquakes should be matched with the design responses, and time histories should be scaled to match the design response spectrum. Besides, AASHTO (2009) says that the earthquakes should be similar in manner of type of faulting, seismic source to site distance, earthquake magnitudes, and seismic velocities.

Seismic Isolation Guideline (1999), prepared by AASHTO, has offered that three pairs of seven earthquakes that are consistent with their source characteristics and magnitudes. Horizontal components of the selected earthquakes should be joined, taking the square root of the sum of the squares (SRSS) of them. Their average amplitudes should be scaled to a value that responses a minimum of 1.3 times the 5% damped design spectrum in the range of 0.5T to 1.5T. T is the dominant modal period of the structure.

CEN (2005) offers to select seven pairs of independent horizontal components of ground motion. Spectral responses of the selected earthquake records should be matched with each other. The horizontal components should be converted into one component taking SRSS as in the Seismic Isolation Guideline. Scaling of the average of the ensemble response of the earthquakes should be done according to at least 1.3 times the amplitude of a 5% damped design spectrum interval of 0.2T – 1.5T.

AASHTO (2009) states that, in case of increasing pore pressure, site-specific ground motion analysis should be conducted with a minimum of seven records. The mean responses of the selected records can be used for the design. The site-specific response spectrum should not be lower than two/thirds of the design spectrum in the interval of 0.5T – 2T.

With the guidelines stated above, the methodology for this study was stated below. Seven earthquakes with transverse and longitudinal direction was selected. These records were selected as their site conditions and magnitudes to be closer to each other. Also, fault types were the strike-slip. Scaling is done between 0.2T and 1.5T, as in Eurocode-8. Also, the average spectrum of the selected seven earthquakes scaled up to minimum 1.3 times of the design spectrum that was calculated for non-liquefaction scenarios.

The site response analysis was performed by using the software Cyclic1D. It is a one-dimensional wave propagation software. The schematic analysis of Cyclic1D software is given in Figure 3.8.

The input motion was the earthquake accelerogram that was taken from the online PEER's database. This software calculates the output motion at the surface with the soil parameters defined by the user. The more detailed information about Cyclic1D analyses was presented in the Section 4.

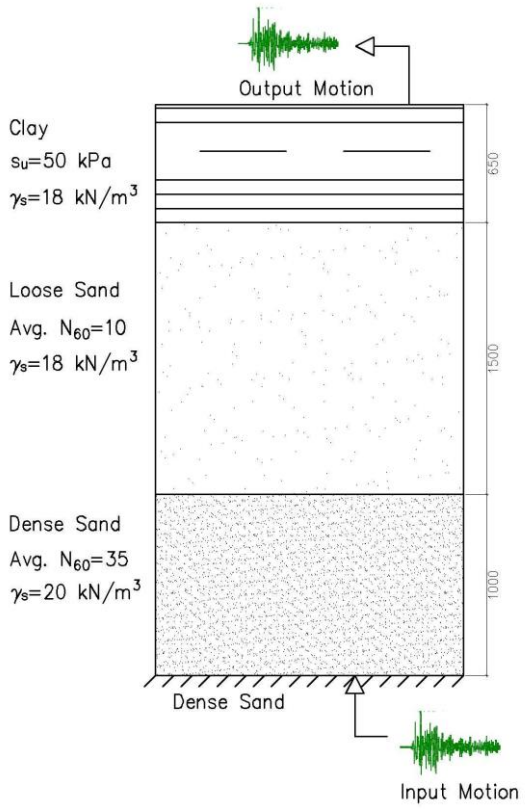

Figure 3.8. Schematic view of site response analysis

3.4. Kinematic Analyses

Kinematic analyses are only about the effect of lateral movement of the soil due to liquefaction. There are some methods for kinematic analyses. These methods were presented in Chapter 2 in detail. In these analyses, basically applied load types are different in this study. The first method for kinematic analysis is a force-based method in which liquefaction effects are applied to the bridge as force. The second one is the displacement-based on which liquefaction effects are applied to bridge as ground displacement.

3.4.1. Force-Based Method

The force-based method on the applied load was assigned to piles and foundation. The force was applied to foundation and piles. In this study, the forces due to liquefaction induced lateral spreading are calculated according to Caltrans (2013). The force-

method driven by the Caltrans (2013) based on the small and large scale shake table tests and field tests. This approach also is a framework for the lateral spreading analysis, which contains equivalent nonlinear static analysis.

The crust layer lays on the liquefiable soil zone in this approach. Moving off that zone under the effects of liquefaction triggers crust movement in the same direction with the liquefiable soil layer. Since the crust does not act like a liquid, it creates a large amount of forces to piles and foundation. Only forces driven by the crust were considered in this approach. The schematic analysis model for Caltrans (2013) was shown in Figure 3.9. F_{ult} is the ultimate load due to crust moving because of liquefaction. The calculation of F_{ult} was presented in the Chapter 4. It is acting on foundations and piles on liquefiable soil.

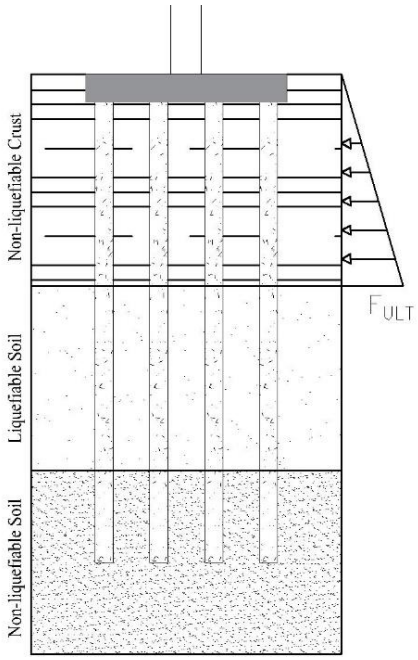

Figure 3.9. Force-Based model configuration

3.4.2. Displacement-Based Method

The displacement-based method is based on the applied loading type, displacement. The ground displacement was applied to piles and foundations with the help of multilinear links. These links have the soil-pile interaction with p-y curves. These p-y

curves were given in the Chapter 4. The ground displacements were applied to these links to displace the piles in a governing forces gathered from the p-y (force-displacement) curves as shown in the Figure 3.10.

The displacements are applied from ground to bottom of the liquefiable soil layer in displacement-based method. The CSR values were used to estimate the displacements. Since the soil moves at same extent in every its depth, they have the same displacement in every depth in non-liquefiable crust.

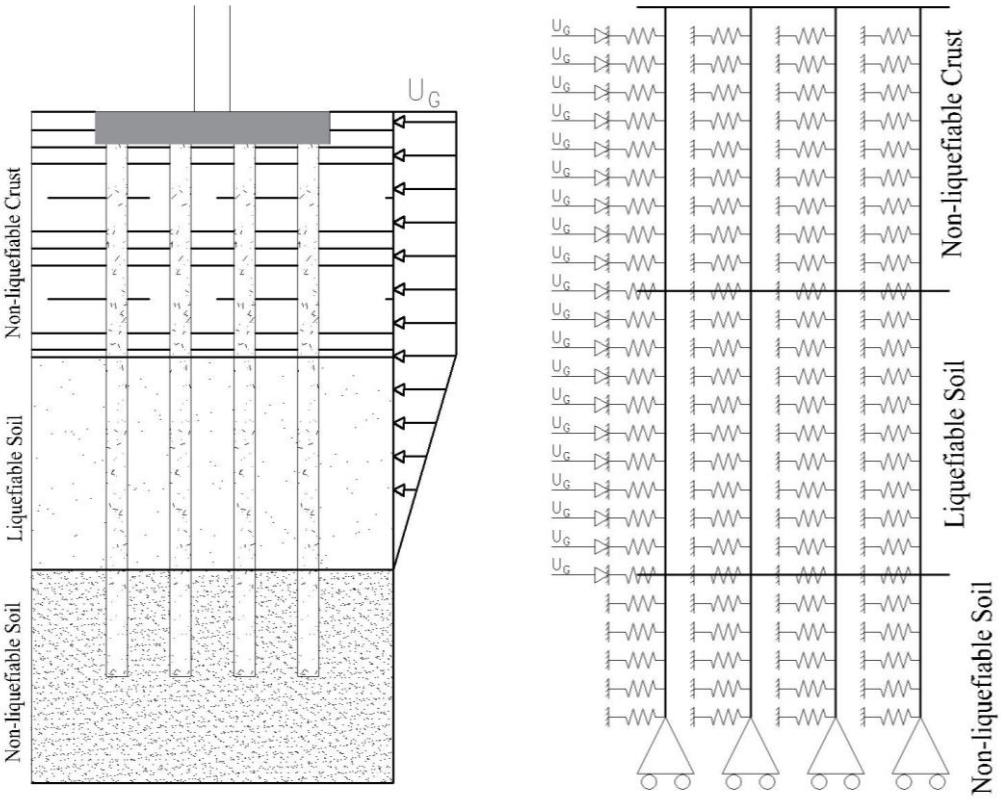

Figure 3.10. Displacement based model configuration and analytical model

At every different soil depth, U_G was changed and these displacements are assigned to fixed restrains that are linked to pile in every 1 meter depth. To be able to find the displacements, soil strain proposed by Shamoto et al. (1998) was used. To see the dramatic effect of strain, method of Shamoto et al. (1998) which underestimates the strain values according to Cetin et al (2002) was used for estimating the shear strain

soil in this study. In Shamoto's findings, to find the soil shear displacements $N_{1,60,cs}$ and CSR values should be found according to Fig 3.12.

In order to find the ground displacements for each earthquake, CSR values of these earthquakes was found. Spectral accelerations of critical earthquake spectrum, average spectrum and design spectrum were used for finding CSR values. For the every response, PGA values were gathered from the liquefaction affected response spectra for each soil profile. After finding the PGA values, CSR values were found according to eq. 2-2.

Shear strains of the soils was found according to Figure 3.11. But before getting the maximum shear strain $(\gamma_r)_{max}$, SPT-N values should be corrected with fine content correction factor given in Table 3.3.

Table 3.3. *Correlation factor calculation for SPT-Na value (Tokimatsu and Yoshimi, 1983)*

Fines content	ΔN_f
0-5	0
5-10	Interpolate
10-	0.1*FC+4

In order to get CSR values, fine content correction should be employed. For this purpose fine content correction is used. Tokimatsu and Yoshimi (1983) developed fine content (FC) correction for liquefiable soils from the test results. In this study this approach was used.

The calculations were made according to these steps. The values used in the analysis were given in the Section 4. Also, it was stated that how to apply these displacements and forces to models.

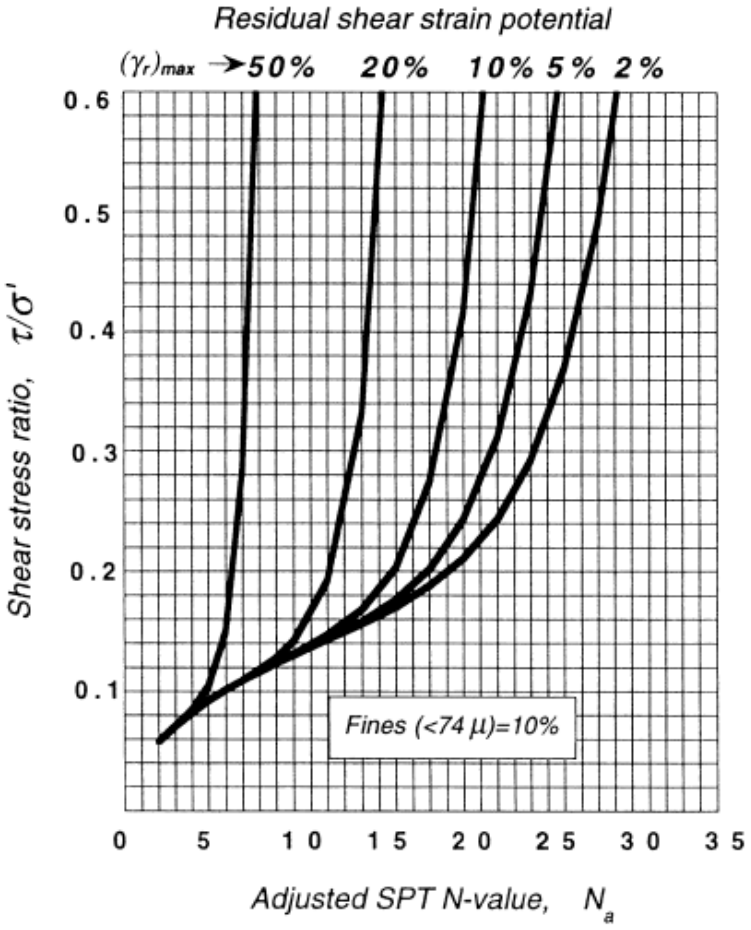

Figure 3.11. Residual shear strain potential by Shamoto et al (1998)

CHAPTER 4

CALCULATIONS FOR MODELS

4.1. Soil Profiles

The generic soil profile consists of 3 layers from top to bottom. The first layer is non-liquefiable layer which is medium clay, second is liquefiable loose sand, and if lays on dense sand layer. Layer thicknesses are changing in each model. All these soil profiles are evaluated in Table 4.1, with their type, classification according to Unified Soil Classification System, thicknesses, design parameters, and weights.

The 1st type of soil is 5m thick medium stiff clay, 15m loose sand, and 10m dense sand. It is abbreviated as SP1 and z1. The 2nd type of soil is 15m thick medium stiff clay, 5m thick loose sand, and 10m thick dense sand. It is abbreviated as SP2 or z2. The 3rd type of soil profile is 10m thick medium stiff clay, 10m thick, loose sand, and 10m thick, dense sand. It is abbreviated as SP3 or z3. These profiles are concluded in Table 4.1 and shown in Figure 4.1. s_u is the undrained shear strength in terms of kPa and the N_{60} is the energy correlated SPT-N value.

Table 4.1. *Soil profiles*

		Thicknesses (m)				
Soil Type	**USCS**	**SP1**	**SP2**	**SP3**	**Parameter**	**Unit Weight (kN/m^3)**
Clay	CH	5	15	10	s_u=50 kPa	18
Loose Sand	SP	15	5	10	N_{60}=10	18
Dense Sand	SW	10	10	10	N_{60}=35	18

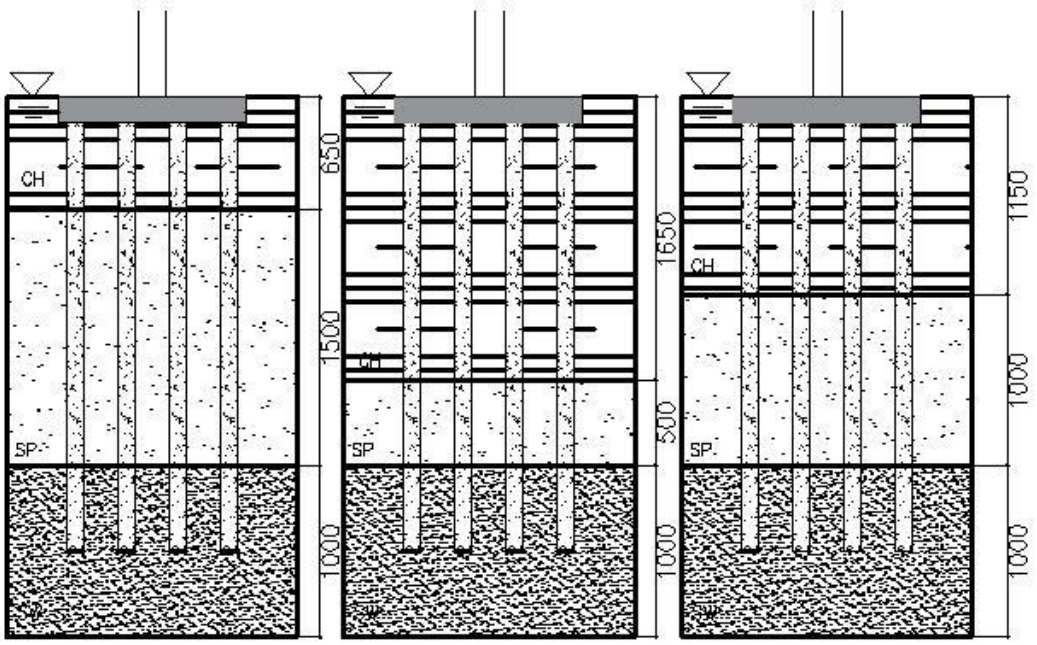

Figure 4.1. Sketch of the soil profiles SP1 (a), SP2 (b), SP3 (c)

The reason for difference between the thicknesses of the first 2 level was to see the effect of the moving crust thickness because of the movement of loose sand after liquefaction. Also, it should be noted that the groundwater table (GWT) is on the surface.

4.1.1. Determination of Friction Angle of Sands

The friction angle of the sands should be gathered for bearing capacity of piles and site response analysis. Four different methods are selected for finding proper friction angle,ϕ, of soils. These methods are Schmertmann's chart (1975), Lambe and Whitman table (1969), and Hatanaka and Uchida's equation (1996).

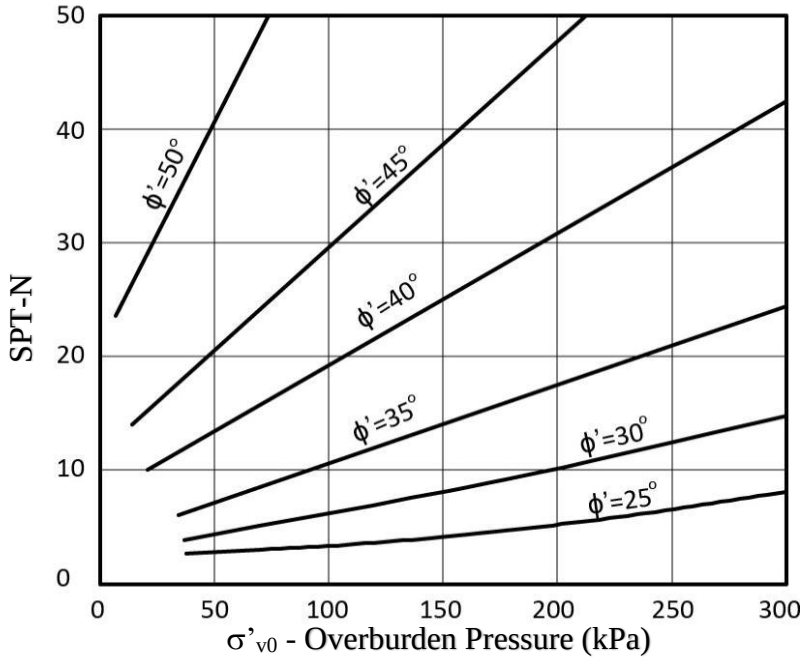

Figure 4.2. Determination of friction angle (Schmertmann, 1975)

Schmertmann's Table given in Figure 4.2. was used for determining the angle of friction of sands. Lambe and Whitman (1969) had also studied friction angles of sands and they gave range for the type of sand. These values were shown in Table 4.2. Hatanaka and Uchida (1996) had produced an empirical relation for sandy soil that was given in eq 4-1.

$$\phi = 20° + \sqrt[2]{15.4(N1)_{60}} \qquad 4\text{-}1$$

Soil parameters are decided with four different correlations are listed in Table 4.2;

Table 4.2. *Friction angle of the sands with different approaches*

Soil Type	**Schmertmann (1975)**	**Lambe Whitman (1969)**	**Hatanaka Uchida (1996)**
Loose Sand	36°	28°-30°	32.41°
Dense Sand	39°	36°-41°	43.22°

Soil parameters were selected for soil layers were shown below;

1. Layer (Medium Stiff Clay), Undrained Shear Strength of Clay soil, Cu=50 kPa
2. Layer (Loose Sand), SPT-N = 10, Internal Friction Angle, ϕ=32°
3. Layer(Dense Sand), SPT-N = 35, Internal Friction Angle, ϕ=40°

4.1.2. Bearing Capacity of Piles

The bearing capacities of piles were calculated by static formula given in eq. 4-2.

$$Q_{all} = \frac{Q_{ult}}{FS} = \frac{Q_s + Q_p}{FS} \tag{4-2}$$

Q_s is the skin friction (shaft resistance), Q_p is Resistance at the tip of the pile, Q_{ult} is ultimate pile capacity, Q_{all} is the allowable pile capacity, FS is the factor of safety. The length of the pile was calculated as 25m. Corresponding forces in dead load of the structure was given in Table 4.3. These values are calculated by SAP2000 bridge model under only dead load condition.

Table 4.3. *Maximum pile force*

P (kN)	Vx (kN)	Vy (kN)	Mxx (kN.m)	Myy (kN.m)
1460	106	106	235	235

The safe bearing capacity of a pile in foundation was calculated as 3167 kN from the eq. 4-2. It was near doubled the necessary static bearing capacity, which is 1460 kN, given in Table 4.3. The bearing calculations were done according to the liquefied case, and only dense sand was involved in calculation. The factor of safety, FS, is taken as 2.5. (Eurocode-8, 2005). Calculations were shown in APPENDIX A.

4.1.3. Shear Wave Velocity of the Layers

Shear wave velocities are required for determining the soil class to gather the design spectrum. Shear wave velocities are estimated according to SPT values of the soils given above. The approaches are listed in Table 4.4.

Table 4.4. *Shear wave velocities of layers of given soil profile, Marto et al. (2013)*

Author	**Imai and Yoshimura (1990)**	**Sisman (1995)**	**Iyisan (1996)**	**Anbazhagan et al. (2012)**
Formula	**$Vs = 76N^{0.33}$**	**$Vs = 32.8N^{0.51}$**	**$Vs = 51.5N^{0.516}$**	**$Vs = 68.96N^{0.51}$**
Layer 1	162 m/s	106 m/s	169 m/s	223 m/s
Layer 2	162 m/s	106 m/s	169 m/s	223 m/s
Layer 3	246 m/s	201 m/s	323 m/s	423 m/s

Shear wave velocities were selected as taking average of four approaches listed in Table 4.4;

V_s (Layer 1) = 165 m/s, V_s (Layer 2) = 165 m/s, V_s(Layer 3) = 300 m/s

To be able to determine the soil class specified in AASHTO (2017) average shear wave velocity should be found. It is indicated that the evaluation should be done for the top 30m ground level as stated in eq. 4-3.

$$(V_S)_{30} = \frac{30}{\sum_{i=1}^{N}\left(\frac{h_i}{V_{S,i}}\right)} \tag{4-3}$$

$V_{S,i}$ is the shear wave velocity of each layer, and h_i is the height of the corresponding layer. Average seismic velocity for 30 thickness, $(V_s)_{30}$ value equals to 210 m/s for all the soil profiles. The soil class according to AASHTO (2009) is D. The soil type classification table was given in Chapter 3.

4.2. Ground Motion Record Selection and Scaling of Response Spectra

Ground motion record selection in analysis problems is a vital issue since liquefaction behavior can be altered by selected earthquake characteristics. Selected earthquake records for this study are gathered from PEER's NGA-WEST2 Database, which can be accessible online (ngawest2.berkeley.edu). Guidelines that were represented in subsection 3.3.2, seven different earthquake records were selected which are listed in Table 4.5.

Table 4.5. *Selected Earthquake Records from PEER database*

Earthquake Name	Station	Magnitude	Rjb (km)	Rrup (km)	Vs30 (m/s)	Fault Mechanism
Darfield (2010)	ROLC	7	0	1.54	295.74	SS
Duzce (1999)	Duzce	7.14	0	6.58	281.86	SS
Imperial Valley (1979)	Aeropuerto Mexicali	6.53	0	0.34	259.86	SS
Kobe (1995)	Takarazuka	6.9	0	0.27	312	SS
Kocaeli (1999)	Yarimca	7.51	1.38	4.83	297	SS
Parkfield (2004)	Parkfield - Fault Zone 1	6	0.02	2.51	178.27	SS
Tottori (2000)	TTRH02	6.61	0.83	0.97	310.21	SS

Rjb is the shortest distance to surface projection and it is also known as Joyner-Boore distance (PEER, 2010). Rrup is the shortest distance to the rupture plane. Magnitudes, distances to fault and fault mechanism was selected to be closer to each other as possible as.

These earthquake records are gathered from the PEER NGA-WEST2 database. For non-liquefied spectra, bi-directional earthquake records are converted into single accelerograms for 3D analysis. They are converted to elastic response spectra which has %5 damping with the help of SeismoSignal which uses Newmark integration.

Newmark Integration can solve second-order differential equations without transforming first-order differential equations. This method is widely used in the dynamic response of the systems according to George Lindfield and John Penny (2012).

To be able to scale the earthquakes, response spectra of the earthquake records listed in Table 4.5 should be gathered. The response spectrum of earthquakes is used in analysis and design of the structures subjected to motion. They are the simulation of simple oscillator subjected to ground acceleration concerning natural period and damping.

PGA is selected as 0.7g for gathering a strong earthquake design spectrum. Soil class was defined as "D" as indicated in the soil class definition table given in Chapter 3. S_S and S_1 values was found in a place having 0.7g and located in North-Anatolian Fault from AFAD's acceleration databases for Turkey. The longitude and latitude values for this place were 38.65, 40.05, respectively. The snapshot of the place that was used was shown in APPENDIX B.

The average shear wave velocity along 30 meters depth of soil profile was 210 m/sec (~700ft/sec), therefore site class was selected as D. According to the site class, F_{pga} F_a, and F_v coefficients were selected according to that site class from AASHTO. These tables were given in Chapter 3. According to figures 4.6 through 4.8 and the equations 3.3-1 through 3.3-3 selected and calculated parameter for design spectrum were given in Table 4.6

Table 4.6. *Values of design spectrum parameters*

SS	1.699
S1	0.480
Soil Class	D
SDS	1.70
SD1	0.72
TO (s)	0.08
TS (s)	0.42

Fa	1
Fv	1.5
TL (s)	6
PGA	0.700

The %5 damped design spectrum for 0.7g PGA earthquake was gathered from the steps above are shown in Figure 4.3. The design spectrum was shown in Figure 4.3. CSR values was calculated as stated in Chapter 2. The CSR calculations were done for the ground level (z=0m), therefore depth reduction factor, r_d, was calculated as one in CSR formula given in eq. 2.1-2. The formula became a simple correlation between PGA and CSR. The ratio between PGA and CSR equals to 0.65 as stated in Seed et al. (1975).

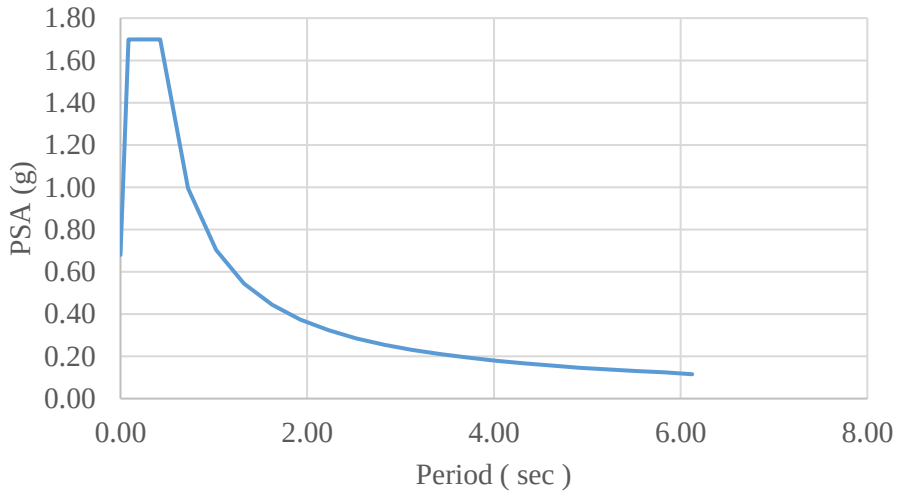

Figure 4.3. Design spectrum according to AASHTO (2017) for D soil class

Response spectra of the earthquakes given in Table 4.3. were calculated via SeismoSignal software from accelerograms that are gathered from PEER NGA2 Database. Design spectrum according to AASHTO (2017) and the maximum spectrum that governs for the period of the structure. These spectra are shown in Figure 4.4.

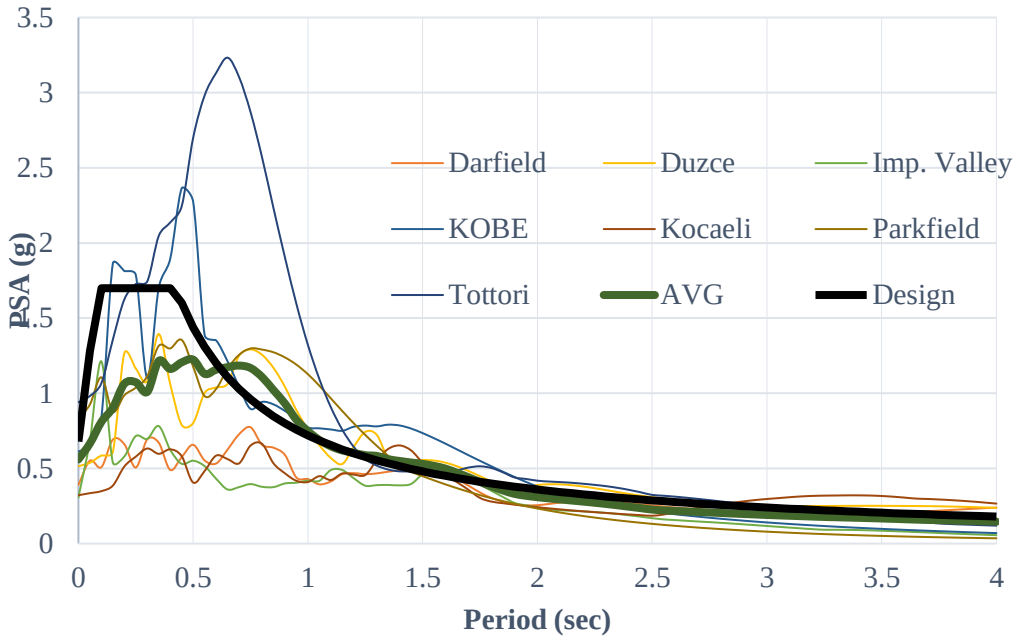

Figure 4.4. 5% Damped response spectra of earthquake records

Scaling of earthquake spectra is done with the 0.2T – 1.5T interval. The fundamental period of structures will be shown in Table 3.6. Lower bound of the scaling 0.2T is multiplied by 1.112 which is the minimum of the periods given in Table 4.7. 1.5T is based on 1.42s which is the maximum period given in Table 4.7. These periods were calculated using SAP2000 software.

Table 4.7. *Fundamental periods of structure in different soil profiles with no-liquefaction configuration*

	No-Liquefaction Scenario			Liquefaction Scenario		
		X	Y		X	Y
Uncracked	SP1	1.112	0.641	SP1	1.168	0.669
	SP2	1.150	0.662	SP2	1.168	0.669
	SP3	1.149	0.662	SP3	1.164	0.667
Cracked	SP1	1.360	0.652	SP1	1.420	0.680
	SP2	1.406	0.674	SP2	1.420	0.680
	SP3	1.405	0.673	SP3	1.417	0.679

The differences between these period values were discussed later on Chapter 6. To be able to perform scaling such periods, one period was selected from the Table 4.7. The minimum fundamental period of the structure was accepted as 1.112 sec. The maximum fundamental period of the structure is 1.42 sec. The scaling will be based on those periods. As in the Eurocode-8, the average spectrum will be scaled according the interval of 0.2T – 1.5T and it will not fall below 1.3 times of design spectrum. The scaling will be done between 0.23 sec and 2.13 sec of the spectrum given in Figure 4.4.

Non-linear p-y curves were used for soil-pile interaction. For the modal analysis, initial stiffness of p-y curves is used. For every node of the piles, these effective stiffness values are linked to joints. Within these effective stiffness values, the fundamental period of the structure is changing for 3 different soil types. Also, p-y curves of the given periods belong to the soil profile without non-liquefiable sand configuration.

The average spectrum of the earthquakes is scaled up to 2.1 so that the average spectrum does not fall below 1.3 times of design spectrum. However, this scale factor were not used in the further analysis. The reason for not using it, if the scale factor was necessary, the forces gathered from that average spectra could be multiply with that scale factor.

The scaled spectra were shown in the Figure 4.5 and Figure 4.6. As AASHTO (2009) implies that the scaled of the ground motions should be lower than the two thirds of the design spectrum. The scaled period range is between 0.5T and 1.5T, which are 0.575 sec and 2.13 sec. In this configuration, scale factor was found as 1.15. In this case, AASHTO created the lower bound and Eurocode-8 created the upper bound. The scaled spectra can be seen in Figure 4.5 and 4.6, for Eurocode-8 and AASHTO respectively.

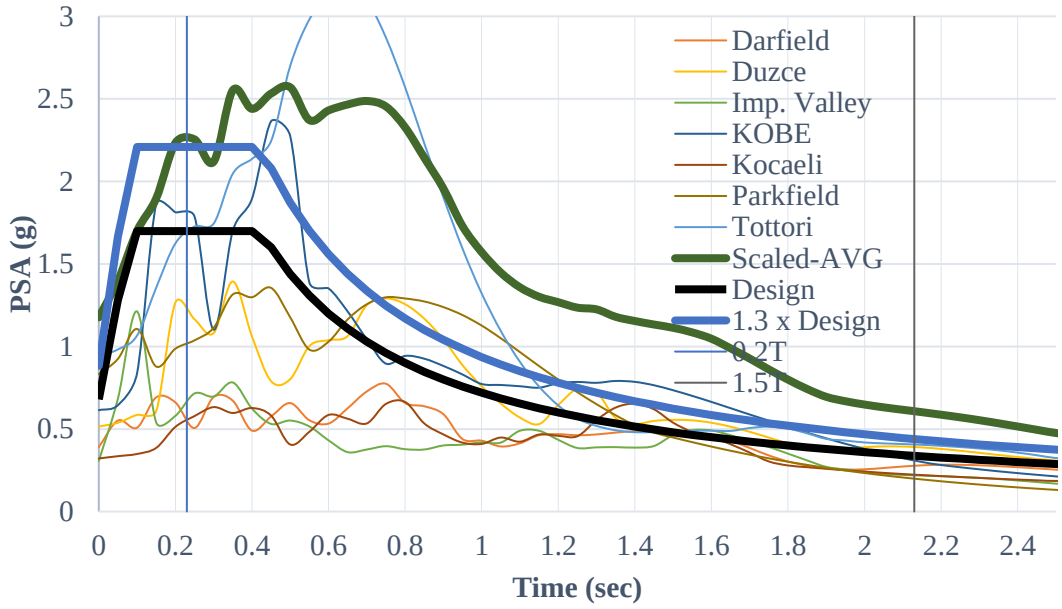

Figure 4.5. Scaled spectra of earthquakes according to CEN (2005)

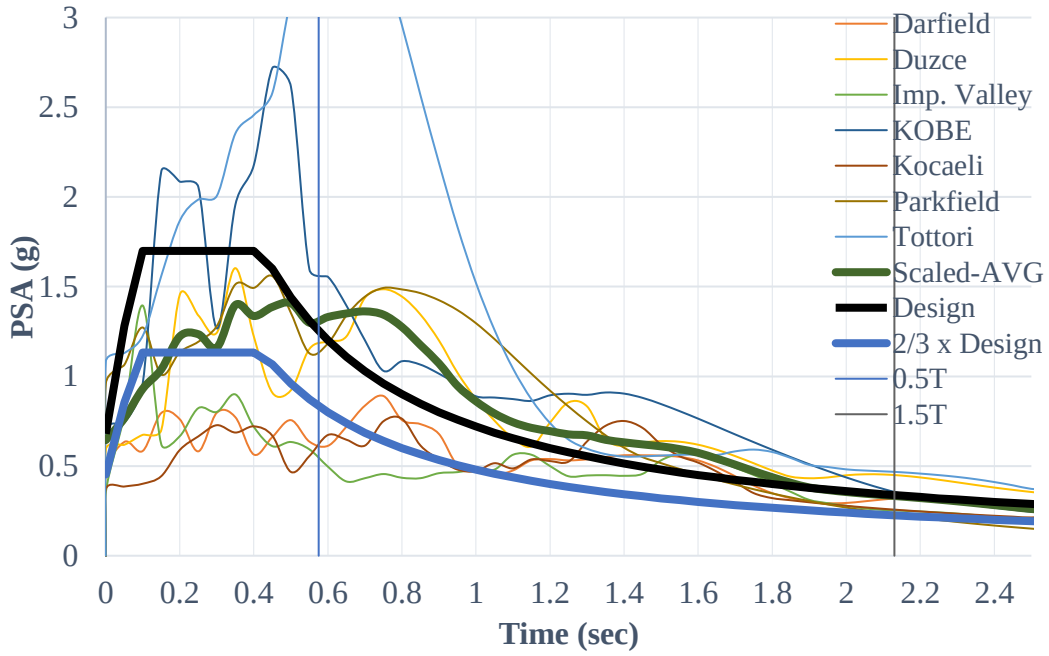

Figure 4.6. Scaled spectra of earthquakes according to AASHTO (2009)

4.3. Liquefaction Effects in Earthquake Ground Motions

As stated in the previous section, liquefaction has to change the impact on the spectra. 1-D site response analysis was done with 3 constitutive models for a different type of soil profiles given Table 4.1 Cyclic1D software was used for this purpose. This process was done for the seen liquefaction effects on response spectra.

Soil layers are uniform in the horizontal direction. Lu (2006) states that under these conditions it is sufficient to study the one dimensional (1D) behavior of a flat or inclined soil column exposed to earthquake motion at the base. Soil effects on the earthquake records are considered via one-dimensional nonlinear site response software Cyclic1D. It is a nonlinear finite element (FEM) program developed to perform one-dimensional field amplification and liquefaction simulations.

The liquefaction model based on flow plasticity material model given in Figure 4.7. Within this plasticity material model, in each step, the stiffness of soil will be evaluated. Soil gains some strain and in each step of the earthquake data, it changes. The soil particles come closer as stresses increase and their stiffness changes again. This behavior is modeled with the conical plasticity model in Figure 4.7.

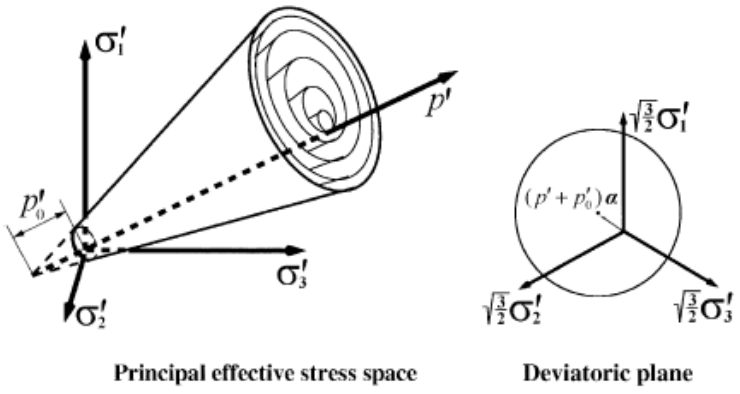

Figure 4.7. Conical yield surface used in Cyclic1D (Elgamal , 2002)

The soil parameters are modeled as very loose in the Cyclic1D software. Therefore, dilative effects of the liquefiable soils are not considered in this situation. Number of yield surfaces are selected as 30 in this model to include high non-linearity of the soil

according to Figure 4.8. Increasing yield parameter shows elastic-perfectly plastic response according to Elgamal et. al. (2015).

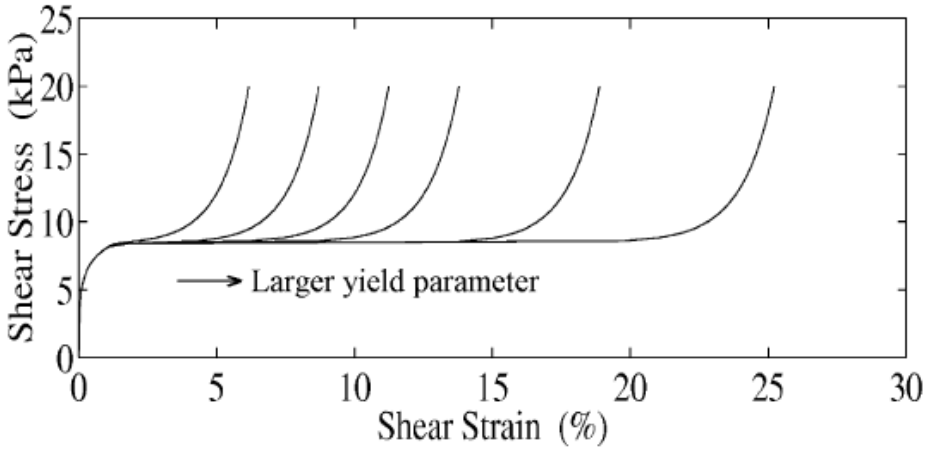

Figure 4.8. Yield performance of the Cyclic 1D (Elgamal et al., 2015)

The accelerograms were converted to spectra by the Newmark method stated before. Newmark time integration which has two user coefficients β and γ is used in Cyclic1D. For the conditionally stable solution β is taken as 1/6 and γ is taken as ½ (Elgamal et al. 2015).

The effect of soil profiles with liquefiable soil layer on each earthquake spectrum are given in the APPENDIX C. Each earthquake record in the longitudinal and transverse direction was combined with SRSS method. After that, these records were propagated from dense sand which is proper for D Soil Type. This process is done for each earthquake with different soil profiles stated in Table 4.1.

According to the results given in APPENDIX C, liquefiable soil layer has a noticeable impact on the spectrum. On short periods of the spectrum (T < 1 sec) decrease in spectral acceleration was observed. It is observed that liquefiable soils have a beneficial effect on a short period of structures when comparing to no liquefaction scenario. On the other hand, longer periods of the spectrum, liquefaction has devastating effects when comparing to no liquefaction scenario. Spectral accelerations

of liquefied soils are much greater and site-specific response became a vital requirement for these types of soils.

Soil thicknesses affected spectra also. All results gathered from each earthquake are similar. When the thickness of moving crust is greater than the liquefying soil equals to each other, spectral accelerations tend to go up. In contrast, if the thickness of the moving crust is smaller than the liquefiable soil, spectral accelerations still tend to go up. However, they are not effective as higher crust thickness does.

4.4. Soil-Pile Interaction

All 3 different types of soil profiles are modeled in LPILE software to gather their nonlinear p-y curves. Non-linear behavior of the piles was integrated SAP2000 software models via LPILE software. For the clay, Matlock (1970) Soft Clay p-y curves are used. For the second layer, liquefiable sand, liquefiable hybrid sand model by Franke and Rollins (2013) was used. For non-liquefaction configuration, API (2014) sand model for the p-y curve was used in the second layer. For the last layer, dense sand, Reese (1974) p-y curve for sand was used. These methods are widely used in the design. These p-y curves for liquefaction and no-liquefaction configurations were given in APPENDIX D.

A pile in a group resists less than single pile and stand against the less lateral load. The main reason that the piles losing lateral capacity is overlapping stress regions of each other. The p-multiplier that is calculated below turn a single pile to a group of piles. Leading row of the pile group gathers more load than the trailing rows. To be able to match the group behavior of the piles to single pile, group reduction factor (GRF) should be applied as p-multiplier to piles. For this p-multiplier, Mokwa's chart in Figure 4.9 was used, since it was used in the design example of Theryo (2005).

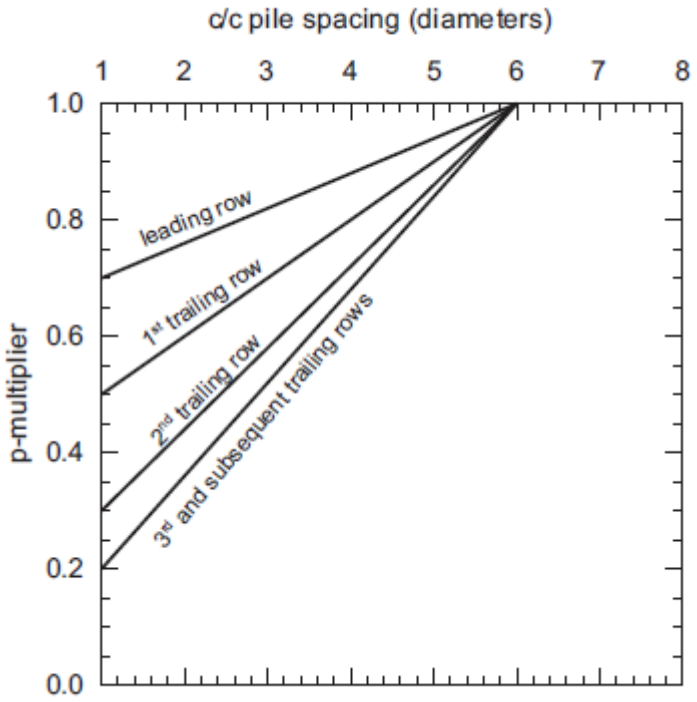

Figure 4.9. P-multiplier for group effects (Mokwa, 2000)

According to the Figure 4.9, group reduction factor (GRF) is calculated as;

$$\frac{0.82+0.67+0.58+0.52}{4} = 0.65$$

Pile group capacity is considered in this analysis, therefore those multipliers are set to 0.65 in LPILE software as done in the Caltrans Example (2013). The linked nonlinear p-y curves are given in APPENDIX D.

4.5. Calculation for Inertial Models

4.5.1. No-Liquefaction Analysis

As stated in the previous section, design spectrum was used in non-liquefied inertial model. These are the models without considering liquefaction effects on acceleration response spectrum. Since AASHTO (2017) proposed analyze bridges in liquefiable site with design spectrum, non-liquefied inertial model had been prepared. For this purpose, Site Class was found “D” as specified in according to the AASHTO (2017).

The design spectrum stated in Chapter 3.4 was used in these analyses. In order to able find the design spectrum, a place which has a PGA of 0.7g was selected. This place locates in the North-Anatolian Fault which its latitude is 38.65° and longitude is 40.05°. The bridge model consists up of superstructure, columns, and piled foundation was shown in Figure 4.10. The soil-structure interaction were modeled with p-y curves. P-y curves belong second layer was arranged as soil does not liquefy. These p-y curves were given in APPENDIX D.

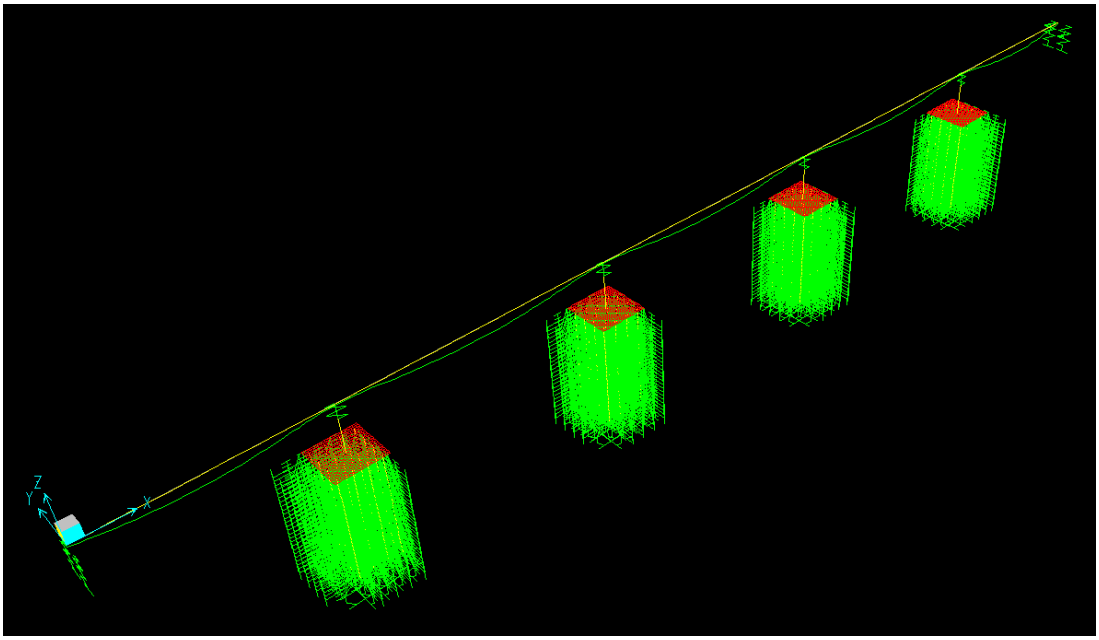

Figure 4.10. Bridge model for Non-liquefied Inertial Model

4.5.2. Liquefaction Analysis

These are the models considering liquefaction effects on the response spectrum that were considered in the analysis. Site response analysis for 3 types of soil profiles was conducted for the inertial analysis of bridge in liquefaction scenario. Non-linear soil springs are gathered from LPILE software (given in Appendix D) and the response spectra that were gathered from the Cyclic 1D were used for response spectrum analysis. The effects of the liquefiable soils on acceleration response of earthquake was discussed. How the structure affected from its mode shapes and spectrum were discussed. Also, CEN (2005) states that the bridge should be designed with the critical

one of the design spectrum or spectra of corresponding accelerogram set. It should be granted that the maximum values of the seismic action should be taken. Therefore, site-specific response spectra analyzed in this section.

Average of the selected earthquake motions was used in the analysis of liquefied inertial models. These average site specific spectrums were not scaled as it was done in non-liquefied inertial model. These average spectra that were used in analysis of liquefied inertial models was given in Chapter 5. Also, the earthquake records affected by the liquefaction was given in APPENDIX C.

4.6. Calculations for Kinematic Models

In this section of this study, kinematic analysis models was represented. It has 2 subsections which are force-based method and displacement-based method.

4.6.1. Force-Based Method

In this section, forces created by the moving crust was calculated according to Caltrans (2013). These forces are applied to foundation and piles. The calculation steps were described in detail. Caltrans (2013) offered two different possible failure cases which are Case-A and Case-B. The forces should be found according to both cases and the minimum one should be selected for design. The failure cases that are log-spiral passive forces and rankine passive forces were shown in Figure 4.11.

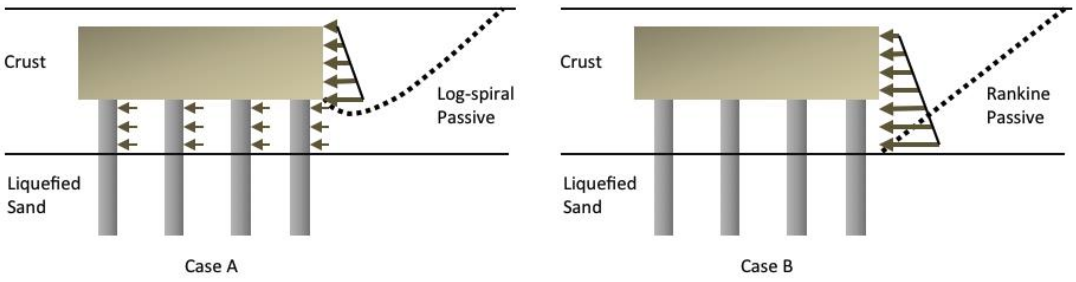

Figure 4.11. Log-Spiral passive zone & Rankine passive zone (Caltrans, 2013)

Case – A states that pile cap is in passive range and piles has same force on them. The maximum crust load acting on the foundation is determined by using equation below.

$$F_{ult} = F_{passive}+F_{sides}+F_{piles} \quad (4\text{-}4)$$

$F_{passive}$ acts on only the foundation. F_{sides} is the force because of adhesion that occurs while soil is moving. F_{piles} is the force acting on the piles due to moving soil.

$$F_{piles} = n\ GRF\ P_{ult}\ L_c \quad (4\text{-}5)$$

$$P_{ult} = 9\ c\ B \quad (4\text{-}6)$$

n is the number of piles, GRF is the group reduction factor, P_{ult} is the ultimate pile resistance, L_c is the length of through the clay layer. B is the pile diameter.

According to API (1993) estimation of $P_{ult;}$

Case – B states that the passive side has effect on pile cap and piles increasingly according to depth.

$$F_{ult} = F_{passive}+F_{sides} \quad (4\text{-}7)$$

Caltrans (2013) already stated that the second case Case – B considers in many situations. It is depend on the soil type and crust thickness. Since the crust was cohesive soil, Case – B was regarded.

$$F_{passive} = \left(4 + \frac{\gamma(D+T)}{2} + \frac{D+T}{4WT} + 2a\right) cWT\,\frac{(D+T)}{2} \quad (4\text{-}8)$$

$$F_{sides} = 2acWLT \quad (4\text{-}9)$$

Caltrans (2013) solves an example in its design guide about the force-displacement method. They applied the force single point on a pile cap calculated from the lateral spread to equivalent super pile that is governs for the all piles. That force is the F_{ult} that is given in the eq 4-7. However, in this study, since the fully bridge model developed, $F_{passive}$ and F_{sides} were applied to foundations and piles individually. $F_{passive}$ was applied on the foundation perpendicular edges to flow and piles, and piles along crust thickness. F_{sides} was applied on the foundation edges in the same direction with

lateral spreading. Therefore, passive and side forces were distributed over foundation and piles linearly as shown in Figure 4.12.

The values in the Figure 4.12 which are 82.7kN for passive and 59.8kN for side forces were found by dividing the number of joints that are perpendicular to lateral spreading action and the depth of composite block. These values were given in the Table 4.8 through 4.10 for SP-1, SP-2 and SP-3.

Table 4.8. *Fpassive and Fsides Values of SP-1*

Symbol	**Value**	**Unit**	**Description**
γ	18	kN/m3	Unit Weight Of Crust
D	0	m	Depth To Top Of Cap D
T	5	m	Pile Cap Thickness
c	50	kPa	Undrained Shear Strength
W_T	11	m	Transverse Width Dimensions
α	0.5		Adhesion Factor
B	1	m	Pile Diameter
$F_{passive}$	**9506.25**	kN	
F_{sides}	**2750**	kN	

Table 4.9. *Fpassive and Fsides Values of SP-2*

Symbol	**Value**	**Unit**	**Description**
γ	18	kN/m3	Unit Weight Of Crust
D	0	m	Depth To Top Of Cap D
T	15	m	Pile Cap Thickness
c	50	kPa	Undrained Shear Strength
W_T	11	m	Transverse Width Dimensions
α	0.5		Adhesion Factor
B	1	m	Pile Diameter
$F_{passive}$	**44306.3**	kN	
F_{sides}	**8250**	kN	

Table 4.10. *Fpassive and Fsides Values of SP-3*

Symbol	Value	Unit	Description
γ	18	kN/m3	Unit Weight Of Crust
D	0	m	Depth To Top Of Cap D
T	10	m	Pile Cap Thickness
c	50	kPa	Undrained Shear Strength
W_T	11	m	Transverse Width Dimensions
α	0.5		Adhesion Factor
B	1	m	Pile Diameter
$F_{passive}$	**24275**	kN	
F_{sides}	**5500**	kN	

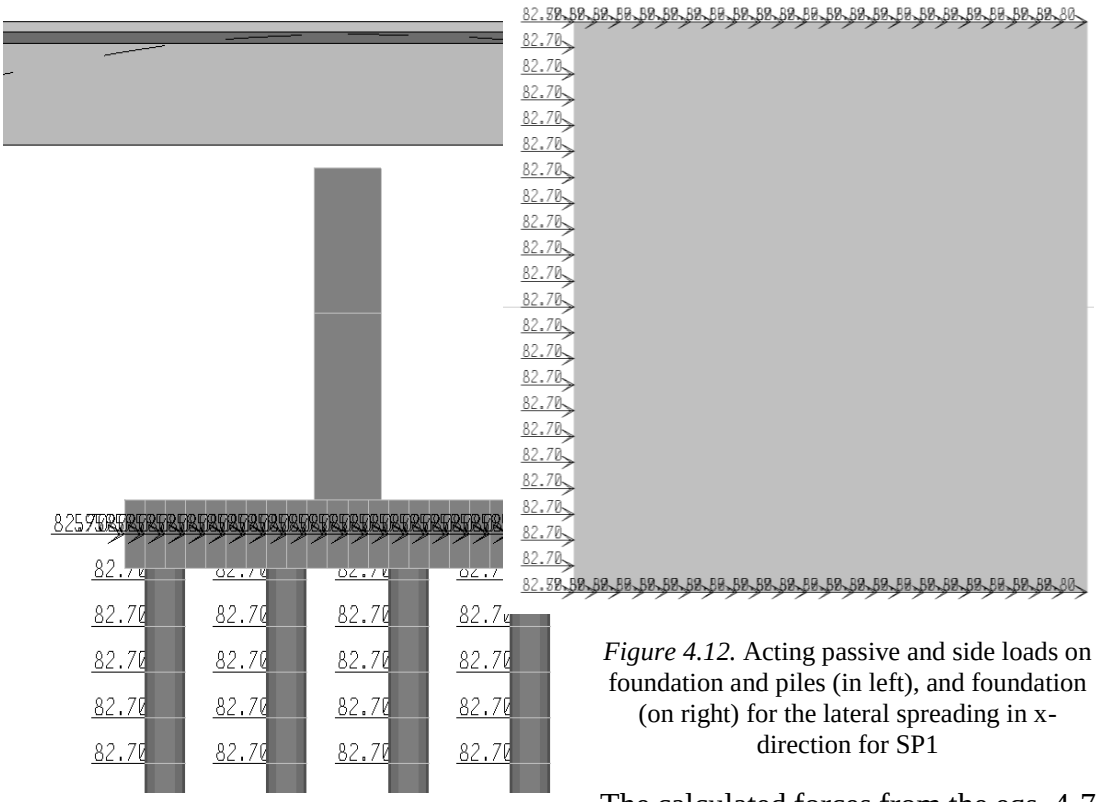

Figure 4.12. Acting passive and side loads on foundation and piles (in left), and foundation (on right) for the lateral spreading in x-direction for SP1

The calculated forces from the eqs. 4-7 through 4-9 are shown in the Table 4.8, 4.9 and 4.10. Also, parameter "T" is corresponds to depth of composite block according to Caltrans (2013). Depth of composite block equals to crust thickness in this study, since soil does not overlay on

foundation. It should be indicated again, the values gathered in Table 4.8 thorough 4.10 are applied on foundation and the piles along crust thickness linearly. They were divided the crust thickness and the number of joints of edge of a foundation. These forces were assigned to all foundations and piles in the piers.

4.6.2. Displacement-Based Method

In this section, the ground displacement were calculated according to section 3.4.2. These displacements was applied to foundations and piles. Shear strains were found by using Shamoto (1998) approach as stated before. Firstly, fine content of the soils were accepted as 10%. After the correlating SPT-N values with the values given in Table 3.11, corrected SPT-N_a was summed in Table 3.12. These values are required to get the CSR values of the earthquakes.

Table 4.11. *Fines corrected SPT-Na values*

Soil Layer	SPT-N	Na	FC %
Layer 1	-	-	10
Layer 2	10	15	10
Layer 3	35	40	10

Responsible displacements of the moving soil are given in Tables 4.12, 4.13 and 4.14. Application in the analytical model shown in Figure 4.13. Also analytical models were given in the previous sections. In the results part, only the average displacements were applied and listed as a result.

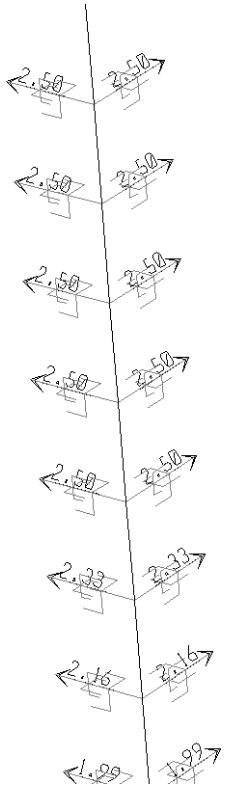

Figure 4.13. Application of displacements to piles for average of the earthquakes in SAP2000

The displacements for each soil profile were shown in Tables 4.12, 4.13 and 4.14 in the following pages. It was showed that the ground displacements were applied to links. There are two links for a joint to apply the different directions and see the maximum effects in X and Y-direction. All the applied ground displacements shown in the Tables 4.12, 4.13 and 4.14 was used in the calculations

Table 4.12. *Ground displacements of average of ground motions for SP-1*

Depth (m)	rd	CSR	Strain	Displacement (m)
0	1	0.41	0.18	2.5
1	0.988	0.40	0.18	2.5
2	0.976	0.40	0.18	2.5
3	0.964	0.39	0.18	2.5
4	0.952	0.39	0.18	2.5
5	0.94	0.38	0.17	2.5
6	0.928	0.38	0.17	2.33
7	0.916	0.38	0.17	2.16
8	0.904	0.37	0.17	1.99
9	0.892	0.37	0.17	1.82
10	0.88	0.36	0.17	1.65
11	0.868	0.36	0.17	1.48
12	0.856	0.35	0.17	1.31
13	0.844	0.35	0.17	1.14
14	0.832	0.34	0.17	0.97
15	0.82	0.34	0.17	0.8
16	0.808	0.33	0.16	0.64
17	0.796	0.33	0.16	0.48
18	0.784	0.32	0.16	0.32
19	0.772	0.32	0.16	0.16
20	0.76	0.31	0.16	0

Table 4.13. *Ground displacements of average of ground motions for SP-2*

Depth (m)	rd	CSR	Strain	Displacement (m)
0	1	0.47	0.2	0.68
1	0.988	0.46	0.2	0.68
2	0.976	0.46	0.2	0.68
3	0.964	0.45	0.19	0.68
4	0.952	0.45	0.19	0.68
5	0.94	0.44	0.19	0.68
6	0.928	0.43	0.19	0.68
7	0.916	0.43	0.19	0.68
8	0.904	0.42	0.19	0.68
9	0.892	0.42	0.19	0.68
10	0.88	0.41	0.18	0.68
11	0.868	0.41	0.18	0.68
12	0.856	0.40	0.18	0.68
13	0.844	0.39	0.18	0.68
14	0.832	0.39	0.18	0.68
15	0.82	0.38	0.17	0.68
16	0.808	0.38	0.17	0.68
17	0.796	0.37	0.17	0.51
18	0.784	0.37	0.17	0.34
19	0.772	0.36	0.17	0.17
20	0.76	0.36	0.17	0

Table 4.14. *Ground displacements of average of ground motions for SP-3*

Depth (m)	rd	CSR	Strain	Displacement (m)
0	1	0.44	0.19	1.52
1	0.988	0.43	0.19	1.52
2	0.976	0.43	0.19	1.52
3	0.964	0.42	0.19	1.52
4	0.952	0.42	0.19	1.52
5	0.94	0.41	0.18	1.52
6	0.928	0.41	0.18	1.52
7	0.916	0.40	0.18	1.52
8	0.904	0.40	0.18	1.52
9	0.892	0.39	0.18	1.52
10	0.88	0.39	0.17	1.52
11	0.868	0.38	0.17	1.52
12	0.856	0.38	0.17	1.35
13	0.844	0.37	0.17	1.18
14	0.832	0.37	0.17	1.01
15	0.82	0.36	0.17	0.84
16	0.808	0.35	0.17	0.67
17	0.796	0.35	0.17	0.5
18	0.784	0.34	0.17	0.33
19	0.772	0.34	0.17	0.16
20	0.76	0.33	0.16	0

CHAPTER 5

NUMERICAL INVESTIGATIONS AND DISCUSSIONS

In many design guides like AASHTO, Eurocode, JRA liquefaction-induced lateral spreading is analyzed in different stages. These stages were referred to in Chapter 3 and 4. In this study, the inertial and kinematic effects of liquefaction will be mentioned. Two different methods for each inertial and kinematic analyses were used and presented in this section.

The inertial analysis was made by considering two methods. The first one includes the liquefaction effects on response spectra. The other one does not include. Response Spectrum Analysis stated in Chapter 3.4 was used for the inertial analysis of the bridge. Design spectra and the spectra that were found after site response analysis was used in the analyses. It should be noted that AASHTO (2009) demands that liquefied configuration should also be designed with the design spectrum that does not considers liquefaction. Therefore, the design spectrum and average spectra will be used in inertial analyses.

The kinematical analysis is made for estimating the damage of moving soil because of liquefaction. In this study, it includes the displacement-based method using shear strain charts proposed by Shamoto et al. (1998) and the force-based method proposed by Caltrans (2013). In the displacement-based method, piles are linked to fixed boundary conditions. These fixed restrains are subjected to ground displacements that are calculated according to Shamoto et al. (1998). In the force-based method, estimation of the force produced by moving soil is based. Caltrans (2013) prepared a guideline for the estimation of these forces developed by liquefaction induced lateral spread. These two methods were employed, and the results were discussed. All analysis model contained nonlinear soil-structure interaction.

After all the analysis, inertial effects and kinematic effects are combined for the design purpose. For example, Caltrans (2013) says that 100% of kinematic effects and 50% of inertial effect or reverse combination should be combined for design purposes. This situation can differ from other specifications. Superstructure and columns were modeled, as stated in Chapter 3.1. The piled foundation was modeled, and the p-y (force-displacement) curves were used to ensure the soil-pile interaction.

As it was stated, SAP2000 software will be used for nonlinear static analysis and response spectrum analysis. To achieve high mass participation ratio (>90%), the mode number was set to a very high number.

The results for displacements for columns and piles, pier forces, and pile forces in different scenarios and different methods were concluded in previous sections. Moreover, effects of the different soil profiles were shown and discussed. In this part of the study, the steps taken in previous sections were represented. In addition, analysis results will be compared and commented on.

Liquefaction-induced lateral spreading analysis for bridges was performed, combining the inertial analyses and kinematic analyses — inertial analysis based on the structure response against earthquake motion. Kinematical analysis was based on the displacement of the liquefying soil. As stated in previous chapters, the inertial analysis performed under two scenarios; non-liquefied and liquefied configurations, according to AASHTO (2017). There are two known methods that are employed in this study for kinematical analysis, force-based method, and displacement-based method. It was investigated that which scenario should be employed and which method could be critical for the specific type of bridge. In addition, moment of inertia of columns is separated, whether they are cracked or not. In order to see the effects of cracked columns, they were used in the analysis models.

5.1. Inertial Analyses

Firstly inertial analysis, liquefied, and non-liquefied configuration was compared. In the non-liquefied scenario design spectrum for a specific site class was studied, as proposed in AASHTO (2017). For this purpose, friction angle and shear wave velocities are calculated according to many approaches. In the liquefied scenario, seven different earthquakes were selected, and site-specific earthquake response analysis were made for different soil profiles within these records. One-dimensional wave propagation software, Cyclic1D, was used in these analyses, as stated in Section 4.5.2. All spectrums were computed. In figure 5.1, the spectrum used in these scenarios was shown.

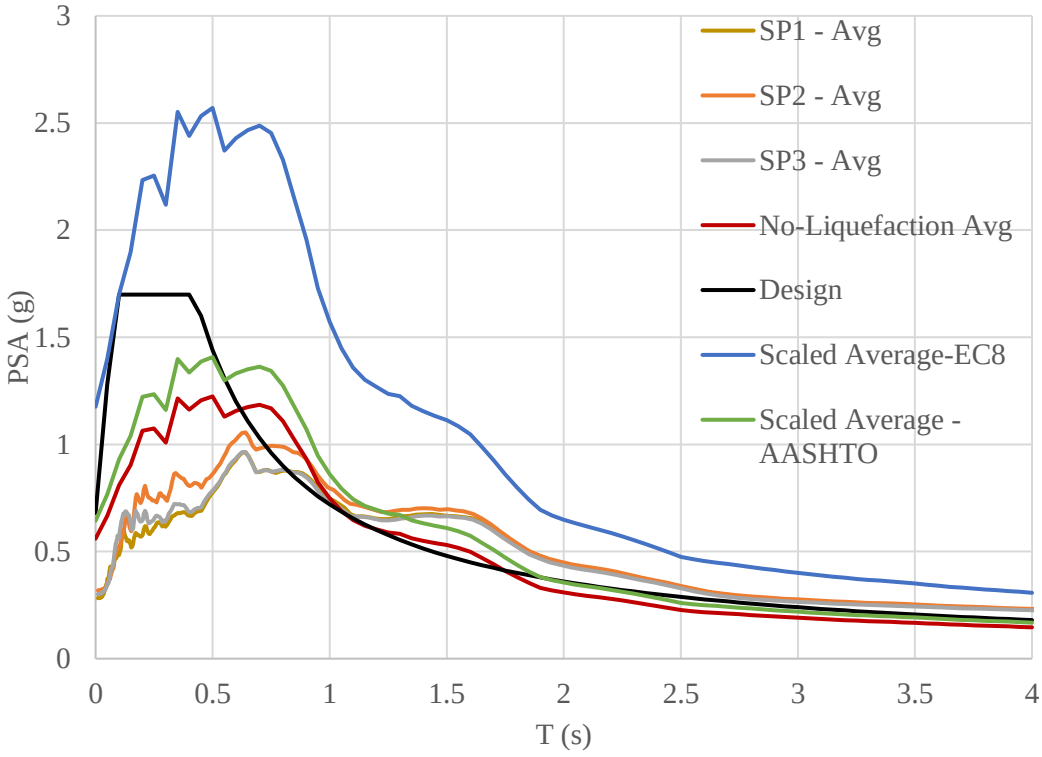

Figure 5.1. Spectra used in models

"SP -1 Avg", "SP - 2 Avg", "SP - 3 Avg" are the spectra were the average of the seven earthquake records after the site response analysis. "Design" is the design spectrum gathered from AASHTO (2017), as specified in Chapter 4. The "Scaled Average –

EC8" spectrum is the spectrum that is gathered after scaling of the seven earthquakes, according to CEN (2005). The "Scaled Average – AASHTO" spectrum is the spectrum that is gathered after scaling of the seven earthquakes, according to AASHTO (2009). As it was indicated in the graph, site response analysis results show that in case the crust thickness was higher than the liquefiable layer thickness, spectral accelerations were higher after analysis. In contrast, in case the liquefiable layer thickness was lower than the crust thickness, spectral accelerations after site response analysis were lower.

The scale factor of the scaled average spectrum was 2.1 for CEN (2008), 1.15 for AASHTO (2009). "SP -1 Avg", "SP - 2 Avg", "SP - 3 Avg," showed that after a period, spectral acceleration was more critical than the design spectrum. It was stated that site response analysis should be done for a long period of structures in AASHTO (2017). The periods of the models were given in Table 5.1.

Table 5.1. *Periods of the models*

	No-Liquefaction Scenario			Liquefaction Scenario			Change in X (%)	Change in Y (%)
		X	Y		X	Y		
Uncracked	SP1	1.112	0.641	SP1	1.168	0.669	5.0	4.4
	SP2	1.150	0.662	SP2	1.168	0.669	1.6	1.0
	SP3	1.149	0.662	SP3	1.164	0.667	1.3	0.8
Cracked	SP1	1.360	0.652	SP1	1.420	0.680	4.4	4.3
	SP2	1.406	0.674	SP2	1.420	0.680	1.1	1.0
	SP3	1.405	0.673	SP3	1.417	0.679	0.9	0.8

Change in X and Y directions are based on the following formula, eq 5-1. In addition, it should be noted that positive results mean that increase in liquefaction scenario, negative sign means that decrease in liquefaction scenario when comparing to no-liquefaction scenario.

$$Change\ in\ (\%) = \frac{\mathrm{LQ-NOLQ}}{NOLQ} * 100 \qquad \text{(Eq 5-1)}$$

"LQ" indicates the liquefaction case results, "NOLQ" indicates the no-liquefaction case results. The change in crack situation was about %22 in X direction. In Y direction, this change was observed to be %1.7. Soil-pile interaction was provided with p-y curves, however since it was a response analysis, effective stiffness values were used in these models. As it can be seen from the graph, these curves did not affect periods excessively. The change in periods was observed for different p-y setups according to table 5.1. The maximum change seen in SP1, which was reasonable, since it has the higher liquefiable soil layer. As it was stated, that layer has different p-y curves. In non-liquefied inertial models API (2014) sand model was used. In liquefied inertial model, liquefiable hybrid sand model by Franke and Rollins (2013) was used. Therefore, the maximum change which is 4.7% was seen in SP1.

Although, the different soil profiles did not affect the periods of structure excessively, it affected the spectral accelerations gathered from the site response analysis, as shown in Figure 5.1. Therefore, the difference of the displacements and forces gathered from non-liquefied and liquefied configuration were not in the same extent. The comparison between the displacements between non-liquefied and liquefied scenarios were given in Table 5.2 and Table 5.3. It should be noted that, No-liquefied scenario and uncracked results were based on in the change rates. The formulation was given in Eq. 5-1. Also change in crack situation is given Eq. 5-2.

$$Change\ in\ (\%) = \frac{\mathrm{CR-UNCR}}{\mathrm{UNCR}} * 100 \qquad \text{(Eq 5-2)}$$

"CR" represents the cracked model results and "UNCR" represents the uncracked model results. The results compared in the table in the following pages, were given in the APPENDIX E. In order to see the results in terms of forces and displacements, one should check the APPENDIX E.

Table 5.2. *Comparison of displacement values of non-liquefied vs. liquefied scenario in column-x direction*

	No-Liquefied Scenario		Liquefied Scenario			
Axis - Soil Profile	Column-X-UNCR	Column-X-CR	Column-X-UNCR	Column-X-CR	Change in Crack Situation (%)	Change in Scenario (%)
P1-SP1	0.011	0.014	0.004	0.005	30.3	-63.2
P2-SP1	0.013	0.017	0.005	0.006	29.8	-63.5
P3-SP1	0.193	0.238	0.215	0.330	53.8	38.4
P4-SP1	0.008	0.010	0.003	0.004	31.5	-62.5
P1-SP2	0.012	0.015	0.004	0.006	44.1	-60.9
P2-SP2	0.014	0.018	0.005	0.007	43.4	-60.0
P3-SP2	0.200	0.247	0.228	0.343	50.2	38.7
P4-SP2	0.009	0.012	0.003	0.004	45.7	-63.0
P1-SP3	0.011	0.015	0.004	0.006	35.4	-61.2
P2-SP3	0.013	0.017	0.004	0.006	28.8	-66.7
P3-SP3	0.200	0.247	0.213	0.325	52.8	31.5
P4-SP3	0.009	0.012	0.004	0.006	43.3	-51.4

In Table 5.2, it was seen that if the analysis model has cracked section columns, cracked models showed more displacement than the uncracked model. Since the cracked section is half of the uncracked moment of inertia, displacements are greater. In scenario change, the non-liquefied scenario was compared to the liquefied scenario. In this comparison, only the P3 axis has a greater in liquefied inertial analysis model, about 14%~20%. The reason for this situation was the difference in spectral accelerations and the different periods for each scenario. It should be noted that only displacements in X directions were concerned, and the maximum change based on non-liquefied results. These displacements were given in Figure 5.2 for the simplicity. In general, it was shown that the in SP-2, column displacements were shown to be higher than other profiles.

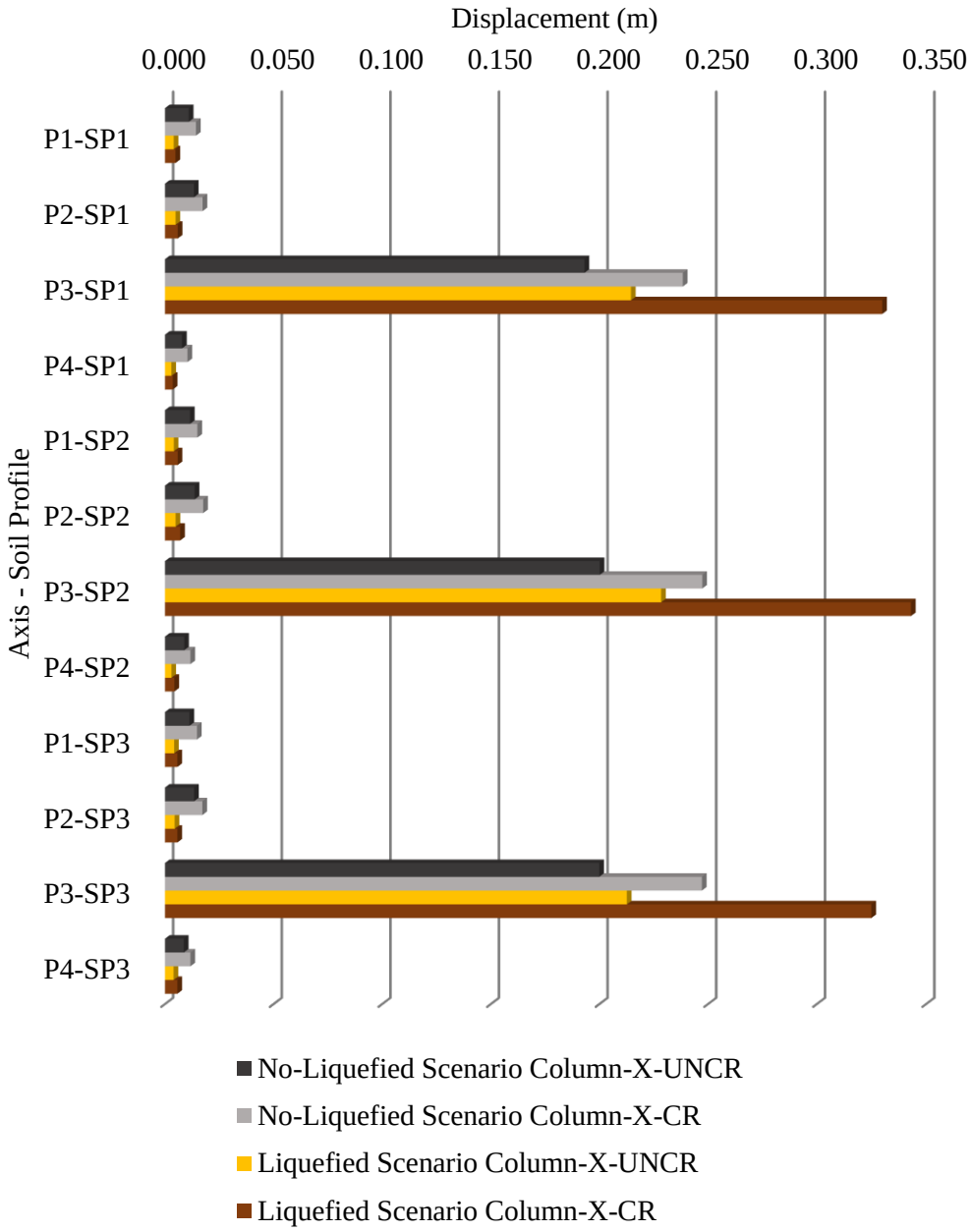

Figure 5.2. Displacements of columns in x-direction

Column displacements in Y direction were shown in Figure 5.3. In this figure, no-liquefaction and liquefaction scenario was discussed. It was seen that the forces are higher in SP-2 results.

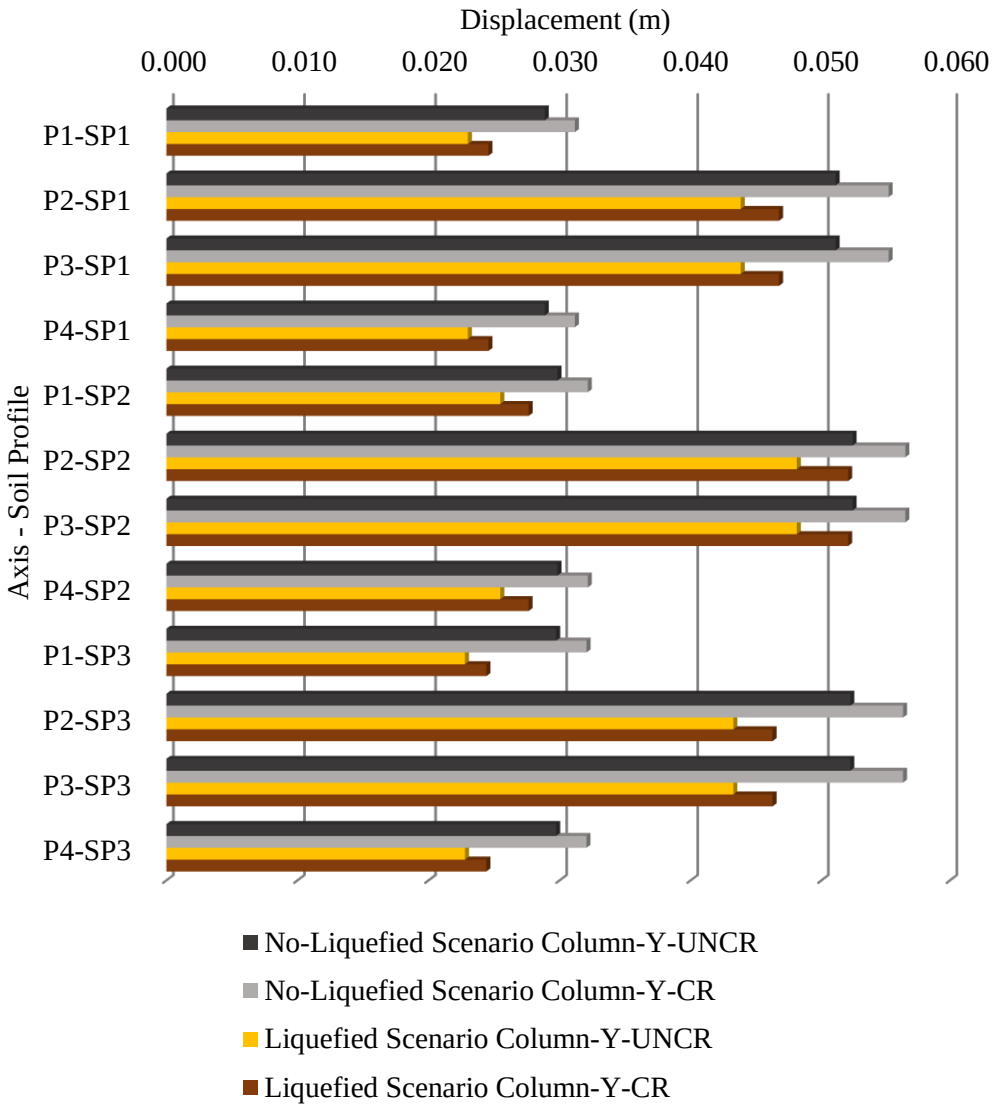

Figure 5.3. Displacements of columns in y-direction

In the Y direction, it was observed that non-liquefaction configuration had greater results in uncracked properties about 20% comparing the liquefaction scenario. Moreover, when the configurations were compared, no-liquefaction scenario shows larger displacements. The displacements of columns and piles in Y direction was given in Table 5.3.

Table 5.3. . *Comparison of displacement values of non-liquefied vs. liquefied scenario in column y-direction*

	No-Liquefied Scenario		Liquefied Scenario			
Axis - Soil Profile	Column-Y-UNCR (m)	Column-Y-CR (m)	Column-Y-UNCR (m)	Column-Y-CR (m)	Change in Crack Situation (%)	Change in Scenario (%)
P1-SP1	0.029	0.031	0.023	0.025	7.9	-20.3
P2-SP1	0.051	0.055	0.044	0.047	8.1	-14.3
P3-SP1	0.051	0.055	0.044	0.047	8.1	-14.3
P4-SP1	0.029	0.031	0.023	0.025	7.9	-20.3
P1-SP2	0.030	0.032	0.025	0.028	8.5	-14.0
P2-SP2	0.052	0.057	0.048	0.052	8.3	-7.9
P3-SP2	0.052	0.057	0.048	0.052	8.3	-7.9
P4-SP2	0.030	0.032	0.025	0.028	8.5	-14.0
P1-SP3	0.030	0.032	0.023	0.024	7.8	-23.4
P2-SP3	0.052	0.056	0.043	0.046	7.9	-17.2
P3-SP3	0.052	0.056	0.043	0.046	7.9	-17.2
P4-SP3	0.030	0.032	0.023	0.024	7.8	-23.4

Pier forces in terms of cracks were compared in Table 5.4. From this table, it was seen that the pier forces were relatively low in Column Top (CT). However, change in the shear causes a great increase in models with cracked property. Therefore, models with cracked moment of inertia were seen to give higher displacements and sectional forces. The changes in pier forces were given in Table 5.4.

Table 5.4. *Pier forces maximum changes in crack situation*

	P	Vx	Vy	Mx	My
P1 - CT	-33.2	-5.4	-2.4	-2.4	-5.4
P2 - CT	-25.8	-8.6	-2.3	-2.3	-8.6
P3 - CT	-32.3	-18.8	-2.3	-2.3	-18.8
P4 - CT	-29.0	2.1	-2.4	-2.4	2.1
P1 - CB	-27.5	-11.6	-2.3	-2.3	-10.5
P2 - CB	-21.2	44.6	0.3	149.7	311.4
P3 - CB	-19.4	-18.3	0.3	149.7	105.5
P4 - CB	-28.4	40.4	0.9	150.7	302.9

Table 5.5. *Maximum changes in pier forces in non-liquefied vs. liquefied scenario*

Axis - Location - Crack Case	Changes in Scenario (%)				
	P	Vx	Vy	Mx	My
P1 - CT - UNC	-23.8	-65.4	-24.1	-24.1	-65.4
P2 - CT - UNC	0.2	-65.7	-18.8	-18.8	-65.7
P3 - CT - UNC	-52.6	7.5	-18.8	-18.8	7.5
P4 - CT - UNC	-1.1	-64.9	-24.1	-24.1	-64.9
P1 - CB - UNC	-25.9	-64.3	-25.8	-24.8	-64.6
P2 - CB - UNC	0.3	-41.8	-17.9	106.5	62.2
P3 - CB - UNC	-51.2	8.1	-17.9	106.5	172.0
P4 - CB - UNC	-1.3	-42.9	-23.4	92.9	60.7
P1 - CT - CR	-11.8	-67.4	-24.5	-24.5	-67.4
P2 - CT - CR	25.6	-66.7	-19.5	-19.5	-66.7
P3 - CT - CR	-52.6	35.4	-19.5	-19.5	35.4
P4 - CT - CR	26.4	-68.8	-24.5	-24.5	-68.8
P1 - CB - CR	-22.2	-66.7	-26.2	-25.2	-66.8
P2 - CB - CR	18.1	-66.9	-20.5	-19.8	-66.9
P3 - CB - CR	-57.8	35.3	-20.5	-19.8	35.4
P4 - CB - CR	24.7	-65.9	-26.2	-25.2	-66.3

At first glance at Table 5.5, it can be said that general conclusion is that no-liquefaction scenario governs. However, the moment and shear forces at Pier-3 in the column bottom had the greatest value in these tables. These values were shown in previous sections. These tables were given to show that there was no constant ratio for

comparing these two methods. However, this attitude was changing in the pile forces. These forces were given in Table 5.6.

Table 5.6. *Maximum changes in pile forces in non-liquefied vs. liquefied scenario*

Axis - Crack Case	Changes in Scenario (%)				
	P	Vx	Vy	Mx	My
P1- UNC	-30.7	-72.0	-15.0	-48.1	-31.2
P2- UNC	-23.6	-68.4	20.4	-37.1	-62.7
P3- UNC	33.0	57.4	-52.4	-19.1	-28.6
P4- UNC	-30.1	-71.6	-6.2	-46.6	-28.2
P1- CR	-30.7	-72.0	-18.2	-48.8	-30.4
P2- CR	-23.7	-68.5	31.2	-34.8	-21.2
P3- CR	14.4	77.5	-45.7	-4.9	-15.6
P4- CR	-30.2	-71.5	-28.0	-50.8	-27.5

It can be said that the pile forces were higher than the liquefied inertial model except the fixed pier in P3 axis. The axial force increase in pier 3 affected piles also. The piles were not affected by the spectral accelerations directly. Forces governing design was considered at the end of this section.

5.2. Kinematic Analyses

In this section, results of the kinematic analyses were compared. The formulations of the change in X and Y direction, scenario and the crack situation were given in Eq. 5-3.

$$Change\ in\ (\%) = \frac{\mathrm{DBM-FBM}}{\mathrm{FBM}} * 100 \qquad \text{(Eq 5-3)}$$

"DBM" indicates the results from displacement-based method results, "FBM" represents the results from force-based method.

The comparison of the displacements and forces were given in the following tables, Table 5.7 and Table 5.8. The values for the column displacements were shown in Figure 5.4.

Table 5.7. *Comparison of the column displacements for FBM vs DBM*

	FBM		DBM			
Axis - Soil Profile	Column-X	Column-Y	Column-X	Column-Y	Change in X (%)	Change in Y (%)
P1-SP1	0.055	0.053	0.313	0.015	471.1	-70.7
P2-SP1	0.055	0.078	0.233	0.026	324.4	-67.0
P3-SP1	0.071	0.078	0.313	0.026	338.8	-67.0
P4-SP1	0.071	0.053	0.313	0.016	338.8	-70.1
P1-SP2	1.219	0.553	0.263	0.021	-78.4	-96.2
P2-SP2	1.229	0.985	0.378	0.033	-69.3	-96.6
P3-SP2	1.229	0.985	0.264	0.035	-78.6	-96.4
P4-SP2	1.219	0.553	0.263	0.022	-78.4	-96.0
P1-SP3	0.139	0.100	0.404	0.028	191.4	-71.7
P2-SP3	0.139	0.152	0.246	0.045	77.1	-70.1
P3-SP3	0.139	0.152	0.405	0.047	191.6	-69.1
P4-SP3	0.139	0.100	0.405	0.029	191.5	-71.1

As it can be seen in Table 5.7, FBM governs the structure in Y-direction. However, in X-direction DBM governed the displacements in piers except Pier 3. The reason was stated before. However, FBM was shown more reacting when the crust thickness was much higher than the liquefiable layer thickness. It should be noted that the changes are based on FBM. This table was drawn in Figure 5.2. In this figure, it was shown that soil layer thickness had an impact on the methods used for analyzing kinematic effects of liquefaction, like FBM, DBM. When the crust thickness was higher than the thickness of liquefiable soil layer, as in SP-2, FBM resulted more displacement than the DBM.

Table 5.8. *Comparison of the pile displacements for FBM vs DBM*

	FBM		DBM			
Axis - Soil Profile	Pile-X	Pile-Y	Pile-X	Pile-Y	Change in X (%)	Change in Y (%)
P1-SP1	0.054	0.056	0.311	0.101	479.4	78.4
P2-SP1	0.000	0.074	0.002	0.093	1448.1	26.4
P3-SP1	0.000	0.074	0.003	0.109	1853.2	47.5
P4-SP1	0.000	0.056	0.003	0.101	2123.4	78.8
P1-SP2	1.210	0.567	0.262	0.032	-78.3	-94.3
P2-SP2	0.040	0.980	0.376	0.040	851.3	-96.0
P3-SP2	0.040	0.980	0.262	0.046	563.4	-95.4
P4-SP2	0.039	0.567	0.262	0.033	575.6	-94.2
P1-SP3	0.133	0.105	0.402	0.042	202.1	-60.0
P2-SP3	0.004	0.143	0.244	0.056	6515.3	-61.0
P3-SP3	0.004	0.143	0.402	0.060	10813.2	-58.2
P4-SP3	0.004	0.105	0.402	0.042	11063.7	-59.4

Large column cap displacements were seen in the Pier 2 and Pier 4 since Pier 3 was fixed to the superstructure. Moving soil has a great effect on the foundation of Pier 3. Therefore it forces to move neighbor piers. These displacement values have serious damage to the columns. If the columns are affected by that damage, all structural elements like foundation, piles are affected.

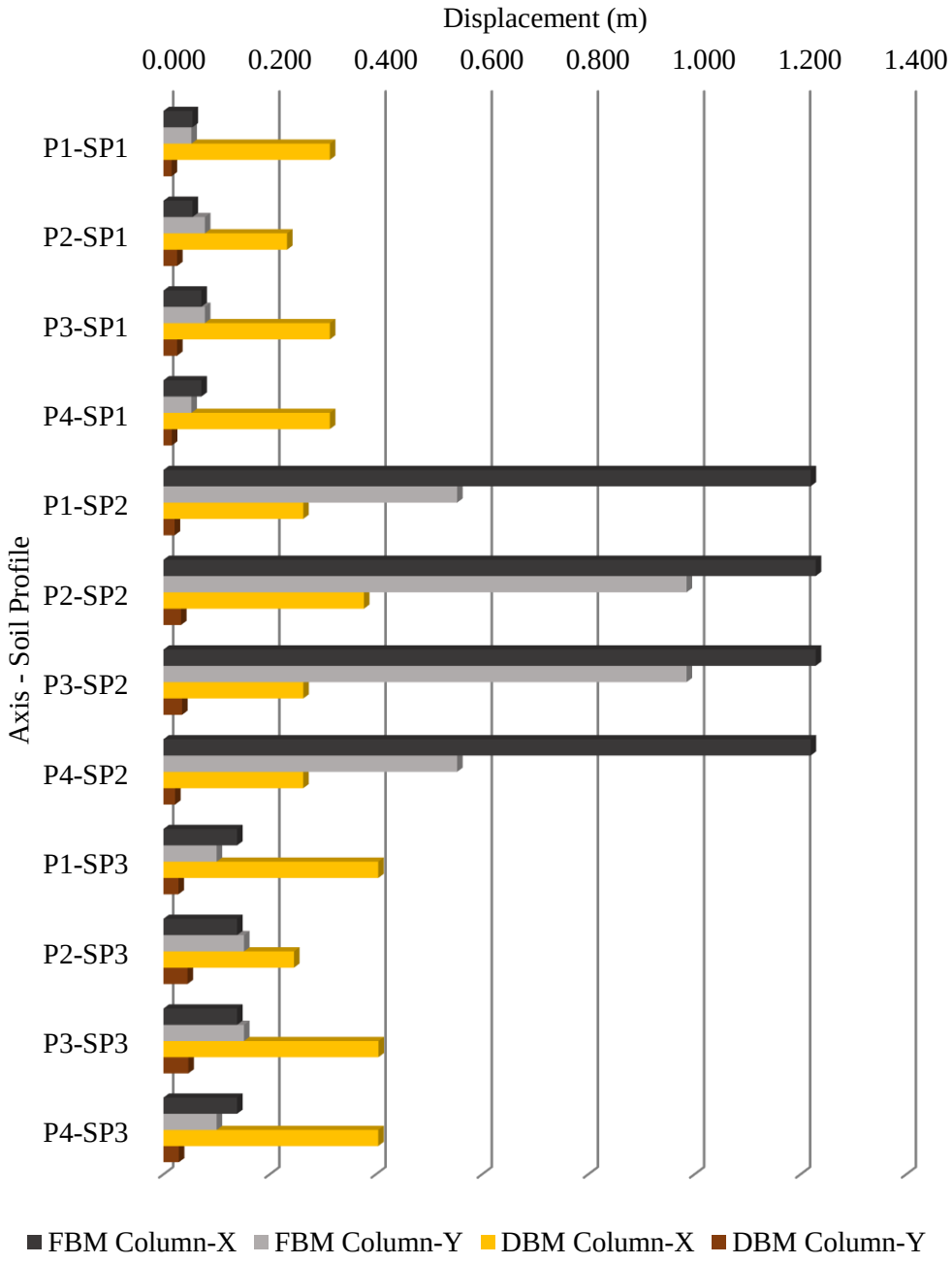

Figure 5.4. Column displacement results for kinematic analyses

In SP-2 highest displacements in columns were observed. In other soil profiles, DBM shows greater results that the FBM. The crust thickness was the identifier factor for the results. The displacement values were given in the Table 5.7.

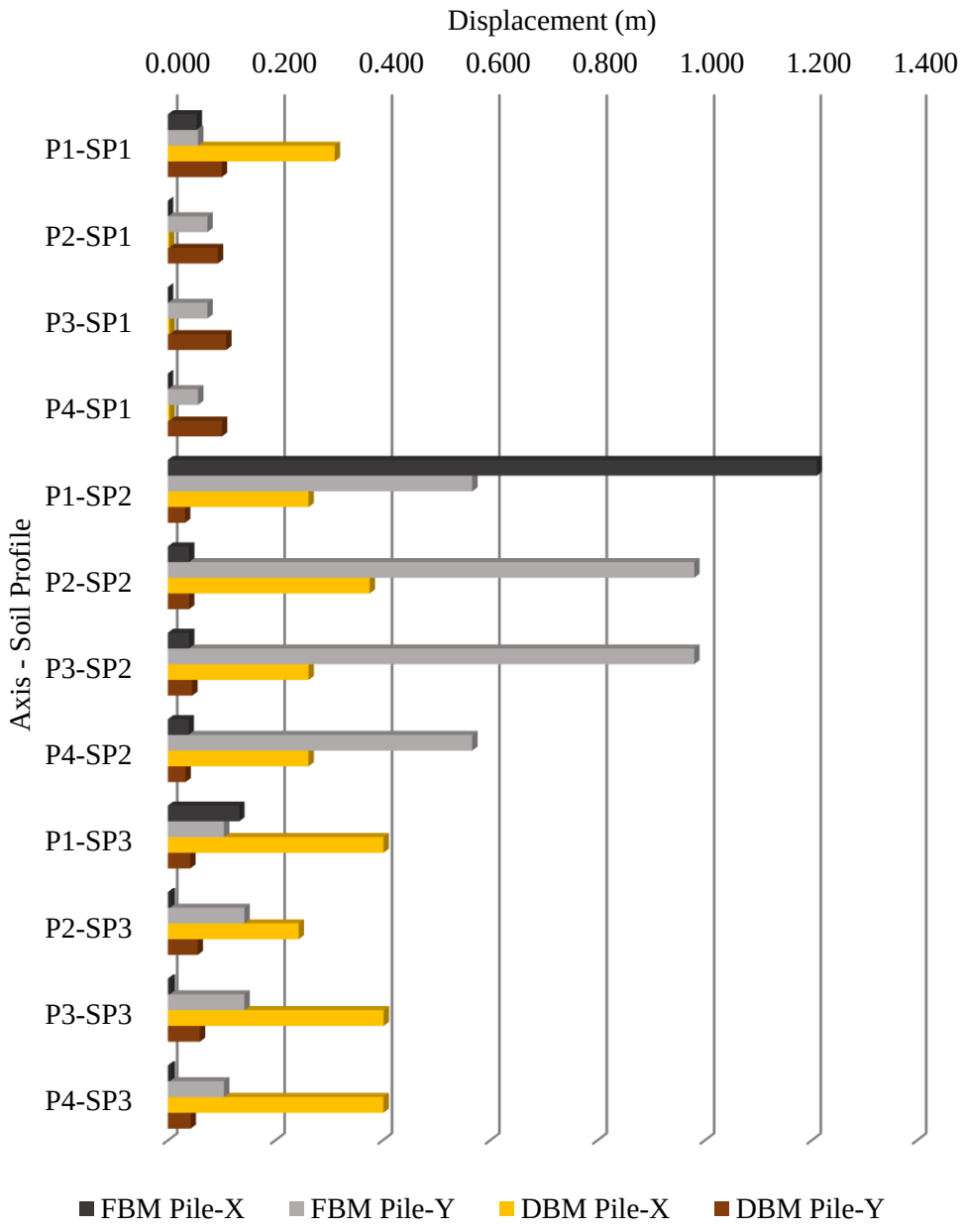

Figure 5.5. Pile displacement results for kinematic analyses

As in the columns, SP-2 showed more X-direction displacements in FBM. In Y direction displacements, DBM showed more displacements in SP-1 which has the lowest crust layer thickness. The values were given in Table 5.8.

5.3. Combinations of the Results

In inertial analysis, displacements are relatively lower than the kinematic analysis. However, force results are much greater. For this kind of problem, many specifications offer superimposed the results of inertial and kinematic forces. For different soil profiles, pier forces were drawn in Figure 5.6, Figure 5.7 and Figure 5.8.

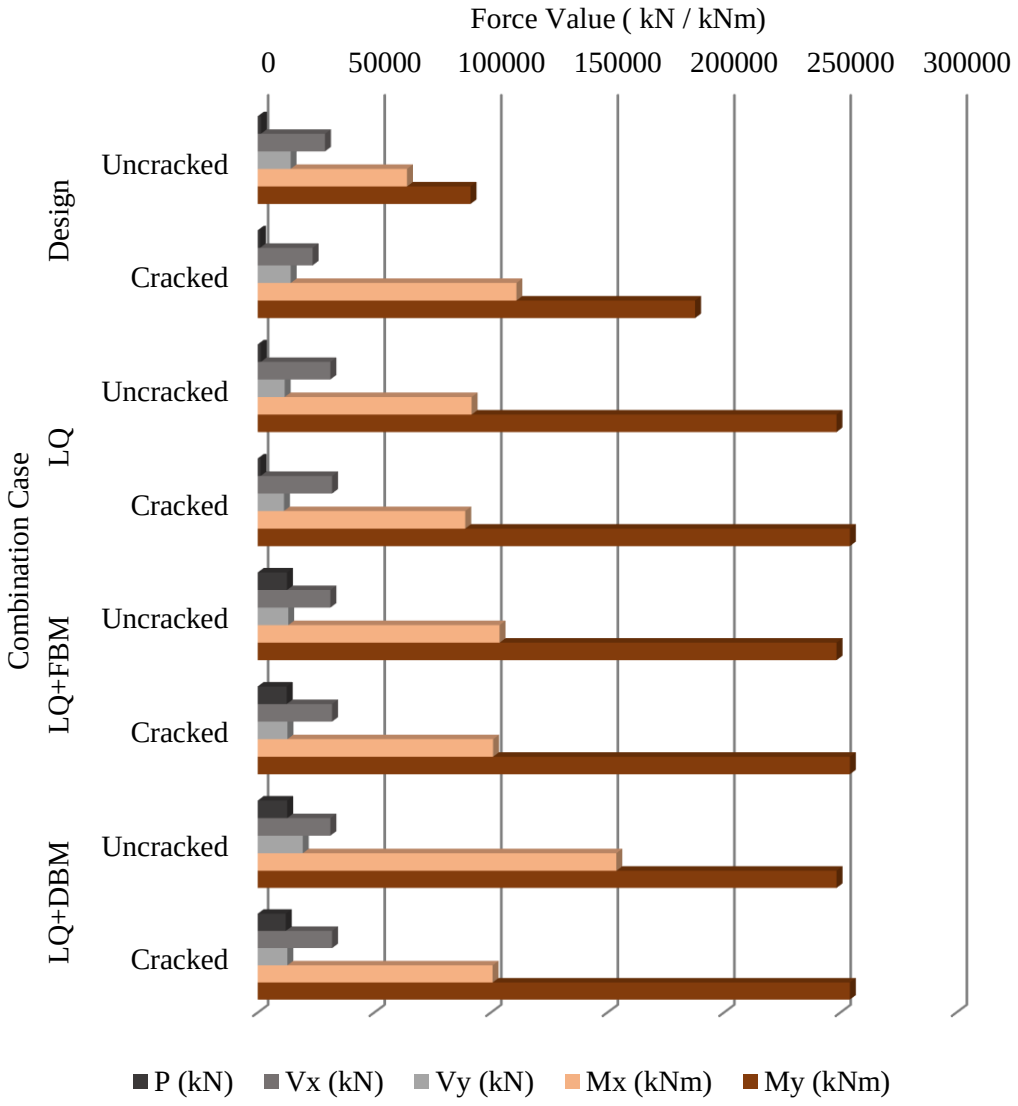

Figure 5.6. Pier forces comparison for SP-1

In SP-1 soil profile, it was seen that the liquefaction scenario had greater results when comparing the no-liquefaction scenario. Combining these forces in liquefaction scenario made liquefaction immortal for pier design concerns. Also, displacement based method showed more critical results than the force-based method. The change between no-liquefaction, liquefaction scenario were given in the Section 5.1. Likely, the change between the FBM and DBM were given in the Section 5.2. DBM showed more forces comparing the FBM.

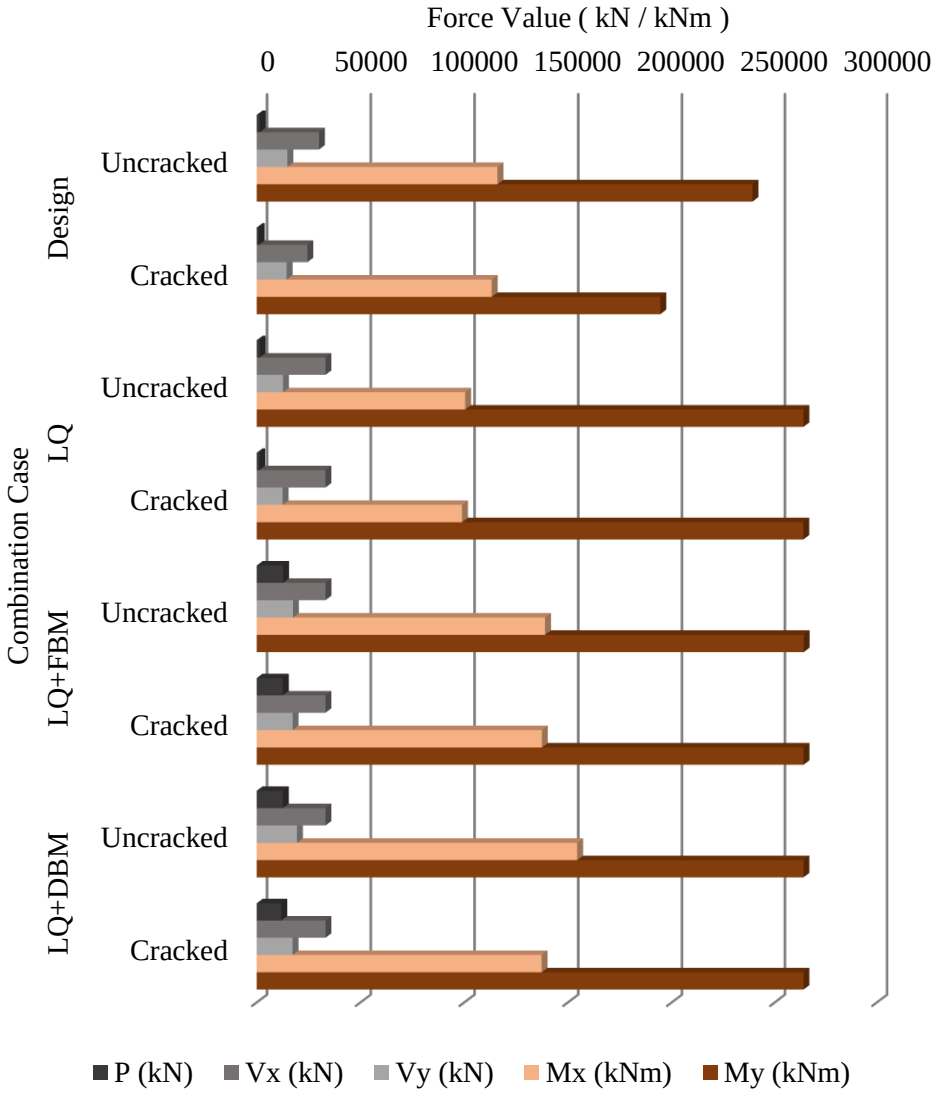

Figure 5.7. Pier forces comparison for SP-2

In Figure 5.3, it was seen that liquefaction was critical in Y-direction moment and X-direction shear forces. The no-liquefaction configuration showed more reaction in X-direction moment and Y direction shear forces. In contrast, liquefaction scenario was higher in other combinations. No-liquefaction situation was seen to be more critical comparing the no-liquefaction design scenario. Also, FBM showed more forces according to DBM.

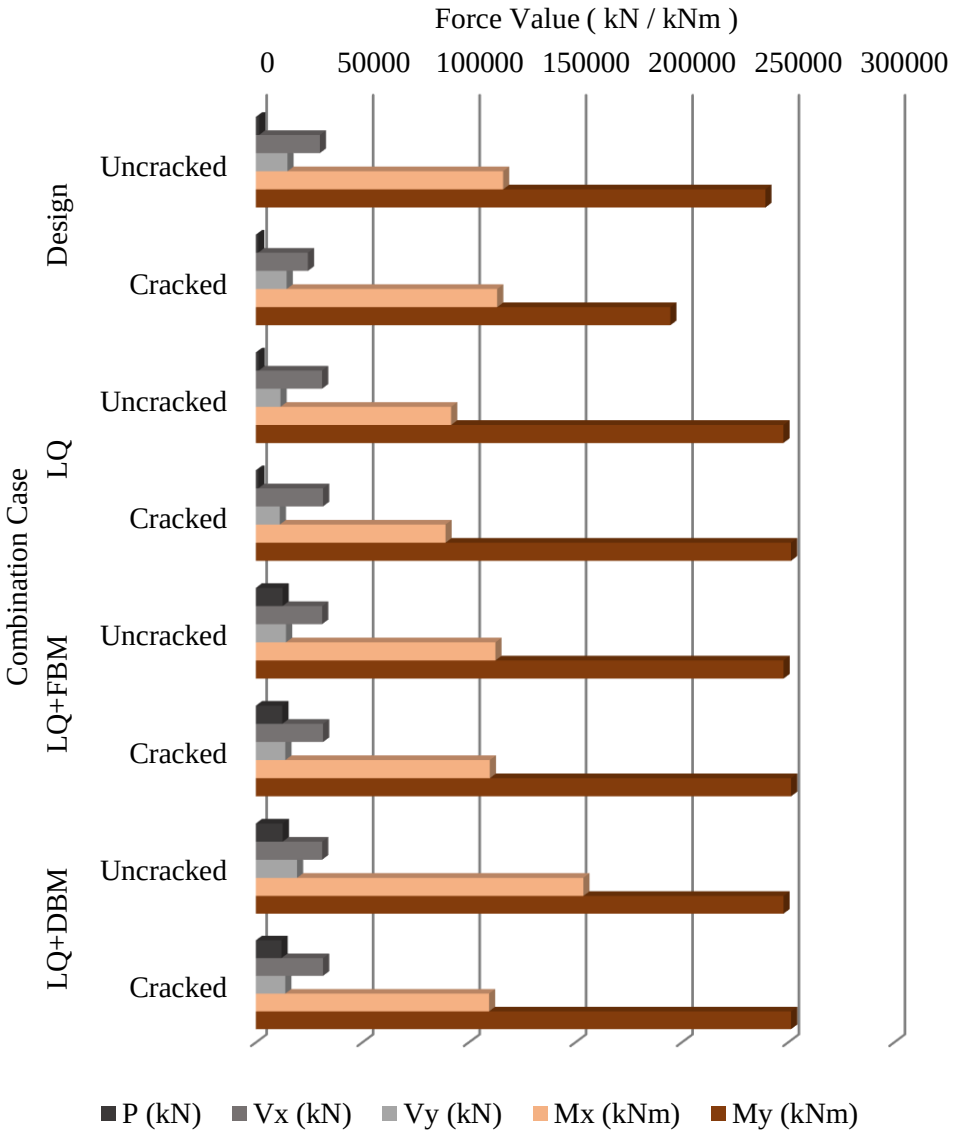

Figure 5.8. Pier forces comparison for SP-3

In SP-3 analyses, it was seen that the no-liquefaction scenario has higher results in Vx and My. However, to proper design, liquefaction scenario should be controlled, since P, Vy and Mx results were higher than the no-liquefaction scenario. This situation is related with the period and the acceleration responded to that period. DBM shows higher results comparing to FBM.

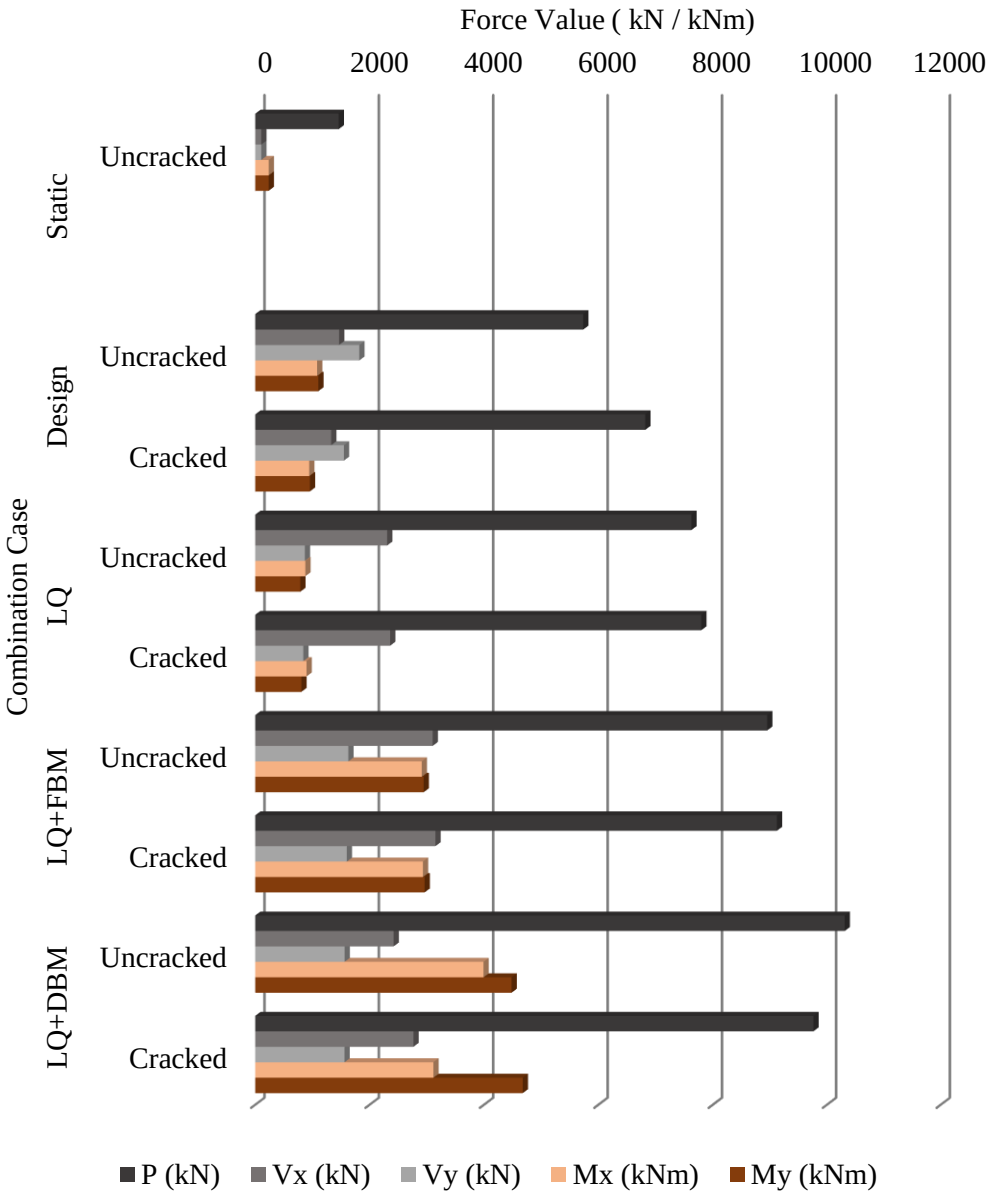

Figure 5.9. Pile forces comparison for SP-1

In pile forces in SP-1, liquefaction scenario govern the design in terms of any force. DBM was seen to cause more forces in piles comparing to FBM. Combining the effects of liquefaction shows nearly 200% more than the design spectrum. Therefore, liquefaction was seen to control the design of piles.

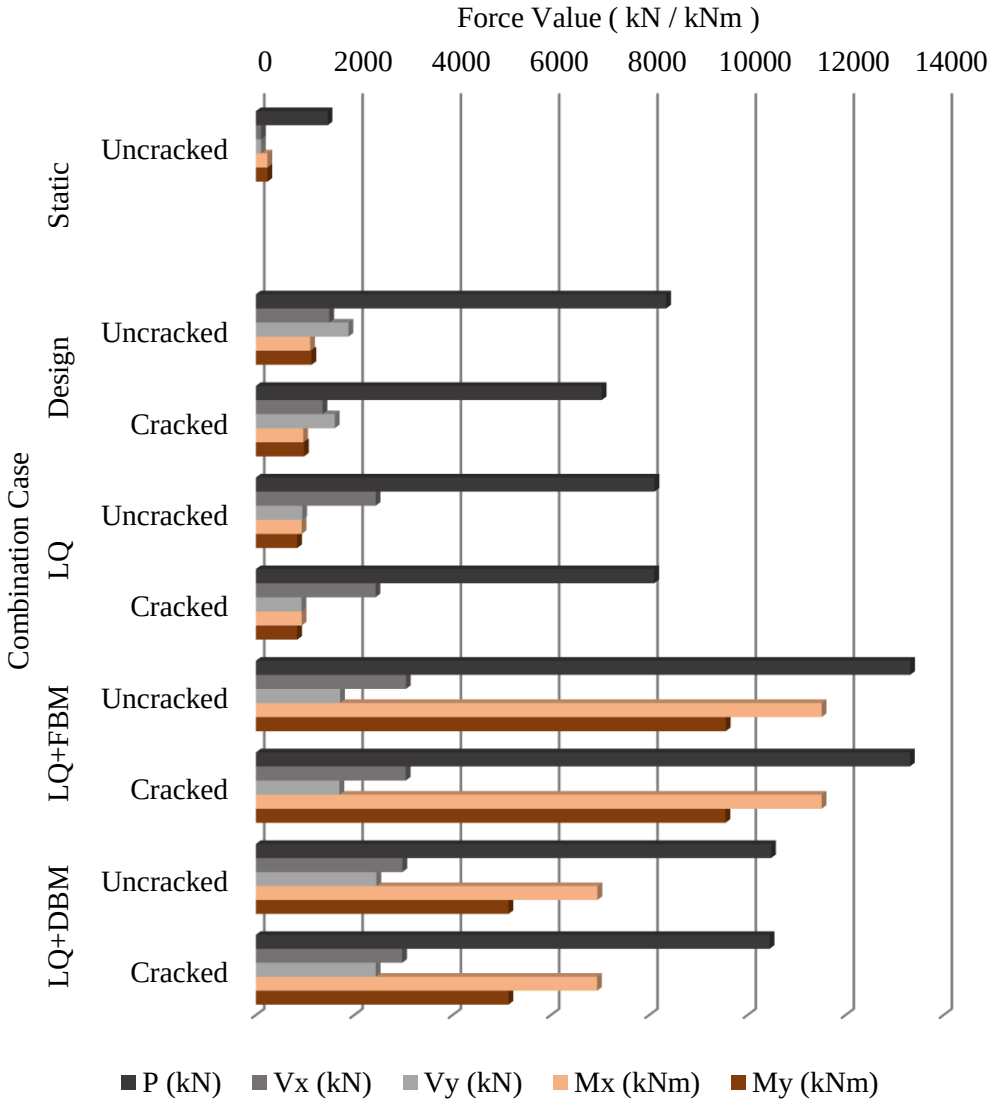

Figure 5.10. Pile forces comparison for SP-2

In the Figure 5.10, no-liquefaction showed more force results than the no-liquefaction scenario in the axial pier forces. However, in the other forces, liquefaction scenario

showed higher results than the design spectrum. In fact, combining inertial and kinematic forces shows greater results than the no-liquefaction scenario. In addition, FBM shows 30% greater results comparing DBM force results. It can be said that the thickness of crust was to increase, the effect of the FBM increased. In this case, it can be said that liquefaction controls the design.

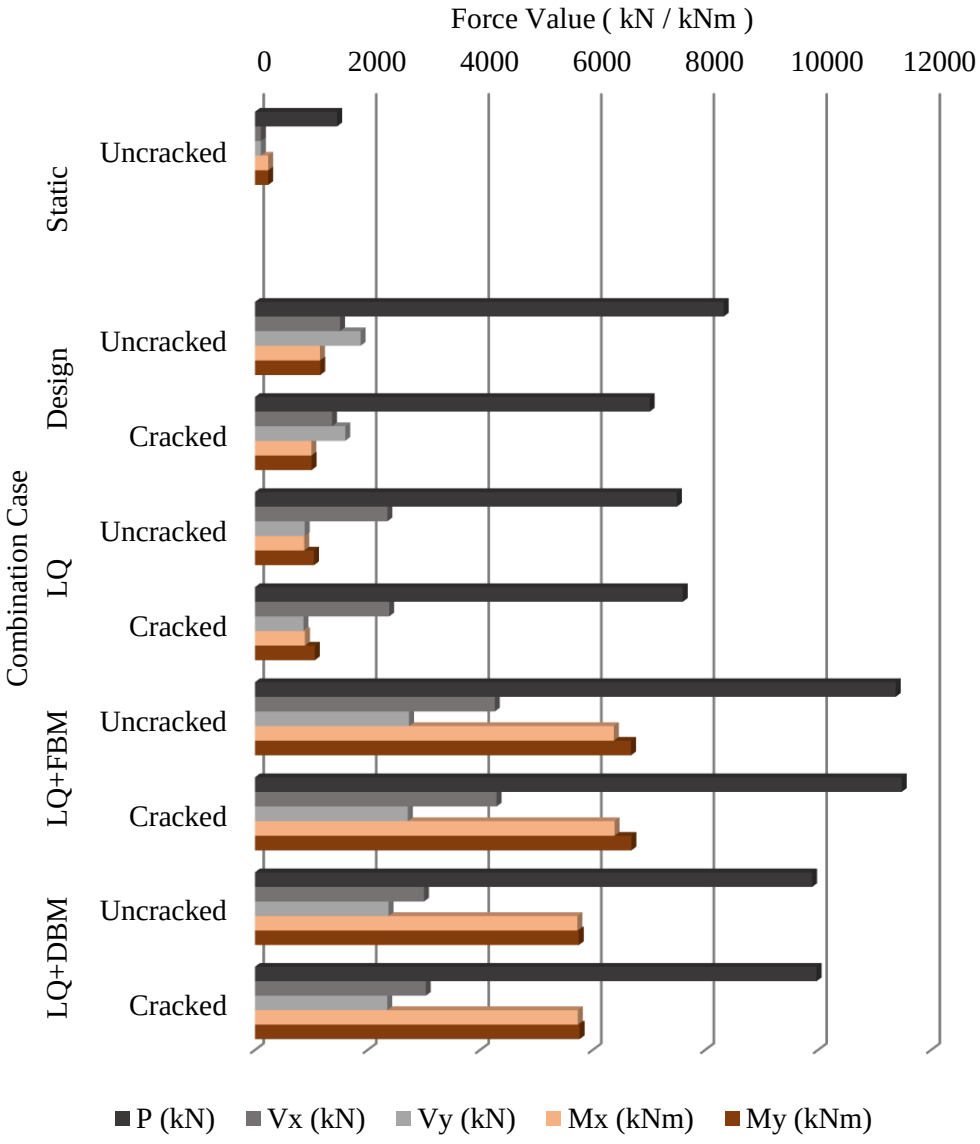

Figure 5.11. Pile forces comparison for SP-3

The forces shown in Figure 5.11, the liquefying layer and crust layer thicknesses were equal. As in the SP-2 profile, no-liquefaction scenario showed more reactions in P, Vy, Mx than the liquefaction scenario models. In addition, if the inertial and kinematic effects are combined, no-liquefaction scenario will have no effect on design purpose. Also, FBM showed more reactions than DBM.

In order to see the difference between the design spectrum and the combination of liquefaction affected response and kinematical analysis, Table 5.9 was given below. One should be note that the liquefaction affected spectra was not scaled. Without scaling, it was seen that liquefaction effects should be included in bridge analysis since the results are critical.

Table 5.9. *No-Liquefaction scenario against combination of liquefaction scenario and kinematic analyses in pier forces*

Comb	Crack Case	P (kN)	Vx (kN)	Vy (kN)	Mx (kNm)	My (kNm)
Design	Uncracked	1525	30051	14820	116102	239302
	Cracked	1076	24440	14465	113311	194626
LQ	Uncracked	1436	33164	12700	100502	264113
	Cracked	1271	33142	12510	98979	264044
LQ+FBM	Uncracked	12769	33175	17511	138991	264206
	Cracked	12604	33154	17321	137468	264136
LQ+DBM	Uncracked	12656	33166	19445	154464	264130
	Cracked	12056	33154	17305	137344	264129

The maximum pier forces gathered from the analysis were listed on Table 5.9. These forces were for all soil profiles. In the stated different soil profiles, different soil p-y

curves, the forces were combined. As it can be seen, the design forces for the pile was critical in liquefied scenario plus displacement-based method. Also, it should be noted that the liquefied scenario results are not scaled up. In that term, it was seen that liquefaction-induced lateral spreading governs the pier design.

Table 5.10. *No-Liquefaction scenario against combination of liquefaction scenario and kinematic analyses in pile forces*

Comb	Crack Case	P (kN)	Vx (kN)	Vy (kN)	Mx (kNm)	My (kNm)
Static	Uncracked	1460	106	106	235	235
Design	Uncracked	8349	1512	1884	1155	1160
	Cracked	7037	1370	1605	1003	1007
LQ	Uncracked	8111	2437	943	932	1049
	Cracked	8105	2434	929	932	1064
LQ+FBM	Uncracked	13322	4263	2739	11514	9560
	Cracked	13315	4294	2717	11514	9554
LQ+DBM	Uncracked	10482	3004	2453	6949	5756
	Cracked	10453	3036	2438	6942	5771

The maximum pile forces were given in the Table 5.10. The values in the table were from all analysis results. In this table it was seen that the combination of liquefaction scenario with kinematic analyses were higher than the design values. Also, it should be noted that, in SP-2 FBM showed higher forces. Therefore, LQ+FBM was the critical forces for the pile design.

CHAPTER 6

CONCLUSIONS AND FUTURE STUDY

6.1. Conclusion

In this thesis study, an analysis of precast cantilever balanced bridge in liquefiable soils was investigated. This bridge consisted up consists up of five spans on a total of 270 meters with two 45 meters exterior span and three 60 meters interior span with box section. In order to see the effects of liquefaction, various methods were employed.

Liquefaction-induced lateral spreading analysis was divided into two types because of its mechanism. These are inertial and kinematic effects of liquefaction. Inertial effects are due to earthquake excitation. These effects were divided into two, which are non-liquefied and liquefied scenario, according to AASHTO (2017). In the non-liquefied scenario, only the design spectrum was used in response analysis of the bridge. In the liquefied scenario, seven earthquake records were selected, site response analysis was made for three different soil profiles, and the average spectra were used in response analysis. Kinematic effects are due to the movement of the soil. In this effect, two different methods for analysis of lateral spreading was used. These are force-based method and displacement-based method. The difference in the methods and scenarios were given in the early chapters.

Liquefaction effects on acceleration spectra of seven earthquakes were gathered from Cyclic1D software. Site response analysis was performed for three different soil profiles. In the early periods of the response spectrum, soil liquefaction decrease the spectral acceleration and beneficial effects on the spectrum. However, as the period increase, the acceleration in liquefied condition had shifted up comparing to the non-

liquefied and design spectrum. This situation may lead to a problem for long-period structures (T>1s).

The periods of the bridge that were modeled for liquefaction and no-liquefaction configuration was seen to be closer to each other. Effective stiffness calculated from the non-linear p-y curves does not affect the periods visibly. However, if the columns were modeled in the cracked moment of inertia, which was half of the uncracked moment of inertia, it was observed that the periods of the bridge was increased by about 20%.

Soil thickness effects on spectra were observed. The results showed that SP1, which has the thickest liquefying layer, decreased the amplitude of spectra more than the others. However, a decrease in the depth of the liquefying layer does not mean an increase in amplitudes of ground motion. Spectral accelerations were seen to rise when the thickness of the crust and liquefying zone were equal to each other.

In analysis of inertial effects of seismic shaking on bridges, liquefaction and no-liquefaction scenarios were considered, and it was observed that the liquefaction configured models are more critical than the non-liquefaction configured model in terms of displacement and forces acting on piers and piles. Response spectra in liquefiable soils tend to raise more than the design spectrum for the longer period ranges in spectra. The differences between liquefaction scenario and no-liquefaction scenario increase when the inertial and kinematic effects are combined.

When the displacement-based method and force-based method is compared, it is seen that the crust layer thickness has an important role for which one controls the design. In SP2, crust layer thickness is three times higher than the liquefiable soil, and force-based method produce greater displacements than the displacement-based method. However, reaction forces are greater in the displacement-based method. In SP1 and SP3, the displacement-based method is more critical than the force-based method.

A large difference was seen between the no-liquefaction scenario and the liquefaction scenario. In no-liquefaction scenario, only the design spectrum was used. However, in

the liquefied scenario for the analysis of the bridge, combining the inertial effects and kinematics effects was necessary, as proposed in Caltrans (2013). When they were compared, it was seen that there combined forces showed more displacements and forces in every soil profile and crack situation. Spectra gathered after site response studies was higher in longer periods comparing to design spectrum. As regards inertial forces in liquefaction scenario was high, additional kinematic forces makes liquefaction scenario more important for design.

6.2. Future Study

- The assumptions and limitations of this study should be removed in future search.
- 3D dynamic analysis for this study could be generated. These results can be controlled with constitutive models.
- Vertical effects of liquefaction could be integrated.

REFERENCES

AASHTO (1999). Guide Specifications I or Seismic Isolation. First Edition, American Association of State Highway and Transportation Officials; Washington, D.C.

AASHTO (2009). Guide Specifications for LRFD Seismic Bridge. First Edition, American Association of State Highway and Transportation Officials; Washington, D.C.

AASHTO (2017). LRFD Bridge Design Specifications, Eight Edition, American Association of State Highway and Transportation Officials; Washington, D.C.

American Petroleum Institute (API) (2014). Petroleum and natural gas industries specific requirements for offshore structures. Part 4—Geotechnical and foundation design considerations, American Petroleum Institute, Washington, DC

Ashford S.A., Boulanger R.W., and Brandenberg S.J. (2011). Recommended Design Practice for Pile Foundations in Laterally Spreading Ground. Pacific Earthquake Engineering Center, Berkeley, California.

Bhattacharya S., Adhikari S., Alexander N.A. (2009). A Simplified Method For Unified Buckling And Free Vibration Analysis Of Pile-Supported Structures In Seismically Liquefiable Soils. Soil Dynamics and Earthquake Engineering.

Bhattacharya, S., Bolton, M.D. and Madabhushi, S.P.G (2005). "A reconsideration of the safety of the existing piled bridge foundations in liquefiable soils", Soils and Foundations (Japan) Vol. 45, No 4. (August 2005 Issue).

Boulanger, R. W. and Idriss, I. M. (2014) "CPT and SPT Based Liquefaction Triggering Procedures", Report UCD/CGM.- 14/01, Department of Civil and Environmental Engineering, University of California, Davis, CA, 138 pp.

Bowen H. J. And Cubrinovski M.(2008) Effective Stress Analysis Of Piles In Liquefiable Soil: A Case Study Of A Bridge Foundation, Bulletin Of The New Zealand Society For Earthquake Engineering, Vol. 41, No. 4, December 2008

Bowen, H. and Cubrinovski, M. (2008). Pseudo-static analysis of piles in liquefied soils: a case study of a bridge foundation. Bulletin of the New Zealand Society for Earthquake Engineering, 41(4), 234-246.

California Department of Transportation (Caltrans), (2013). Guidelines for Foundation Loading and Deformation Due to Liquefaction Induced Lateral Spreading. Sacramento, CA.

CE 468 Geotechnical Design, Lecture Notes. Middle East Technical University, Ankara

CEN (2005). Eurocode 8 - Design of structures for earthquake resistance - Part 2: Bridges. European Committee For Standardization, Brussels

Cetin K. O., Youd T. L., Seed R. B., Bray J. D., Durgunoglu H. T., Lettis W., Yilmaz M. T. Liquefaction-induced lateral spreading at Izmit Bay during the 1999 Kocaeli (Izmit) – Turkey Earthquake. ASCE J. of Geotech. and Geoenvir. Eng. 130(12): 1300-1313, 2004.

Chang, K., Chang, D., Tsai, M., Sung, Y. (2000). Seismic Performance of Highway Bridges. Earthquake Eng. And Eng. Seismology. Vol. 2, No. 1, pp. 55-77.

Cubrinovski M., Ishihara K. and Poulos H. (2009). Pseudostatic analysis of piles subjected to lateral spreading. Special Issue, Bulletin of NZ Society for Earthquake Engineering, 42(1), 28–38.

Day R. W. (2012). Geotechnical Earthquake Engineering Handbook With the 2012 International Building Code. 2nd Edition. McGrawHill

DeMello V. (1971). The Standard Penetration Test - A State of the Art Report. 4th. PanAmerican Conf. on SMFE, 1: 1 – 86.

DLH, (2007). Earthquake Technical Specification for Coastal and Harbor Structures, Railways, Airports (in Turkish). General Directorate of Railways Harbors and Airports Construction, Ankara

Elgamal, A (2010). Calibrated 3D Computational Modeling of Soil- Structure Systems and Liquefaction Scenarios. International Conferences on Recent Advances in Geotechnical Earthquake Engineering and Soil Dynamics. 1.

Elgamal, A., Yang, Z., Para, E., Ragheb, A., (2002). Modeling of cyclic mobility in saturated cohesionless soils, International Journal Plast., 19(6), 883– 905.

Elgamal A., Yang Z., and Lu J. (2015). Cyclic1D: Seismic Ground Response Version 1.4 User's Manual. University of California, San Diego

Escribano D., Bhattacharya S. (2011). Performance of Pile-Supported Bridges In Liquefiable Soils During Major Earthquakes. 5 Th Int. Conf. On Earthquake Geotechnical Engineering, January, Santiago, Chile

FHWA-NHI. 2014. LRFD Seismic Analysis and Design of Bridges Reference Manual. U.S. Department of Transportation Federal Highway Administration, Publication No. FHWA-NHI-15-004.

Franke, K.W., and Rollins, K.M., 2013. Simplified Hybrid p-y Spring Model for Liquefied Soils. Journal of Geotechnical and Geoenvironmental Engineering, ASCE, Vol. 139, No. 4, pp. 564-576.

Hamada, M., Towhata, I., Yasuda, S., Isoyama, R., and Emoto, K. (1987). Study on liquefaction- induced permanent ground displacements. Computers and Geotechnics 4 (1987) pg. 197-220

Hatanaka M. and Uchida A. (1996). "Empirical Correlation between Penetration Resistance and Internal Friction Angle of Sandy Soils" Soils and Foundations, 36(4): 1 – 10.

Idriss, I. M., and Boulanger, R. W. (2008). Soil liquefaction during earthquakes. Monograph MNO-12, Earthquake Engineering Research Institute, Oakland, CA, 261 pp.

Imbsen R. A. (2007). AASHTO Guide Specifications for LRFD Seismic Bridge Design

Isenhower W. M., Wang S.T, Vasquez L. G. (2017). Technical Manual for LPile 2018 (Using Data Format Version 10) Ensoft Inc., Austin, Texas.

Ishihara, K. (1985). Stability of Natural Deposits During Earthquakes. Proceedings of the Eleventh International Conference on Soil Mechanics and Foundation Engineering, vol. 1, San Francisco, pp. 321–376.

Japan Road Association, JRA (2002). Part V, Seismic Design, Specifications for Highway Bridges

Kayen, R. E., Mitchell, J. K., Seed, R. B., Lodge, A., Nishio, S., and Coutinho, R. (1992). "Evaluation of SPT-, CPT-, and Shear Wave-Based Methods for Liquefaction Potential Assessments Using Loma Prieta Data." Proceedings, 4th Japan-U.S. Workshop on Earthquake Resistant Design of Lifeline Facilities and Countermeasures for Soil Liquefaction, NCEER-92-0019. National Center for Earthquake Engineering, Buffalo, NY, pp. 177–192.

Kramer, S. L. (1996). Geotechnical Earthquake Engineering. Prentice-Hall, Englewood Cliffs, NJ.

Lambe, T.W. and Whitman, R.V. (1969) Soil Mechanics. John Wiley & Sons, New York.

Lindfield G.R., Penny J.E.T. (2012). Numerical Methods Using MATLAB®. 3rd edition, Academic Press, Oxford

Liyanapathirana D.S., Poulos H.G. A Numerical Model For Dynamic Soil Liquefaction Analysis

Marto A, Tan C S, Kasim F. and Suhatril M. (2013). A Correlation Of Shear Wave Velocity And Standard Penetration Resistance, Electronic Journal of Geotechnical Engineering, 18c pp. 463 – 471.

Menun C., Kiureghian A. D. (1998). A Replacement for the 30%, 40%, and SRSS Rules for Multicomponent Seismic Analysis. Earthquake Spectra, Volume 14, No. 1, February 1998

Mokwa, R.L., and Duncan, J.M., "Investigation of the Resistance of Pile Caps and Integral Abutments to Lateral Loading", Final Contract Report, February 2000, Virginia Transportation Research Council, Charlottesville, VA

Murashev A.K., Kirkcaldie D.K., Keepa C., Cubrinovski M., Orense R. (2013). Development of the design guidance for bridges in New Zealand for liquefaction and lateral spreading effects, draft report for NZ Transport Agency' research project TAR 12/09

Murashev A.K., Kirkcaldie D.K., Keepa C., Cubrinovski M., Orense R., Lloyd J. N. (2014).The Assessment of Liquefaction and Lateral Spreading Effects On Bridges. NZSEE, New Zealand Society for Earthquake Engineering 2014 Conference Paper. Auckland

NISEE: National Information Services for Earthquake Engineering, University of California, Berkeley

PEER, (2010). User's Manual for the PEER Ground Motion Database Web Application Beta Version – October 1, 2010

Reese, L. C., Cox, W. R., and Koop, F. D., (1974). Analysis of Laterally Loaded Piles in Sand. Proceedings, 6th Offshore Technology Conference, Vol. II, pp. 473-484.

Rocscience Inc. (2018). Laterally Loaded Piles. Toronto

Schmertmann J.H. (1975). "Measurement of In-Situ Shear Strength" 7th PSC, ASCE, 2: 57 -138.

Seed, H. B., and Lee, K. L. (1965). Studies of Liquefaction of Sands Under Cyclic Loading Conditions. Report TE-65-65. Department of Civil Engineering, University of California, Berkeley.

Seed, H. B., Mori, K., and Chan, C. K. (1975). "Influence of Seismic History on the Liquefaction Characteristics of Sands." Report EERC 75-25. Earthquake Engineering Research Center, University of California, Berkeley.

Seed, H. B., Tokimatsu, K., Harder, L. F., and Chung, R. (1985). "Influence of SPT Procedures in Soil Liquefaction Resistance Evaluations." Journal of Geotechnical Engineering, ASCE, vol. 111, no. 12, pp. 1425–1445.

Seismosoft, 2018. A software (SeismoSeignal) capable of adjusting earthquake accelerograms

Shamoto, Y., Zhang, J., and Tokimatsu, K. (1998). New charts for predicting large residual post-liquefaction ground deformations. Soil dynamics and earthquake engineering, Vol. 17, Elsevier, New York, 427–438.

Theryo, T.S. (2005). Precast Balanced Cantilever Bridge Design Using AASHTO LRFD Bridge Design Specifications.American Segmental Bridge Institute.

Tokimatsu K. and Asaka Y. (1998). Effects of liquefaction-induced ground displacements on pile performance in the 1995 Hyogoken-Nambu earthquake, Special Issue on Geotechnical Aspects of the January 15, 1995 Hyogoken-Nambu Earthquake, No. 2, Soils and Foundations, 163−177

Tokimatsu K. and Yoshimi Y. (1983). Emprical correlation of soil liquefaction based on SPT N-Value and Fines Content, Soils and Foundations, Vol. 23, No. 4, Dec. 1983

U.S. Geological Survey Data Series, DDS-21, 1995. Earth Science Photographs From U.S. Geological Survey Library

Wang, R. (2016). Single Piles in Liquefiable Ground: Seismic Response and Numerical Analysis Methods. Springer, Heidelberg

Wu, J., Seed, R.B. and Pestana, J.M. (2003). Liquefaction Triggering and Post Liquefaction Deformations of Monterey 0/30 Sand under Uni-Directional Cyclic Simple Shear Loading. Geotechnical Engineering Report No. UCB/GE-2003/01, April 2003, UC, Berkeley

Yan, L. (2006). Sensor Data Analysis and Information Extraction for Structural Health Monitoring. Ph.D. dissertation, Univ. of California, San Diego, Dept. of Structural Eng, La Jolla, CA.

Yoshida, N., Tazoh, T., Wakamatsu, K., Yasuda S., Towahata I., Nakazawa, H. and Kiku, H. (2007). “Causes of Showa Bridge collapse in the 1964 Niigata earthquake based on eye witness testimony”. Soils and Foundations, 47(6), pp.1075-1087.

Youd T. L, Carter B. (2003). Influence of Soil Softening and Liquefaction on Response Spectra for Bridge Design. Utah Department of Transportation Research and Development Division

Youd, T. L., Hansen, C. M., and Bartlett, S. F. (2002). Revised multilinear regression equations for prediction of lateral spread displacement. Journal of Geotech. Geoenviron. Eng., 128(12), 1007–1017.

APPENDICES

A. Bearing Capacity of Pile

Design Soil Parameters

Sl.No.	Description	Reduced Level		Depth of layer from ground		Soil Parameters			Interaction Parameters		
						c	ϕ	γ_{Sub}	k	δ	α
		From	To	From	To	kN/m^2	deg.	kN/m^3		deg.	
1	Clay	0	-5	0.0	5.0	50	0	18		0	1
2	Loose Sand	-5	-20	5.0	20.0	0	30	18	0.5	23	0
3	Dense Sand	-20	-30	20.0	30.0	0	39	20	0.5	29	0

Pile Details

Existing ground level	=	0	m
Pile Diameter, D	=	1.0	m
Pile Cut-off level	=	0.0	m
Dredge level	=	0.0	m
Scour level	=	0.0	m
Pile Founding level	=	-25.0	m
Depth from G.L.corresponding to F.L.	=	25.0	m
Pile Embedment length	=	25.0	m
Total Pile Length, L	=	25.0	m
Pile Density	=	25.0	kN/m^3
Factor of Safety	=	2.5	
Pile Fixity condition at top	=	fixed	(Fixed or Free)
Grade of Concrete	=	25	N/mm^2

Modulus of subgrade reaction at fixity zone	=	4000	kN/m3
Type of soil in fixity zone	=	Sand	(Sand or Clay)
Unsupported Length of Pile, L1	=	0.0	m
Allowable displacement of pile at head (For Horizontal capacity)	=	7.0	mm

Sketch

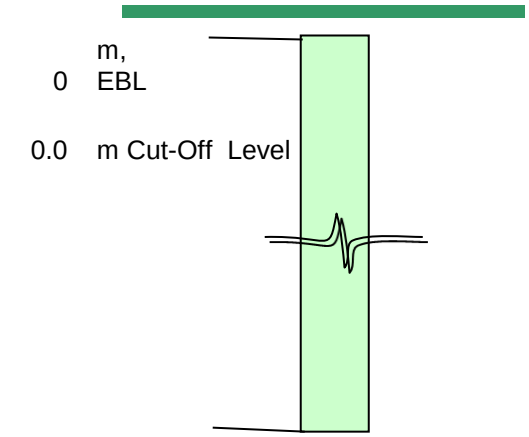

-25.0 m, Found. Level

Calculation of Vertical Capacity

Ultimate Capacity of Pile , Qult = Qb + Qs - Wp

Whetre, Qb = Ultimate End Bearing
Qs = Ultimate Skin Resistance
Wp = Self weight of Pile

Qsafe = Qult / FOS
Where, FOS = Factor of Safety

Calculation of Skin Resistances

Layer-1:

Layer thickness, L_1	=	5	m
Pile embedment in the layer, h_1	=	5	m

Ultimate Skin Resistance, Q_{s1} = $(\alpha * c_1 + K * P_{d1} * \tan\delta) \times A_{s1}$

Where, Reduction factor, α

α	=	1	
Cohesion, c_1	=	50	kN/m^2
Coefficient of Lateral earth pressure, K	=	0	
Unit weight of soil , γ_1	=	18	kN/m^3
Effective Overburden Pressure at middle of layer, P_{d1} $P_{d1} = h_1/2 * \gamma_1$	=	45	kN/m^2
Angle of wall friction, δ	=	0	deg.
Surface area of Pile in layer 1, $A_{s1} = pi * D * h_1$	=	15.7	m^2

Ultimate Skin Resistance, Q_{s1} = $(\alpha * c_1 + K * P_{d1} * \tan\delta) \times A_{s1}$ = 0 kN

Layer-2:

Layer thickness, L_2	=	15	m
Pile embedment in the layer, h_1	=	15	m

Ultimate Skin Resistance, Q_{s2} = $(\alpha * c_2 + K * P_{d2} * \tan\delta) \times A_{s2}$

Where, Reduction factor, α

α	=	0	
Cohesion, c_2	=	0	kN/m^2
Coefficient of Lateral earth pressure, K	=	0.5	
Unit weight of soil, γ_2	=	18	kN/m^3

Effective Overburden Pressure at middle of layer, P_{d2}			
$P_{d2} = P_{d1} + h_1/2 * \gamma_1 + h_2/2 * \gamma_2$	=	225	kN/m^2
Angle of wall friction, δ	=	23	deg.
Surface area of Pile in layer 2, $A_{s2} = pi * D * h_2$	=	47.1	m^2

Ultimate Skin Resistance, Q_{s2} = $(\alpha * c_2 + K * P_{d2} * \tan\delta) \times A_{s2}$ = 0 kN

Layer-3:

Layer thickness, L_3	=	10	m
Pile embedment in the layer, h_3	=	5	m

Ultimate Skin Resistance, Q_{s3} = $(\alpha * c_3 + K * P_{d3} * \tan\delta) \times A_{s3}$

Where, Reduction factor,

α	=	0	
Cohesion, c_3	=	0	kN/m^2
Coefficient of Lateral earth pressure, K	=	0.5	
Unit weight of soil, γ_3	=	20	kN/m^3
Effective Overburden Pressure at middle of layer, P_{d3}			
$P_{d3} = P_{d2} + h_2/2 * \gamma_2 + h_3/2 * \gamma_3$	=	410	kN/m^2
Angle of wall friction, δ	=	29	deg.
Surface area of Pile in layer 3, $A_{s3} = pi * D * h_3$	=	15.7	m^2

Ultimate Skin Resistance, Q_{s3} = $(\alpha * c_3 + K * P_{d3} * \tan\delta) \times A_{s3}$ = 1801.353 kN

Total Ultimate Skin resistance, $Qs = Q_{s1} + Q_{s2} + Q_{s3} + \ldots + Q_{sn}$ = 1801 kN

Ultimate End Bearing Resistance

Ultimate End bearing Resistance, $Q_b = (c^* N_c + P_d * N_q) * A_p$

Where,	Cohesion at Pile Toe, c	=	15	kN/m^2
	Bearing Capacity Factor, N_c	=	9	
	Effective overburden pressure at Pile tip, P_d $P_d = P_{d6} + h_6/2 *\gamma_6$	=	460	kN/m^2
	Angle of internal friction at pile toe,ϕ	=	29	
	Bearing Capacity Factor, N_q	=	18	
	Area of Pile at toe, A_p	=	0.785	m^2
Ultimate End bearing Resistance, $Q_b = (c^* N_c + P_d * N_q) * A_p$		=	6606	kN

Self Weight of the Pile, Wp

Self weight of the Pile , $W_p = A_p * L * \gamma_p$

Where,	Area of pile, A_p	=	0.785	m^2
	Total Length of Pile , L	=	25	m
	Unit Weight of Pile material, γ_p	=	25	kN/m^3
Self weight of the Pile , $W_p = A_p * L * \gamma_p$		=	491	kN

Ultimate Capacity of the Pile , $Q_{ult} = Q_b + Q_s - W_p$

Where,	Ultimate End Bearing, Qb	=	6606	kN
	Ultimate Skin Resistance, Qs	=	1801	kN
	Self weight of the Pile, Wp	=	491	kN
Ultimate Capacity of the Pile , $Q_{ult} = Q_b + Q_s - W_p$		=	7917	kN

Safe Capacity of Pile, $Q_{safe} = Q_{ult}$ / FOS

Where, Ultimate Capacity of Pile, Q_{ult}	=	7917	kN
Factor of Safety	=	2.5	
Safe Capacity of Pile, $Q_{safe} = Q_{ult}$ / FOS	=	3167	kN

Tension Capacity of Pile

Ultimate Tension Capacity of the Pile , $Q_{ult(T)} = 2/3 \times Q_s + W_p$

Where, Ultimate Skin Resistance, Qs	=	1801	kN
Self weight of the Pile, Wp	=	491	kN
Ultimate Tension Capacity of the Pile , $Q_{ult(T)} = 2/3 \times Q_s + W_p$	=	1692	kN

Safe Tension Capacity of the Pile , $Q_{safe(T)} = Q_{ult(T)}$ / FoS

Where, FoS = Factor of Safety	=	2.5	
Safe Tension Capacity of the Pile , $Q_{safe(T)} = Q_{ult(T)}$ / FoS	=	677	kN

B. Site Location for PGA

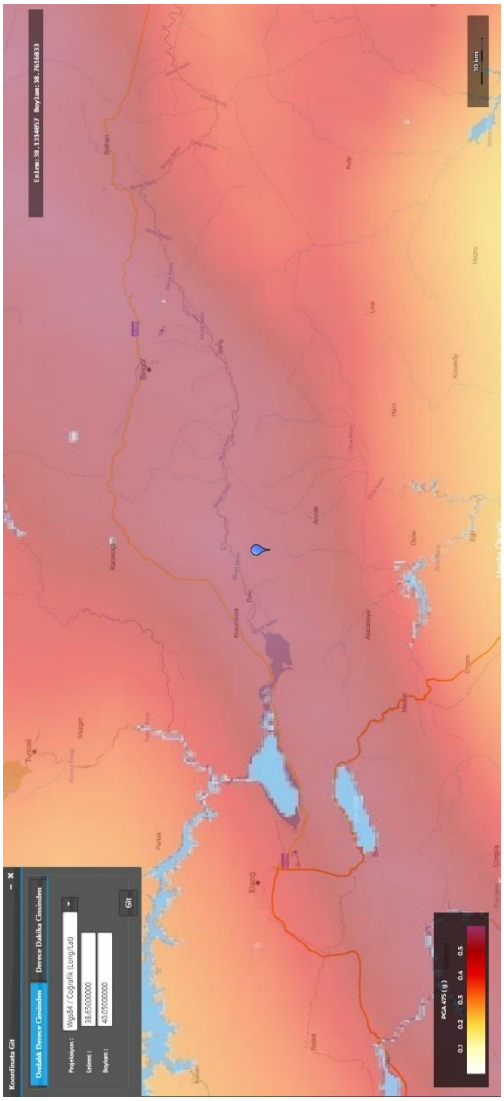

Figure B.1. Location of the selected PGA value

C. Site Spesific Response Analyses

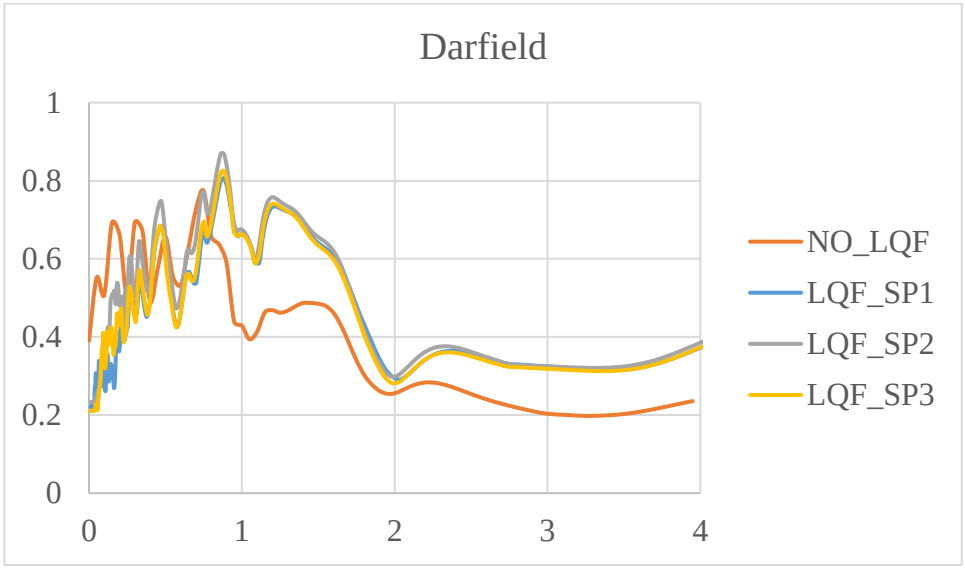

Figure C.1. Acceleration Response Spectra of Darfield Earthquake for non-liquefied and three different liquefied soil conditions

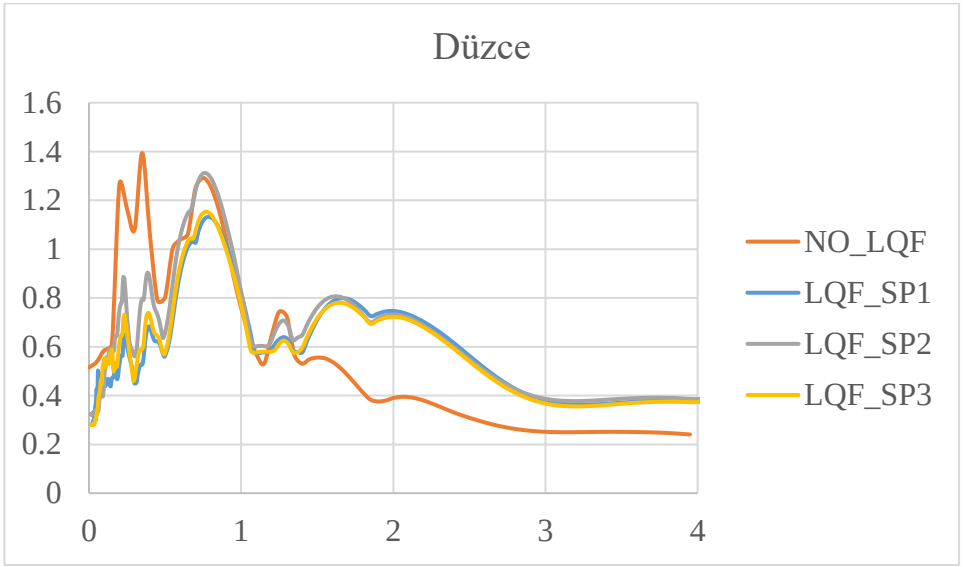

Figure C.2. Acceleration Response Spectra of Duzce Earthquake for non-liquefied and three different liquefied soil conditions

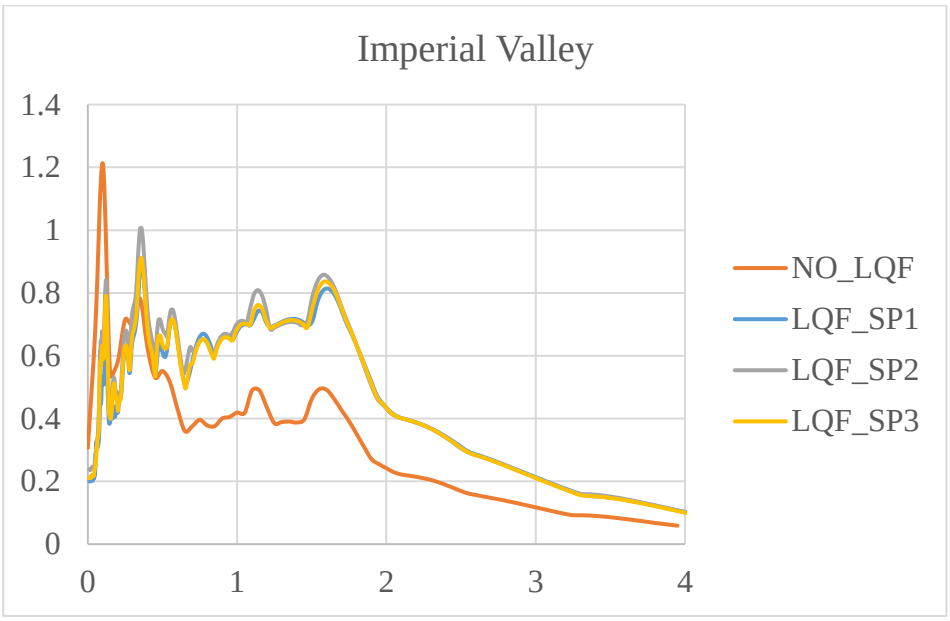

Figure C.3. Acceleration Response Spectra of Imperial Valley Earthquake for non-liquefied and three different liquefied soil conditions

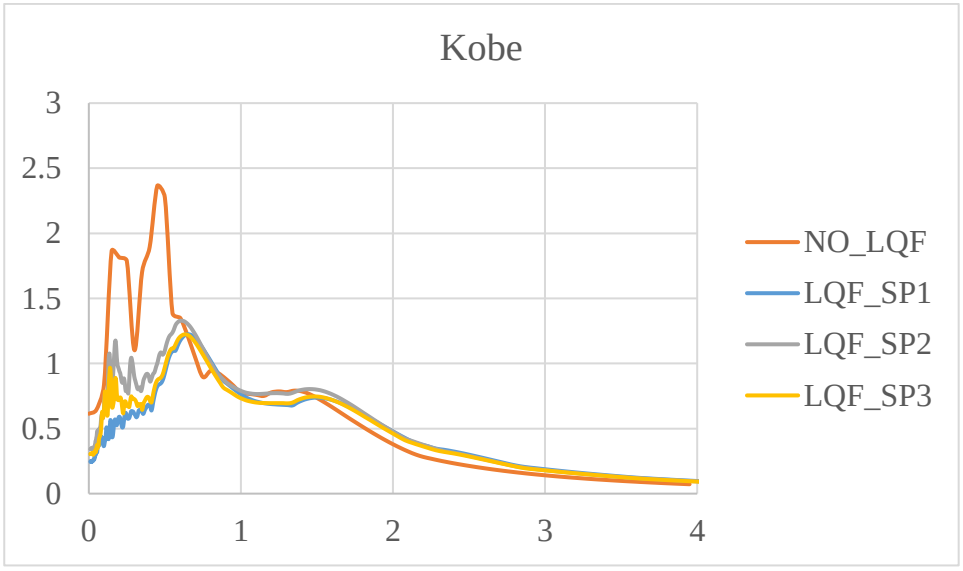

Figure C.4. Acceleration Response Spectra of Kobe Earthquake for non-liquefied and three different liquefied soil conditions

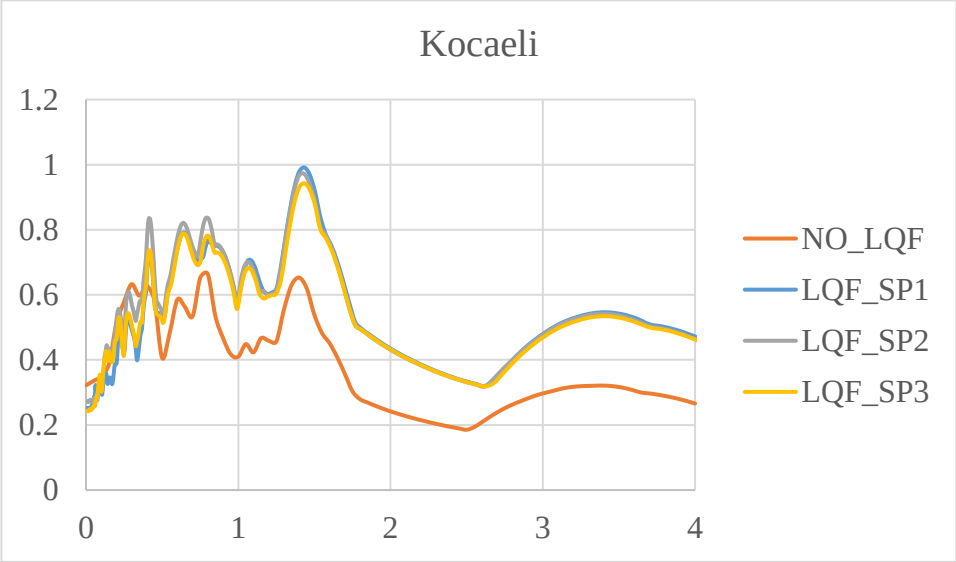

Figure C.5. Acceleration Response Spectra of Kocaeli Earthquake for non-liquefied and three different liquefied soil conditions

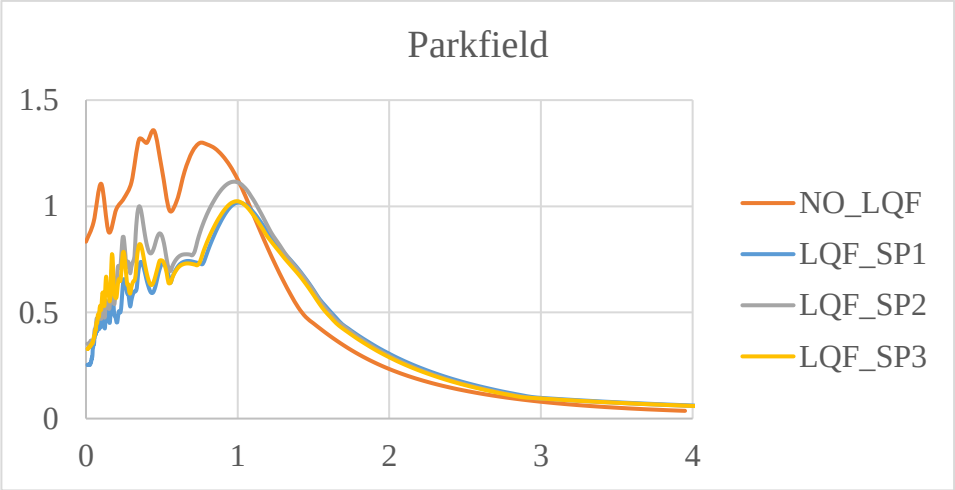

Figure C.6. Acceleration Response Spectra of Parkfield Earthquake for non-liquefied and three different liquefied soil conditions

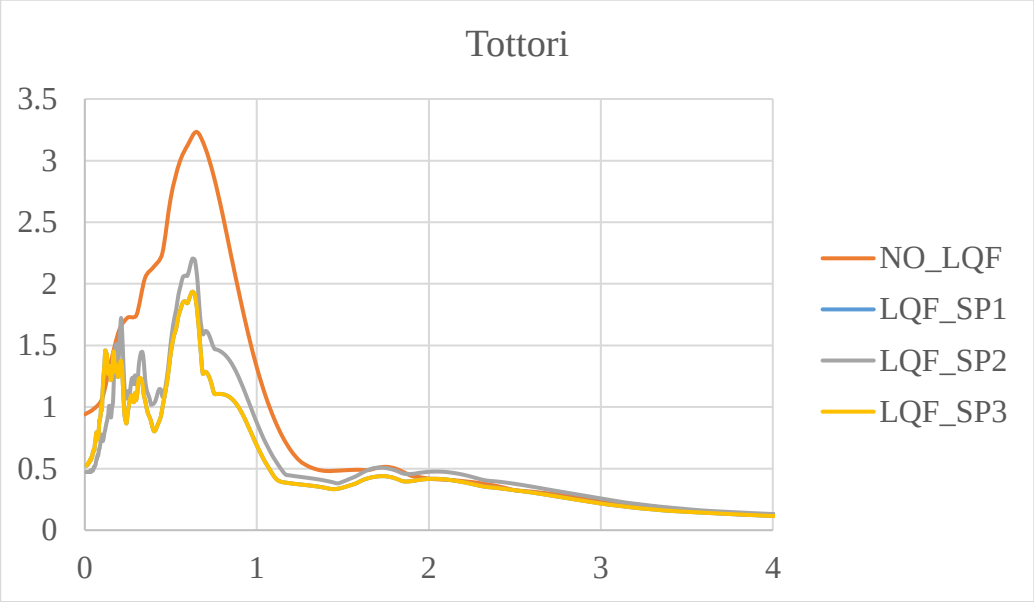

Figure C.7. Acceleration response spectra of tottori earthquake for non-liquefied and three different liquefied soil conditions

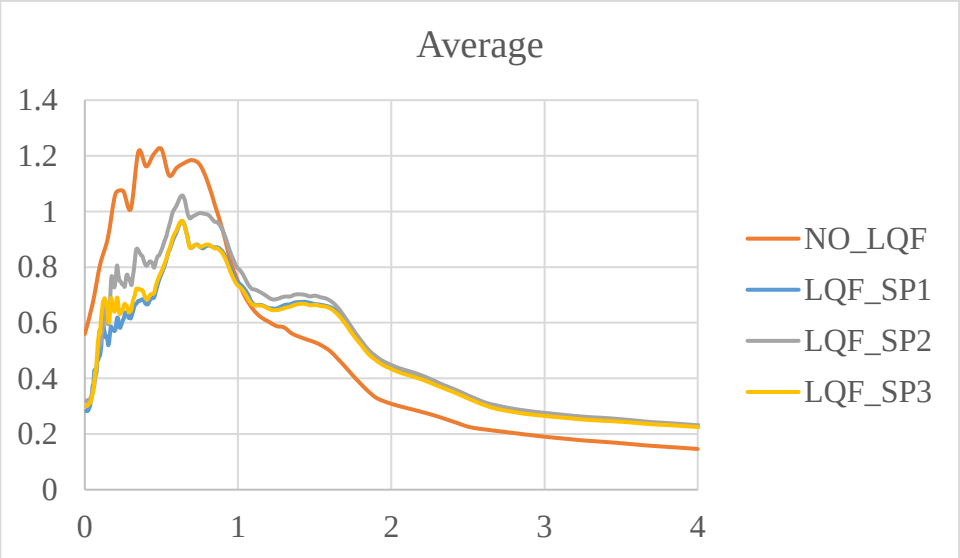

Figure C.8. Acceleration response spectra of average of the ground motions earthquake for non-liquefied and three different liquefied soil conditions

D. P-y Curves of Soils

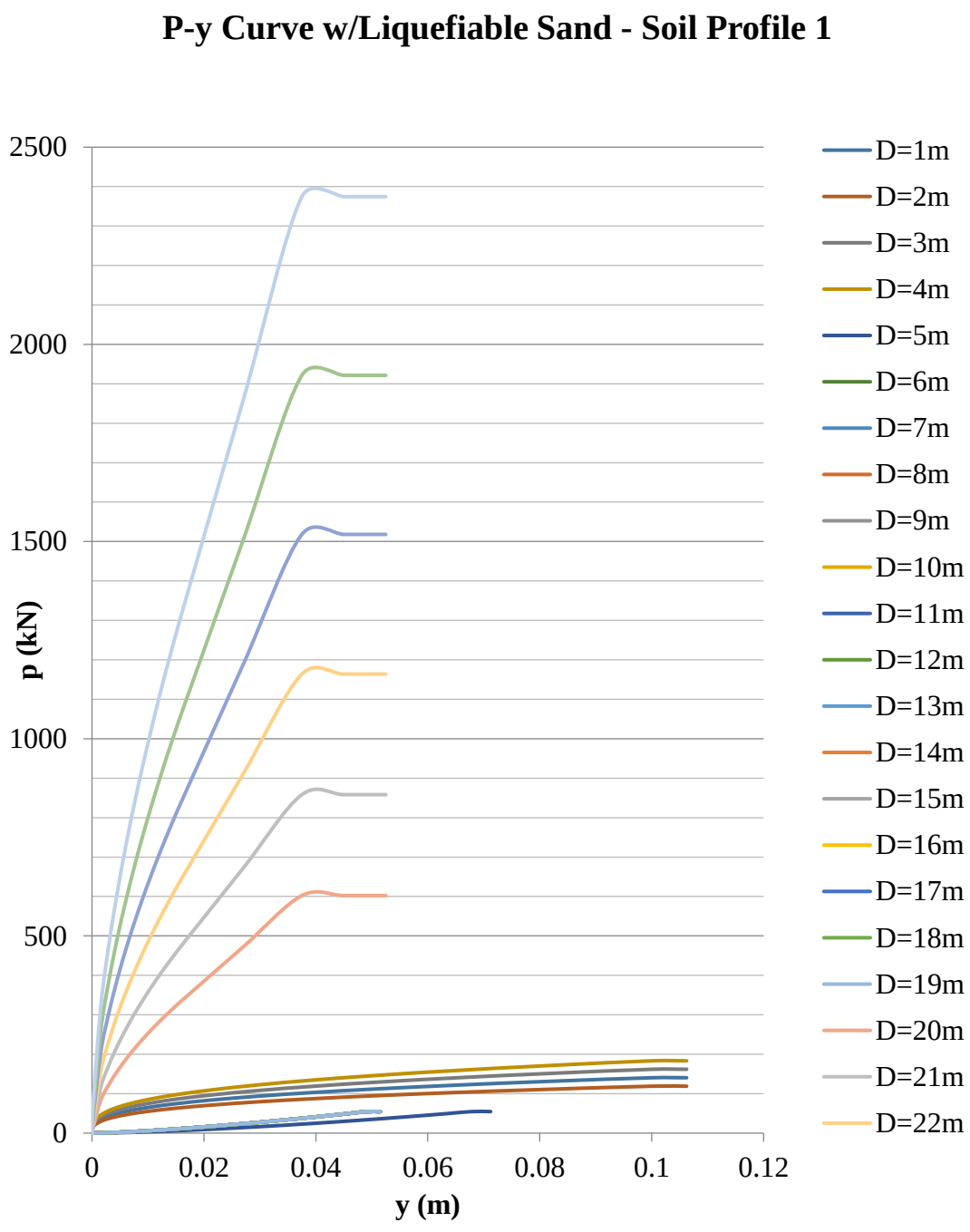

Figure D.1. P-y Curve w/ Liquefiable Sand - Soil Profile 1

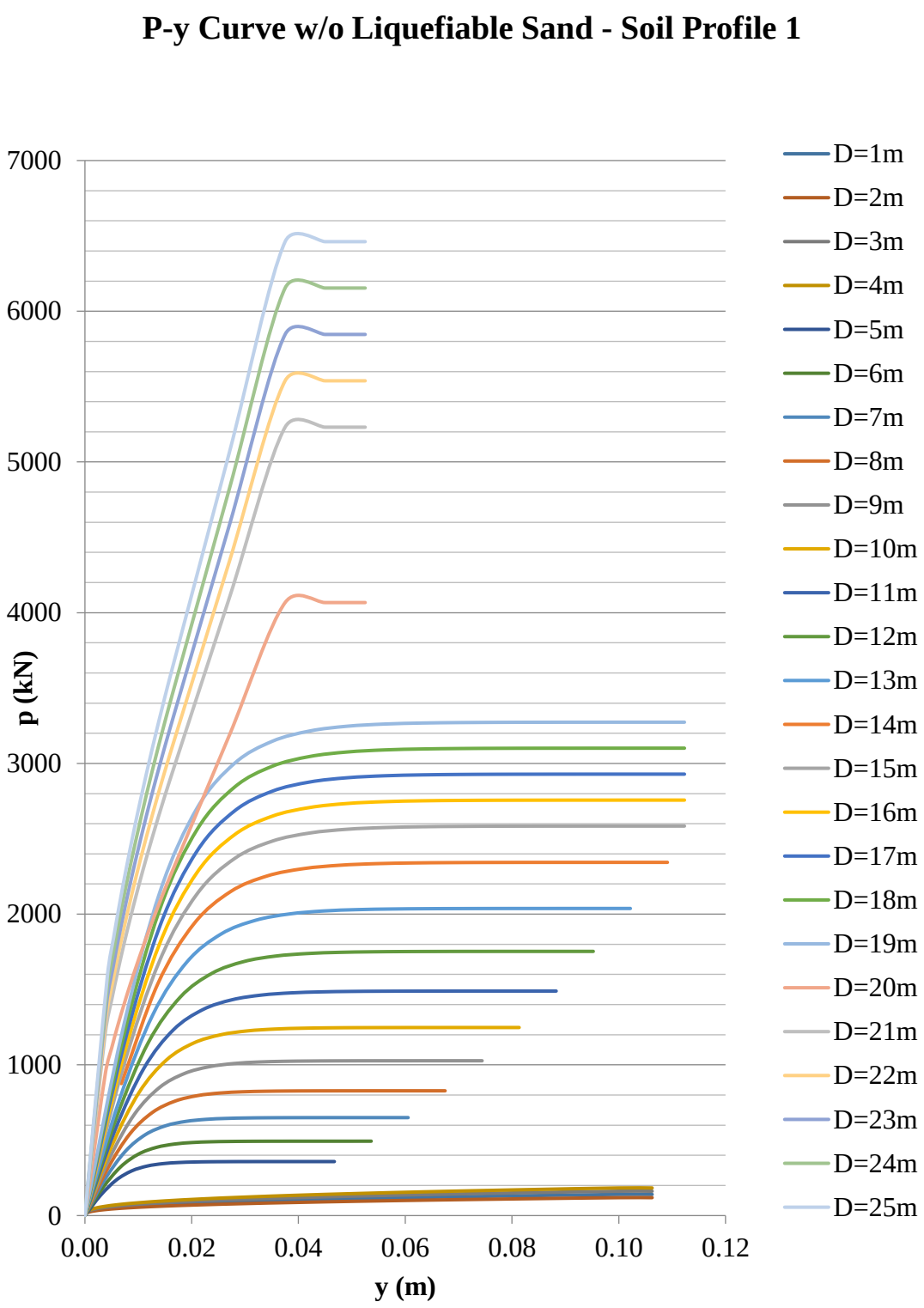

Figure D.2. P-y Curve w/o Liquefiable Sand - Soil Profile 1

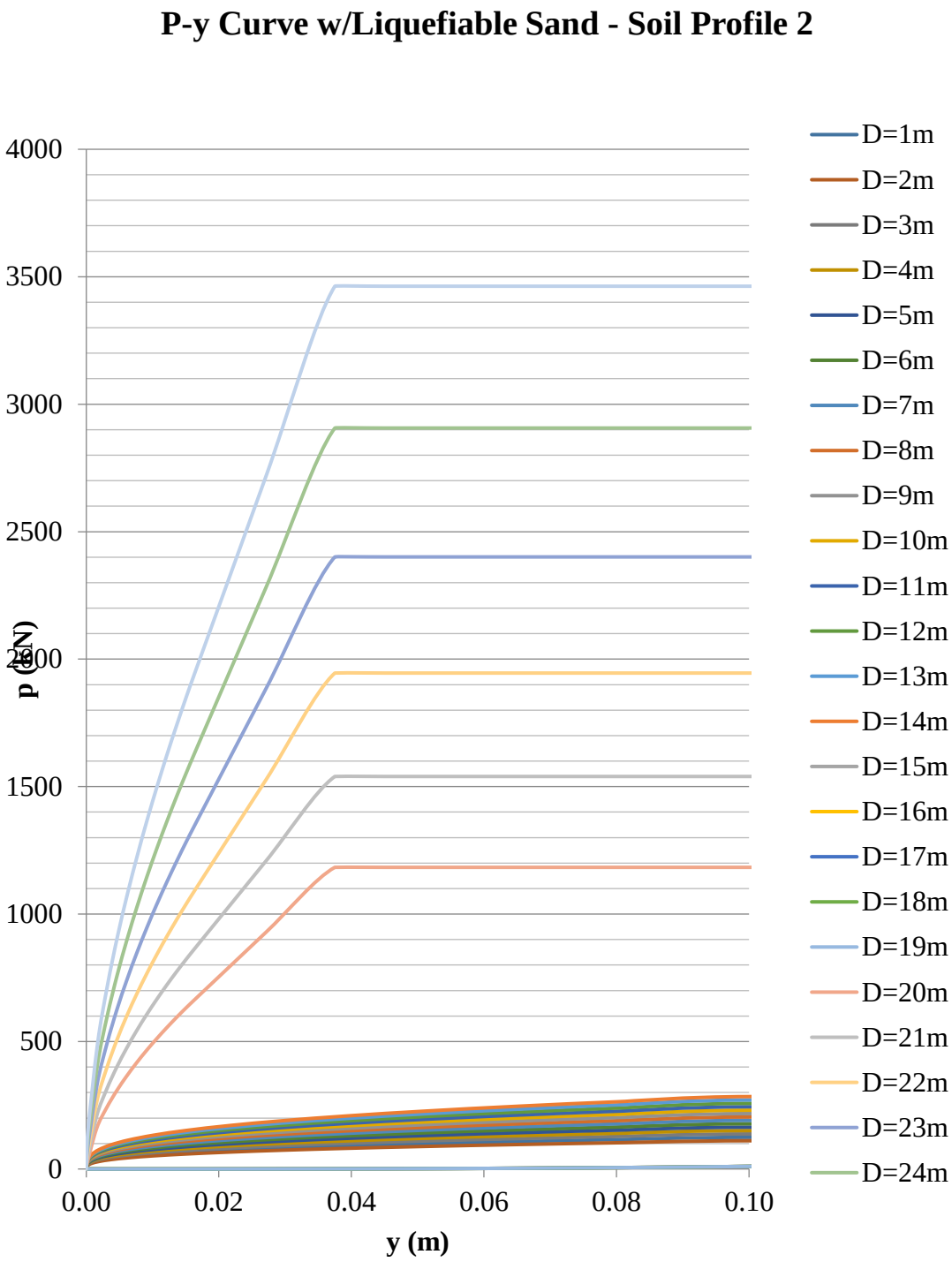

Figure D.3. P-y Curve w/ Liquefiable Sand - Soil Profile 2

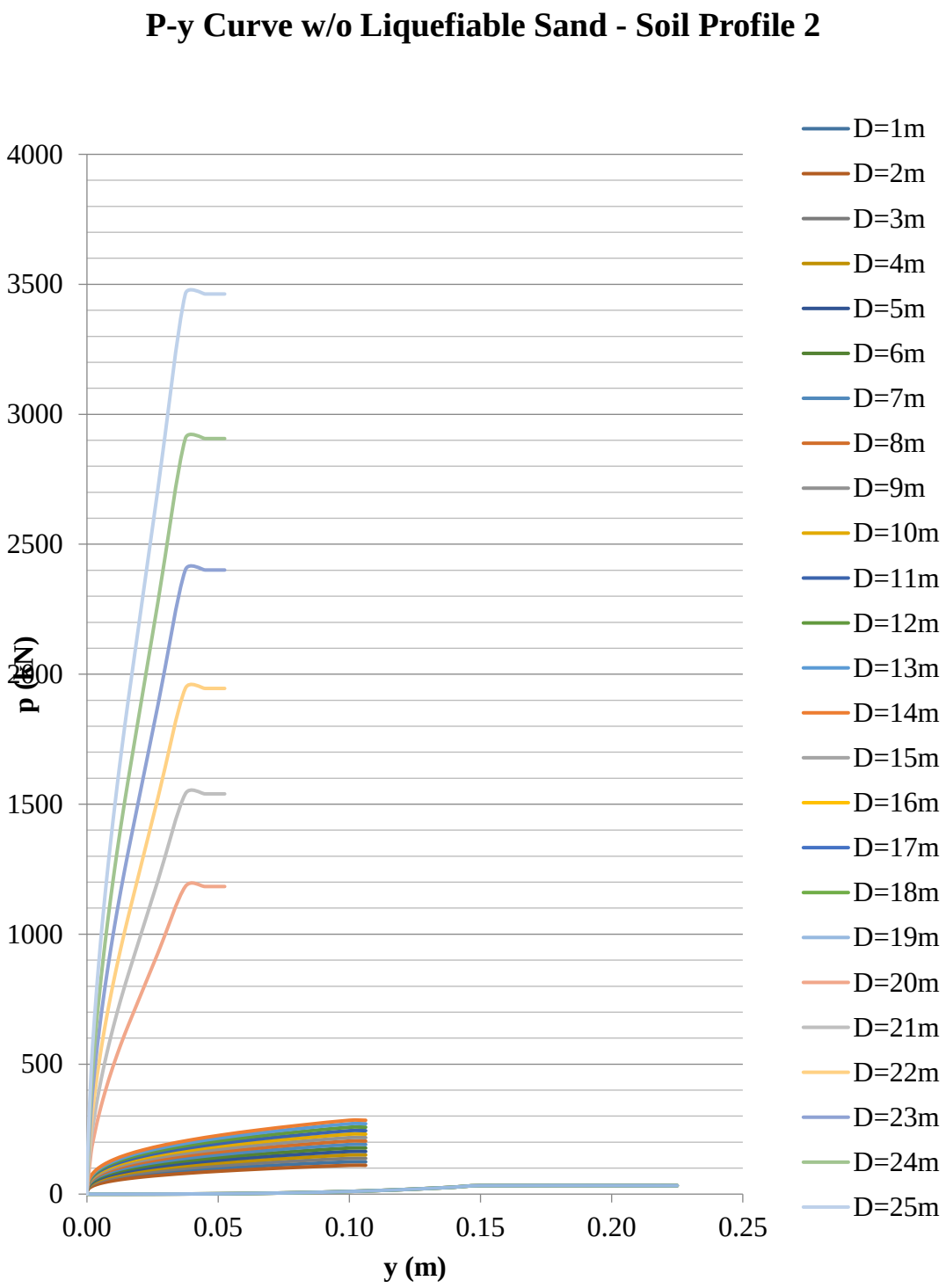

Figure D.4. P-y Curve w/o Liquefiable Sand - Soil Profile 2

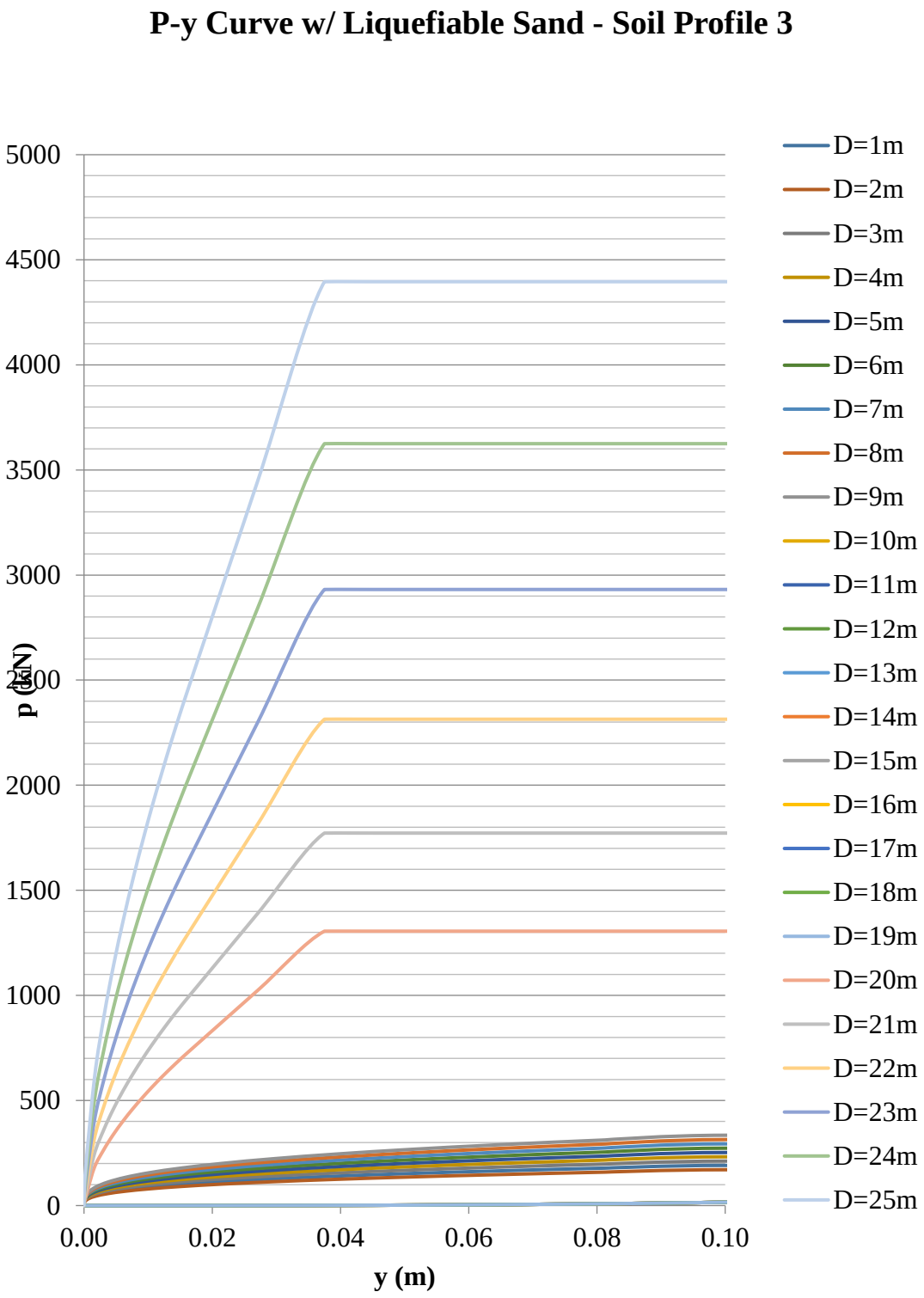

Figure D.5. P-y Curve w/ Liquefiable Sand - Soil Profile 3

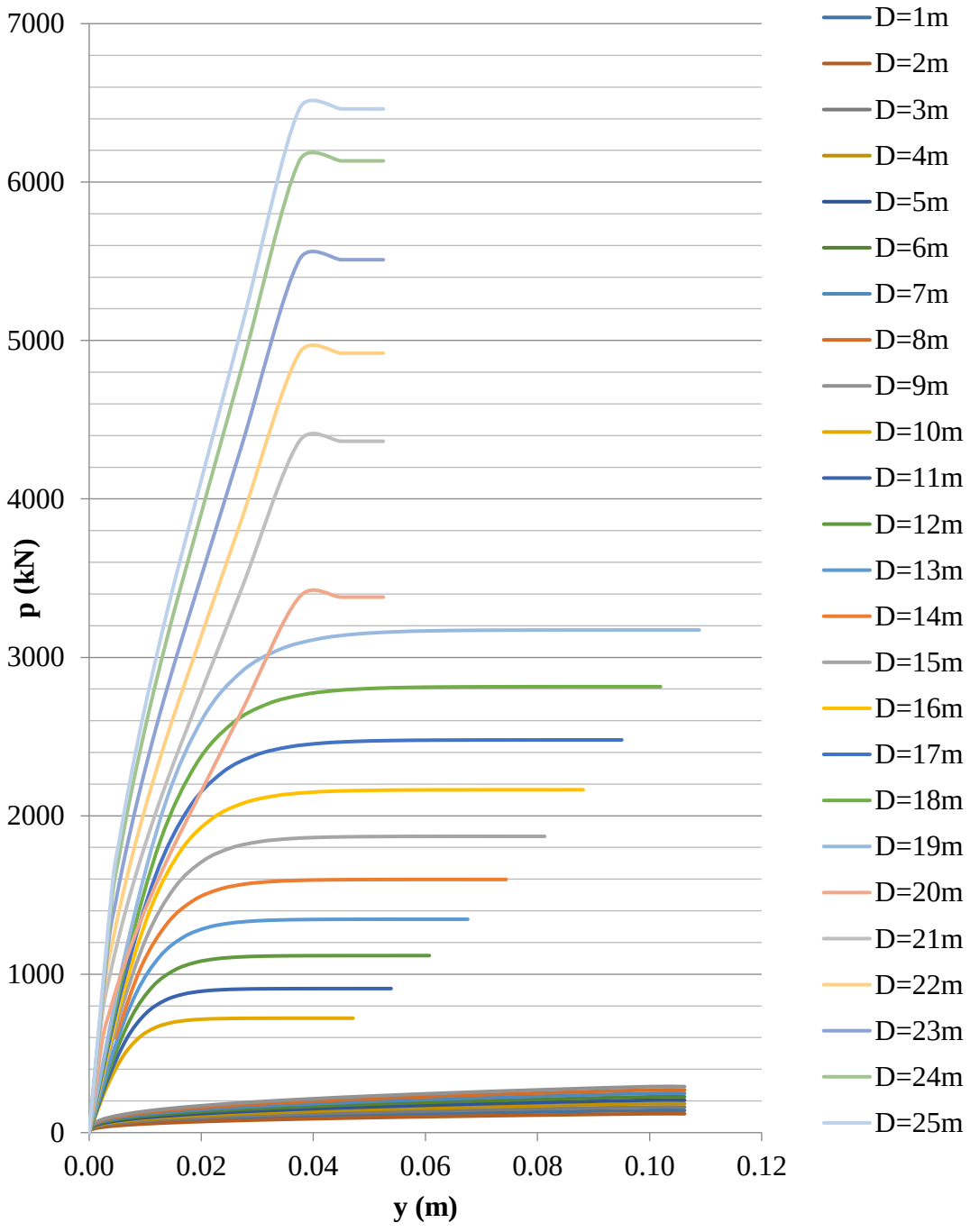

Figure D.6. P-y Curve w/o Liquefiable Sand - Soil Profile 3

E. Results Tables

Table E.1. *Displacements in non-liquefied inertial mode with uncracked parameters for SP-1*

	P1 (m)	P2 (m)	P3 (m)	P4 (m)
Column-X	0.011	0.013	0.193	0.008
Column-Y	0.029	0.051	0.051	0.029
Pile-X	0.001	0.004	0.000	0.000
Pile-Y	0.002	0.001	0.004	0.002

Table E.2. *Displacements in Non-Liquefied Inertial Mode with Cracked Parameters for SP - 1*

	P1 (m)	P2 (m)	P3 (m)	P4 (m)
Column-X	0.014	0.017	0.238	0.010
Column-Y	0.031	0.055	0.055	0.031
Pile-X	0.001	0.000	0.000	0.000
Pile-Y	0.002	0.004	0.004	0.002

Table E.3. *Displacements in Non-Liquefied Inertial Mode with Uncracked Parameters for SP - 2*

	P1 (m)	P2 (m)	P3 (m)	P4 (m)
Column-X	0.012	0.014	0.200	0.009
Column-Y	0.030	0.052	0.052	0.030
Pile-X	0.001	0.000	0.000	0.000
Pile-Y	0.002	0.004	0.004	0.002

Table E.4. *Displacements in Non-Liquefied Inertial Mode with Cracked Parameters for SP - 2*

	P1 (m)	P2 (m)	P3 (m)	P4 (m)
Column-X	0.015	0.018	0.247	0.012
Column-Y	0.032	0.057	0.057	0.032
Pile-X	0.001	0.000	0.000	0.000
Pile-Y	0.002	0.004	0.004	0.002

Table E.5. *Displacements in Non-Liquefied Inertial Mode with Uncracked Parameters for SP - 3*

	P1 (m)	P2 (m)	P3 (m)	P4 (m)
Column-X	0.011	0.013	0.200	0.009
Column-Y	0.030	0.052	0.052	0.030
Pile-X	0.001	0.000	0.000	0.000
Pile-Y	0.002	0.004	0.004	0.002

Table E.6. *Displacements in Non-Liquefied Inertial Mode with Cracked Parameters for SP - 3*

	P1 (m)	P2 (m)	P3 (m)	P4 (m)
Column-X	0.015	0.017	0.247	0.012
Column-Y	0.032	0.056	0.056	0.032
Pile-X	0.001	0.000	0.000	0.000
Pile-Y	0.002	0.004	0.004	0.002

Table E.7. *Pier Forces in Non-Liquefied Inertial Model with Uncracked Parameters for SP - 1*

	P (kN)	Vx (kN)	Vy (kN)	Mx (kNm)	My (kNm)
P1 - ColumnTop	713	281	7783	5934	214
P2 - ColumnTop	1212	336	13908	10605	257
P3 - ColumnTop	472	28645	13908	10605	21842
P4 - ColumnTop	1358	213	7783	5934	162
P1 - ColumnBot	750	2513	8213	64052	13808
P2 - ColumnBot	1216	1868	14122	44449	3625
P3 - ColumnBot	480	28854	14122	44449	91298
P4 - ColumnBot	1371	1153	7958	24963	2255

Table E.8. *Pier Forces in Non-Liquefied Inertial Model with Cracked Parameters for SP - 1*

	P (kN)	Vx (kN)	Vy (kN)	Mx (kNm)	My (kNm)
P1 - ColumnTop	476	266	7597	5793	203
P2 - ColumnTop	900	308	13589	10362	235
P3 - ColumnTop	319	23270	13589	10362	17743
P4 - ColumnTop	965	218	7597	5793	166
P1 - ColumnBot	544	2222	8026	62580	12352
P2 - ColumnBot	958	2701	14159	110971	14914
P3 - ColumnBot	387	23568	14158	110970	187654
P4 - ColumnBot	982	1619	8027	62577	9087

Table E.9. *Pier Forces in Non-Liquefied Inertial Model with Uncracked Parameters for SP - 2*

	P (kN)	Vx (kN)	Vy (kN)	Mx (kNm)	My (kNm)
P1 - ColumnTop	735	295	8020	6115	225
P2 - ColumnTop	1254	352	14226	10848	269
P3 - ColumnTop	498	29654	14226	10847	22611
P4 - ColumnTop	1408	225	8020	6115	172
P1 - ColumnBot	762	2637	8470	66008	14492
P2 - ColumnBot	1266	3138	14820	116078	17225
P3 - ColumnBot	552	30033	14820	116077	239148
P4 - ColumnBot	1459	2030	8471	66005	11101

Table E.10. *Pier Forces in Non-Liquefied Inertial Model with Cracked Parameters for SP - 2*

	P (kN)	Vx (kN)	Vy (kN)	Mx (kNm)	My (kNm)
P1 - ColumnTop	480	279	7816	5960	213
P2 - ColumnTop	922	330	13876	10580	252
P3 - ColumnTop	315	24132	13876	10580	18400
P4 - ColumnTop	1001	217	7816	5960	165
P1 - ColumnBot	509	2322	8264	64389	12919
P2 - ColumnBot	944	2736	14465	113287	15192
P3 - ColumnBot	330	24431	14465	113286	194547
P4 - ColumnBot	1016	1830	8265	64386	10140

Table E.11. *Pier Forces in Non-Liquefied Inertial Model with Uncracked Parameters for SP - 3*

	P (kN)	Vx (kN)	Vy (kN)	Mx (kNm)	My (kNm)
P1 - ColumnTop	760	291	8025	6119	222
P2 - ColumnTop	1260	347	14231	10851	264
P3 - ColumnTop	496	29673	14231	10851	22625
P4 - ColumnTop	1421	224	8026	6119	171
P1 - ColumnBot	875	2597	8468	66017	14276
P2 - ColumnBot	1293	3090	14815	116102	16952
P3 - ColumnBot	559	30051	14815	116101	239302
P4 - ColumnBot	1525	1999	8470	66014	10961

Table E.12. *Pier Forces in Non-Liquefied Inertial Model with Cracked Parameters for SP - 3*

	P (kN)	Vx (kN)	Vy (kN)	Mx (kNm)	My (kNm)
P1 - ColumnTop	489	276	7822	5964	210
P2 - ColumnTop	928	304	13880	10584	232
P3 - ColumnTop	357	24142	13880	10584	18408
P4 - ColumnTop	1019	244	7822	5964	186
P1 - ColumnBot	517	2296	8262	64399	12763
P2 - ColumnBot	935	2689	14461	113311	14838
P3 - ColumnBot	409	24440	14460	113310	194626
P4 - ColumnBot	1076	1832	8263	64396	10269

Table E.13. *Pile Forces in Non-Liquefied Inertial Model with Uncracked Parameters for SP - 1*

	P (kN)	Vx (kN)	Vy (kN)	Mx (kNm)	My (kNm)
P1 Axis	2145	519	539	294	247
P2 Axis	3703	875	720	462	412
P3 Axis	5735	1466	1820	1083	1103
P4 Axis	2127	510	488	286	237

Table E.14. *Pile Forces in Non-Liquefied Inertial Model with Cracked Parameters for SP - 1*

	P (kN)	Vx (kN)	Vy (kN)	Mx (kNm)	My (kNm)
P1 Axis	2083	504	544	290	237
P2 Axis	3597	852	641	433	399
P3 Axis	6820	1329	1550	943	956
P4 Axis	2067	495	577	302	228

Table E.15. *Pile Forces in Non-Liquefied Inertial Model with Uncracked Parameters for SP - 2*

	P (kN)	Vx (kN)	Vy (kN)	Mx (kNm)	My (kNm)
P1 Axis	2215	541	557	307	253
P2 Axis	3793	908	767	489	418
P3 Axis	8349	1493	1884	1105	1132
P4 Axis	2201	534	458	283	244

Table E.16. *Pile Forces in Non-Liquefied Inertial Model with Cracked Parameters for SP - 2*

	P (kN)	Vx (kN)	Vy (kN)	Mx (kNm)	My (kNm)
P1 Axis	2146	525	563	303	242
P2 Axis	3682	883	773	481	402
P3 Axis	7037	1356	1605	963	980
P4 Axis	2125	518	461	279	234

Table E.17. *Pile Forces in Non-Liquefied Inertial Model with Uncracked Parameters for SP - 3*

	P (kN)	Vx (kN)	Vy (kN)	Mx (kNm)	My (kNm)
P1 Axis	2214	544	559	304	266
P2 Axis	3781	900	769	483	439
P3 Axis	8331	1512	1878	1155	1160
P4 Axis	2203	536	472	285	257

Table E.18. *Pile Forces in Non-Liquefied Inertial Model with Cracked Parameters for SP - 3*

	P (kN)	Vx (kN)	Vy (kN)	Mx (kNm)	My (kNm)
P1 Axis	2140	528	565	298	255
P2 Axis	3660	875	627	440	423
P3 Axis	7015	1370	1604	1003	1007
P4 Axis	2136	522	626	313	248

Table E.19. *Displacements in Liquefied Inertial Mode with Uncracked Parameters for SP - 1*

	P1 (m)	P2 (m)	P3 (m)	P4 (m)
Column-X	0.004	0.005	0.215	0.003
Column-Y	0.023	0.044	0.044	0.023
Pile-X	0.000	0.000	0.000	0.000
Pile-Y	0.002	0.003	0.003	0.002

Table E.20. *Displacements in Liquefied Inertial Mode with Cracked Parameters for SP - 1*

	P1 (m)	P2 (m)	P3 (m)	P4 (m)
Column-X	0.005	0.006	0.330	0.004
Column-Y	0.025	0.047	0.047	0.025
Pile-X	0.000	0.000	0.000	0.000
Pile-Y	0.002	0.003	0.003	0.002

Table E.21. *Displacements in Liquefied Inertial Mode with Uncracked Parameters for SP - 2*

	P1 (m)	P2 (m)	P3 (m)	P4 (m)
Column-X	0.004	0.005	0.228	0.003
Column-Y	0.025	0.048	0.048	0.025
Pile-X	0.000	0.000	0.000	0.000
Pile-Y	0.002	0.003	0.003	0.002

Table E.22. *Displacements in Liquefied Inertial Mode with Cracked Parameters for SP - 2*

	P1 (m)	P2 (m)	P3 (m)	P4 (m)
Column-X	0.006	0.007	0.343	0.004
Column-Y	0.028	0.052	0.052	0.028
Pile-X	0.000	0.000	0.000	0.000
Pile-Y	0.002	0.003	0.003	0.002

Table E.23. *Displacements in Liquefied Inertial Mode with Uncracked Parameters for SP - 3*

	P1 (m)	P2 (m)	P3 (m)	P4 (m)
Column-X	0.004	0.004	0.213	0.004
Column-Y	0.023	0.043	0.043	0.023
Pile-X	0.000	0.000	0.000	0.000
Pile-Y	0.001	0.003	0.003	0.001

Table E.24. *Displacements in Liquefied Inertial Mode with Cracked Parameters for SP - 3*

	P1 (m)	P2 (m)	P3 (m)	P4 (m)
Column-X	0.006	0.006	0.325	0.006
Column-Y	0.024	0.046	0.046	0.024
Pile-X	0.000	0.000	0.000	0.000
Pile-Y	0.001	0.003	0.003	0.001

Table E.25. *Pier Forces in Liquefied Inertial Model with Uncracked Parameters for SP - 1*

	P (kN)	Vx (kN)	Vy (kN)	Mx (kNm)	My (kNm)
P1 - ColumnTop	544	97	5908	4505	74
P2 - ColumnTop	1215	115	11286	8606	88
P3 - ColumnTop	224	30789	11286	8606	23477
P4 - ColumnTop	1343	75	5908	4505	57
P1 - ColumnBot	556	897	6097	48163	4888
P2 - ColumnBot	1219	1086	11596	91768	5879
P3 - ColumnBot	234	31186	11596	91767	248365
P4 - ColumnBot	1352	658	6097	48161	3624

Table E.26. *Pier Forces in Liquefied Inertial Model with Cracked Parameters for SP - 1*

	P (kN)	Vx (kN)	Vy (kN)	Mx (kNm)	My (kNm)
P1 - ColumnTop	420	87	5735	4373	66
P2 - ColumnTop	1131	102	10941	8342	78
P3 - ColumnTop	151	31508	10941	8342	24025
P4 - ColumnTop	1220	68	5735	4373	52
P1 - ColumnBot	423	741	5924	46785	4106
P2 - ColumnBot	1132	894	11251	89018	4934
P3 - ColumnBot	163	31895	11251	89017	254108
P4 - ColumnBot	1225	551	5924	46784	3063

Table E.27. *Pier Forces in Liquefied Inertial Model with Uncracked Parameters for SP - 2*

	P (kN)	Vx (kN)	Vy (kN)	Mx (kNm)	My (kNm)
P1 - ColumnTop	588	97	6521	4972	74
P2 - ColumnTop	1295	116	12360	9424	89
P3 - ColumnTop	256	32741	12360	9424	24965
P4 - ColumnTop	1431	73	6521	4972	56
P1 - ColumnBot	591	900	6739	53208	4900
P2 - ColumnBot	1297	1089	12700	100502	5903
P3 - ColumnBot	263	33164	12700	100501	264113
P4 - ColumnBot	1436	661	6739	53206	3616

Table E.28. *Pier Forces in Liquefied Inertial Model with Cracked Parameters for SP - 2*

	P (kN)	Vx (kN)	Vy (kN)	Mx (kNm)	My (kNm)
P1 - ColumnTop	445	104	6430	4903	79
P2 - ColumnTop	1177	120	12164	9275	91
P3 - ColumnTop	166	32740	12164	9275	24964
P4 - ColumnTop	1269	75	6430	4903	57
P1 - ColumnBot	448	889	6652	52510	4925
P2 - ColumnBot	1179	1071	12510	98979	5898
P3 - ColumnBot	170	33142	12510	98978	264044
P4 - ColumnBot	1271	662	6652	52508	3649

Table E.29. *Pier Forces in Liquefied Inertial Model with Uncracked Parameters for SP - 3*

	P (kN)	Vx (kN)	Vy (kN)	Mx (kNm)	My (kNm)
P1 - ColumnTop	547	103	5922	4516	78
P2 - ColumnTop	1215	108	11280	8601	82
P3 - ColumnTop	229	30720	11280	8601	23424
P4 - ColumnTop	1343	97	5922	4516	74
P1 - ColumnBot	569	950	6112	48287	5180
P2 - ColumnBot	1221	1003	11585	91700	5453
P3 - ColumnBot	255	31114	11585	91699	247805
P4 - ColumnBot	1352	898	6112	48285	4884

Table E.30. *Pier Forces in Liquefied Inertial Model with Cracked Parameters for SP - 3*

	P (kN)	Vx (kN)	Vy (kN)	Mx (kNm)	My (kNm)
P1 - ColumnTop	418	100	5761	4393	76
P2 - ColumnTop	1120	100	10948	8348	77
P3 - ColumnTop	148	31171	10948	8348	23768
P4 - ColumnTop	1207	100	5761	4393	77
P1 - ColumnBot	428	877	5952	47011	4855
P2 - ColumnBot	1121	881	11254	89064	4862
P3 - ColumnBot	157	31551	11254	89063	251380
P4 - ColumnBot	1209	878	5953	47009	4846

Table E.31. *Pile Forces in Liquefied Inertial Model with Uncracked Parameters for SP - 1*

	P (kN)	Vx (kN)	Vy (kN)	Mx (kNm)	My (kNm)
P1 Axis	1486	145	458	153	170
P2 Axis	2828	276	867	291	154
P3 Axis	7627	2308	867	877	788
P4 Axis	1486	145	458	153	170

Table E.32. *Pile Forces in Liquefied Inertial Model with Cracked Parameters for SP - 1*

	P (kN)	Vx (kN)	Vy (kN)	Mx (kNm)	My (kNm)
P1 Axis	1443	141	445	148	165
P2 Axis	2743	268	841	282	314
P3 Axis	7799	2358	841	897	807
P4 Axis	1443	141	415	148	165

Table E.33. *Pile Forces in Liquefied Inertial Model with Uncracked Parameters for SP - 2*

	P (kN)	Vx (kN)	Vy (kN)	Mx (kNm)	My (kNm)
P1 Axis	1642	153	502	169	188
P2 Axis	3098	289	943	319	355
P3 Axis	8111	2437	943	932	842
P4 Axis	1642	153	502	169	188

Table E.34. *Pile Forces in Liquefied Inertial Model with Cracked Parameters for SP - 2*

	P (kN)	Vx (kN)	Vy (kN)	Mx (kNm)	My (kNm)
P1 Axis	1620	151	495	167	185
P2 Axis	3051	285	929	314	349
P3 Axis	8105	2434	929	932	842
P4 Axis	1620	151	495	167	185

Table E.35. *Pile Forces in Liquefied Inertial Model with Uncracked Parameters for SP - 3*

	P (kN)	Vx (kN)	Vy (kN)	Mx (kNm)	My (kNm)
P1 Axis	1468	166	468	204	171
P2 Axis	2784	314	884	388	324
P3 Axis	7498	2353	884	876	1049
P4 Axis	1468	166	468	204	171

Table E.36. *Pile Forces in Liquefied Inertial Model with Cracked Parameters for SP - 3*

	P (kN)	Vx (kN)	Vy (kN)	Mx (kNm)	My (kNm)
P1 Axis	1429	161	456	199	166
P2 Axis	2704	305	858	377	315
P3 Axis	7602	2385	862	888	1064
P4 Axis	1429	161	456	199	166

Table E.37. *Displacements in FBM with Uncracked Parameters for SP - 1*

	P1 (m)	P2 (m)	P3 (m)	P4 (m)
Column-X	0.055	0.055	0.071	0.071
Column-Y	0.053	0.078	0.078	0.053
Pile-X	0.054	0.000	0.000	0.000
Pile-Y	0.056	0.074	0.074	0.056

Table E.38. *Displacements in FBM with Cracked Parameters for SP - 1*

	P1 (m)	P2 (m)	P3 (m)	P4 (m)
Column-X	0.055	0.055	0.071	0.071
Column-Y	0.053	0.078	0.078	0.053
Pile-X	0.054	0.000	0.000	0.000
Pile-Y	0.056	0.074	0.074	0.056

Table E.39. *Displacements in FBM with Uncracked Parameters for SP - 2*

	P1 (m)	P2 (m)	P3 (m)	P4 (m)
Column-X	1.219	1.229	1.229	1.219
Column-Y	0.553	0.985	0.985	0.553
Pile-X	1.210	0.040	0.040	0.039
Pile-Y	0.567	0.980	0.980	0.567

Table E.40. *Displacements in FBM with Cracked Parameters for SP - 2*

	P1 (m)	P2 (m)	P3 (m)	P4 (m)
Column-X	1.219	1.229	1.229	1.219
Column-Y	0.553	0.985	0.985	0.553
Pile-X	1.210	0.040	0.040	0.039
Pile-Y	0.567	0.980	0.980	0.567

Table E.41. *Displacements in FBM with Uncracked Parameters for SP - 3*

	P1 (m)	P2 (m)	P3 (m)	P4 (m)
Column-X	0.139	0.139	0.139	0.139
Column-Y	0.100	0.152	0.152	0.100
Pile-X	0.133	0.004	0.004	0.004
Pile-Y	0.105	0.143	0.143	0.105

Table E.42. *Displacements in FBM with Cracked Parameters for SP - 3*

	P1 (m)	P2 (m)	P3 (m)	P4 (m)
Column-X	0.139	0.139	0.139	0.139
Column-Y	0.100	0.152	0.152	0.100
Pile-X	0.133	0.004	0.004	0.004
Pile-Y	0.105	0.143	0.143	0.105

Table E.43. *Pier Forces in FBM with Uncracked Parameters for SP - 1*

	P (kN)	Vx (kN)	Vy (kN)	Mx (kNm)	My (kNm)
P1 - ColumnTop	9478	1	1495	1140	1
P2 - ColumnTop	9870	1	526	401	1
P3 - ColumnTop	9870	3	526	401	2
P4 - ColumnTop	9478	3	1495	1140	2
P1 - ColumnBot	10831	1	1495	11961	11
P2 - ColumnBot	11223	1	526	4206	12
P3 - ColumnBot	11223	3	526	4206	22
P4 - ColumnBot	10831	3	1495	11961	21

Table E.44. *Pier Forces in FBM with Cracked Parameters for SP - 1*

	P (kN)	Vx (kN)	Vy (kN)	Mx (kNm)	My (kNm)
P1 - ColumnTop	9478	1	1467	1119	0
P2 - ColumnTop	9870	1	511	390	0
P3 - ColumnTop	9870	1	511	390	0
P4 - ColumnTop	9478	1	1467	1119	0
P1 - ColumnBot	10831	3	1467	11740	0
P2 - ColumnBot	11223	3	511	4090	0
P3 - ColumnBot	11223	3	511	4090	0
P4 - ColumnBot	10831	3	1467	11740	0

Table E.45. *Pier Forces in FBM with Uncracked Parameters for SP - 2*

	P (kN)	Vx (kN)	Vy (kN)	Mx (kNm)	My (kNm)
P1 - ColumnTop	9244	11	4811	3668	8
P2 - ColumnTop	9980	12	701	535	9
P3 - ColumnTop	9980	12	701	535	9
P4 - ColumnTop	9244	11	4811	3668	8
P1 - ColumnBot	10598	11	4811	38489	85
P2 - ColumnBot	11333	12	701	5610	93
P3 - ColumnBot	11333	12	701	5610	93
P4 - ColumnBot	10597	11	4811	38488	85

Table E.46. *Pier Forces in FBM with Cracked Parameters for SP - 2*

	P (kN)	Vx (kN)	Vy (kN)	Mx (kNm)	My (kNm)
P1 - ColumnTop	9244	11	4796	3657	8
P2 - ColumnTop	9980	12	706	539	9
P3 - ColumnTop	9980	12	706	539	9
P4 - ColumnTop	9244	11	4796	3657	8
P1 - ColumnBot	10598	11	4796	38365	85
P2 - ColumnBot	11333	12	706	5650	93
P3 - ColumnBot	11333	12	706	5650	93
P4 - ColumnBot	10597	11	4796	38365	85

Table E.47. *Pier Forces in FBM with Uncracked Parameters for SP - 3*

	P (kN)	Vx (kN)	Vy (kN)	Mx (kNm)	My (kNm)
P1 - ColumnTop	9474	7	2598	1981	5
P2 - ColumnTop	9872	7	860	656	5
P3 - ColumnTop	9872	7	860	656	5
P4 - ColumnTop	9474	7	2598	1981	5
P1 - ColumnBot	10827	7	2598	20787	55
P2 - ColumnBot	11225	7	860	6883	57
P3 - ColumnBot	11225	7	860	6883	57
P4 - ColumnBot	10827	7	2598	20786	55

Table E.48. *Pier Forces in FBM with Cracked Parameters for SP - 3*

	P (kN)	Vx (kN)	Vy (kN)	Mx (kNm)	My (kNm)
P1 - ColumnTop	9474	7	2554	1947	5
P2 - ColumnTop	9872	7	837	639	5
P3 - ColumnTop	9872	7	837	639	5
P4 - ColumnTop	9474	7	2554	1947	5
P1 - ColumnBot	10827	7	2554	20431	55
P2 - ColumnBot	11225	7	837	6700	57
P3 - ColumnBot	11225	7	837	6700	57
P4 - ColumnBot	10827	7	2554	20431	55

Table E.49. *Pile Forces in FBM with Uncracked Parameters for SP - 1*

	P (kN)	Vx (kN)	Vy (kN)	Mx (kNm)	My (kNm)
P1 Axis	707	669	285	1230	1702
P2 Axis	1324	793	285	1230	2158
P3 Axis	1324	796	761	2035	2157
P4 Axis	1148	669	761	2035	1702

Table E.50. *Pile Forces in FBM with Cracked Parameters for SP - 1*

	P (kN)	Vx (kN)	Vy (kN)	Mx (kNm)	My (kNm)
P1 Axis	716	671	285	1230	1708
P2 Axis	1323	792	285	1230	2155
P3 Axis	1323	792	761	2035	2109
P4 Axis	1148	671	761	2035	1708

Table E.51. *Pile Forces in FBM with Uncracked Parameters for SP - 2*

	P (kN)	Vx (kN)	Vy (kN)	Mx (kNm)	My (kNm)
P1 Axis	5147	243	766	10515	4963
P2 Axis	5210	615	771	10582	8718
P3 Axis	5210	615	771	10582	8718
P4 Axis	5147	243	766	10515	4963

Table E.52. *Pile Forces in FBM with Cracked Parameters for SP - 2*

	P (kN)	Vx (kN)	Vy (kN)	Mx (kNm)	My (kNm)
P1 Axis	5147	218	766	10515	5017
P2 Axis	5210	615	771	10582	8713
P3 Axis	5210	615	771	10582	8713
P4 Axis	5147	218	766	10515	5017

Table E.53. *Pile Forces in FBM with Uncracked Parameters for SP - 3*

	P (kN)	Vx (kN)	Vy (kN)	Mx (kNm)	My (kNm)
P1 Axis	3856	1694	1855	5499	4695
P2 Axis	3879	1910	1855	5502	5634
P3 Axis	3879	1910	1855	5502	5634
P4 Axis	3856	1694	1855	5499	4695

Table E.54. *Pile Forces in FBM with Cracked Parameters for SP - 3*

	P (kN)	Vx (kN)	Vy (kN)	Mx (kNm)	My (kNm)
P1 Axis	3856	1697	1855	5499	4706
P2 Axis	3879	1909	1855	5502	5627
P3 Axis	3879	1909	1855	5502	5627
P4 Axis	3856	1697	1855	5499	4706

Table E.55. *Displacements in DBM with Uncracked Parameters for SP - 1*

	P1 (m)	P2 (m)	P3 (m)	P4 (m)
Column-X	0.341	0.263	0.341	0.341
Column-Y	0.016	0.026	0.027	0.017
Pile-X	0.339	0.005	0.005	0.004
Pile-Y	0.109	0.090	0.118	0.109

Table E.56. *Displacements in DBM with Cracked Parameters for SP - 1*

	P1 (m)	P2 (m)	P3 (m)	P4 (m)
Column-X	0.341	0.259	0.341	0.341
Column-Y	0.022	0.035	0.036	0.022
Pile-X	0.339	0.003	0.004	0.004
Pile-Y	0.035	0.046	0.049	0.035

Table E.57. *Displacements in DBM with Uncracked Parameters for SP - 2*

	P1 (m)	P2 (m)	P3 (m)	P4 (m)
Column-X	0.288	0.402	0.289	0.288
Column-Y	0.023	0.036	0.038	0.024
Pile-X	0.287	-0.004	-0.003	-0.003
Pile-Y	0.034	-0.043	-0.049	-0.035

Table E.58. *Displacements in DBM with Cracked Parameters for SP - 2*

	P1 (m)	P2 (m)	P3 (m)	P4 (m)
Column-X	0.288	0.402	0.289	0.288
Column-Y	0.023	0.036	0.038	0.024
Pile-X	0.287	-0.004	-0.003	-0.003
Pile-Y	0.036	-0.044	-0.051	-0.037

Table E.59. *Displacements in DBM with Uncracked Parameters for SP - 3*

	P1 (m)	P2 (m)	P3 (m)	P4 (m)
ColumnX	-0.386	-0.225	-0.387	-0.386
ColumnY	-0.027	-0.044	-0.045	-0.028
PileX	-0.384	-0.005	-0.002	-0.008
PileY	-0.040	0.053	0.057	0.041

Table E.60. *Displacements in DBM with Cracked Parameters for SP - 3*

	P1 (m)	P2 (m)	P3 (m)	P4 (m)
ColumnX	-0.386	-0.225	-0.387	-0.386
ColumnY	-0.027	-0.043	-0.045	-0.028
PileX	-0.384	-0.005	-0.008	-0.008
PileY	-0.043	0.055	0.060	0.043

Table E.61. *Pier Forces in DBM with Uncracked Parameters for SP - 1*

	P (kN)	Vx (kN)	Vy (kN)	Mx (kNm)	My (kNm)
P1 - ColumnTop	9484	0	4800	3664	0
P2 - ColumnTop	9867	0	3333	2545	0
P3 - ColumnTop	9867	0	4705	3592	0
P4 - ColumnTop	9484	0	4786	3653	0
P1 - ColumnBot	10837	0	4753	38174	0
P2 - ColumnBot	11220	0	3261	26428	0
P3 - ColumnBot	11220	0	4607	37313	0
P4 - ColumnBot	10837	0	4716	38055	0

Table E.62. *Pier Forces in DBM with Cracked Parameters for SP - 1*

	P (kN)	Vx (kN)	Vy (kN)	Mx (kNm)	My (kNm)
P1 - ColumnTop	9484	0	6153	4692	0
P2 - ColumnTop	9867	0	4895	3732	0
P3 - ColumnTop	9867	0	5879	4483	0
P4 - ColumnTop	9484	0	6145	4686	0
P1 - ColumnBot	10837	0	6150	49209	0
P2 - ColumnBot	11220	0	4890	39141	0
P3 - ColumnBot	11220	0	5874	47017	0
P4 - ColumnBot	10837	0	6140	49145	0

Table E.63. *Pier Forces in DBM with Uncracked Parameters for SP - 2*

	P (kN)	Vx (kN)	Vy (kN)	Mx (kNm)	My (kNm)
P1 - ColumnTop	9500	2	6746	5144	1
P2 - ColumnTop	9866	2	4356	3321	2
P3 - ColumnTop	9885	2	6409	4887	1
P4 - ColumnTop	9484	2	6728	5130	1
P1 - ColumnBot	10838	2	6745	53962	13
P2 - ColumnBot	11219	2	4354	34839	17
P3 - ColumnBot	11221	2	6406	51261	13
P4 - ColumnBot	10837	2	6725	53815	13

Table E.64. *Pier Forces in DBM with Cracked Parameters for SP - 2*

	P (kN)	Vx (kN)	Vy (kN)	Mx (kNm)	My (kNm)
P1 - ColumnTop	9500	2	6698	5108	1
P2 - ColumnTop	9866	2	4313	3289	2
P3 - ColumnTop	9885	2	6368	4856	1
P4 - ColumnTop	9487	2	6680	5094	1
P1 - ColumnBot	10838	2	6695	53572	13
P2 - ColumnBot	11219	2	4309	34493	17
P3 - ColumnBot	11239	2	6362	50924	13
P4 - ColumnBot	10840	2	6675	53425	13

Table E.65. *Pier Forces in DBM with Uncracked Parameters for SP - 3*

	P (kN)	Vx (kN)	Vy (kN)	Mx (kNm)	My (kNm)
P1 ColumnTop	9487	3	7760	5917	3
P2 ColumnTop	9934	3	5822	4439	2
P3 ColumnTop	9869	3	7319	5581	3
P4 ColumnTop	9487	3	7744	5904	3
P1 ColumnBot	10840	3	7759	62075	27
P2 ColumnBot	11287	3	5819	46563	21
P3 ColumnBot	11222	3	7316	58542	28
P4 ColumnBot	10835	3	7741	61939	27

Table E.66. *Pier Forces in DBM with Cracked Parameters for SP - 3*

	P (kN)	Vx (kN)	Vy (kN)	Mx (kNm)	My (kNm)
P1 ColumnTop	9487	3	7694	5867	3
P2 ColumnTop	9934	3	5771	4400	2
P3 ColumnTop	9869	4	7262	5537	3
P4 ColumnTop	9487	3	7679	5855	3
P1 ColumnBot	10840	3	7690	61533	27
P2 ColumnBot	11287	3	5765	46149	21
P3 ColumnBot	11219	3	7255	58072	28
P4 ColumnBot	10840	3	7673	61411	27

Table E.67. *Pile Forces in DBM with Uncracked Parameters for SP - 1*

	P (kN)	Vx (kN)	Vy (kN)	Mx (kNm)	My (kNm)
P1 Axis	2238	24	318	826	3687
P2 Axis	2601	112	697	3115	2862
P3 Axis	2685	24	307	944	3694
P4 Axis	2240	24	317	829	3694

Table E.68. *Pile Forces in DBM with Cracked Parameters for SP - 1*

	P (kN)	Vx (kN)	Vy (kN)	Mx (kNm)	My (kNm)
P1 Axis	1921	24	392	516	3694
P2 Axis	1880	407	719	2218	3870
P3 Axis	1963	24	375	351	3694
P4 Axis	1917	24	391	511	3694

Table E.69. *Pile Forces in DBM with Uncracked Parameters for SP - 2*

	P (kN)	Vx (kN)	Vy (kN)	Mx (kNm)	My (kNm)
P1 Axis	2370	59	425	1490	2537
P2 Axis	2218	544	1510	6017	4297
P3 Axis	2292	60	402	1290	2540
P4 Axis	2363	60	424	1478	2540

Table E.70. *Pile Forces in DBM with Cracked Parameters for SP - 2*

	P (kN)	Vx (kN)	Vy (kN)	Mx (kNm)	My (kNm)
P1 Axis	2348	59	422	1457	2537
P2 Axis	2218	544	1509	6010	4297
P3 Axis	2272	60	399	1260	2540
P4 Axis	2340	59	421	1445	2537

Table E.71. *Pile Forces in DBM with Uncracked Parameters for SP - 3*

	P (kN)	Vx (kN)	Vy (kN)	Mx (kNm)	My (kNm)
P1 Axis	2400	65	500	1063	3933
P2 Axis	2084	651	1490	4854	4707
P3 Axis	2307	67	472	828	3939
P4 Axis	2395	65	499	1055	3934

Table E.72. *Pile Forces in DBM with Cracked Parameters for SP - 3*

	P (kN)	Vx (kN)	Vy (kN)	Mx (kNm)	My (kNm)
P1 Axis	2375	65	496	1026	3933
P2 Axis	2068	651	1489	4849	4707
P3 Axis	2289	67	468	796	3939
P4 Axis	2369	65	495	1017	3934